UNCLASSIFIED

URITY CLASSIFICATION OF THIS PAGE (When Data Entered)

## REPORT DOCUMENTATION PAGE

READ INSTRUCTIONS BEFORE COMPLETING FORM

REPORT NUMBER: AFIT/CI/NR 88- 25

2. GOVT ACCESSION NO.

3. RECIPIENT'S CATALOG NUMBER

TITLE (and Subtitle): ORIGIN OF TROPOSPHERIC OZONE OVER CENTRAL UNITED STATES

5. TYPE OF REPORT & PERIOD COVERED: MS THESIS

6. PERFORMING ORG. REPORT NUMBER

AUTHOR(s): DONNA P. McNAMARA

8. CONTRACT OR GRANT NUMBER(s)

PERFORMING ORGANIZATION NAME AND ADDRESS: AFIT STUDENT AT: UNIVERSITY OF MARYLAND

10. PROGRAM ELEMENT, PROJECT, TASK AREA & WORK UNIT NUMBERS

11. CONTROLLING OFFICE NAME AND ADDRESS

12. REPORT DATE: 1988

13. NUMBER OF PAGES: 121

14. MONITORING AGENCY NAME & ADDRESS (if different from Controlling Office): AFIT/NR, Wright-Patterson AFB OH 45433-6583

15. SECURITY CLASS. (of this report): UNCLASSIFIED

15a. DECLASSIFICATION/DOWNGRADING SCHEDULE

16. DISTRIBUTION STATEMENT (of this Report)

DISTRIBUTED UNLIMITED: APPROVED FOR PUBLIC RELEASE



17. DISTRIBUTION STATEMENT (of the abstract entered in Block 20, if different from Report)

SAME AS REPORT

18. SUPPLEMENTARY NOTES

Approved for Public Release: IAW AFR 190-1
LYNN E. WOLAVER 18 July 88
Dean for Research and Professional Development
Air Force Institute of Technology
Wright-Patterson AFB OH 45433-6583

19. KEY WORDS (Continue on reverse side if necessary and identify by block number)

20. ABSTRACT (Continue on reverse side if necessary and identify by block number)

ATTACHED

[illegible] product- [illegible] black and [illegible]

DD FORM 1 JAN 73 1473 EDITION OF 1 NOV 65 IS OBSOLETE

UNCLASSIFIED

SECURITY CLASSIFICATION OF THIS PAGE (When Data Entered)

# INTRODUCTION

Ozone ($O_3$) is a key species in the troposphere for several reasons. It is a key ingredient of "Los Angeles-type smog" as a result of photochemical reactions. Tropospheric $O_3$ also impacts the radiation budget and may cause climate change because it is a greenhouse gas with a strong absorption band centered at 9.6 μm in the atmospheric window region (Fishman et al., 1979). Also, photolysis of $O_3$ by radiation of wavelengths less than 318 nm is the primary source of hydroxyl (OH) radicals in the troposphere.

$$O_3 + h\nu \rightarrow O(^1D) + O_2 \quad (1)$$

$$O(^1D) + M \rightarrow O(^3P) + M \quad (2)$$

$$O(^1D) + H_2O \rightarrow 2 \cdot OH \quad (3)$$

$O(^1D)$ is an excited state of atomic oxygen; $O(^3P)$ is the ground state. OH radicals are important in the cleansing of the atmosphere through oxidation of pollutant species such as carbon monoxide (CO), methane ($CH_4$), non-methane hydrocarbons (NMHCs) and some halocarbons (Levy, 1971).

Sources of tropospheric $O_3$ have been under much debate in the past few years. $O_3$ is known to be photochemically active in the stratosphere where it strongly absorbs ultraviolet radiation, causing the reversal in lapse rate there. As explained by Fishman (1985), earliest studies considered $O_3$ inert in the troposphere; deposition at the surface was believed balanced by injection from the stratosphere (Junge, 1962). Photochemical production of $O_3$ in the troposphere was first considered after the discovery of $O_3$ as a key species in "Los

Angeles-type smog". In the early 1970's, the idea that significant amounts of $O_3$ may be produced outside the polluted planetary boundary layer (PBL) was proposed (Chameides and Walker, 1973; Crutzen, 1973). It is now quite clear that photochemistry and transport both effect the observed $O_3$ distribution in the troposphere. What remains is to determine the relative contributions of each process under specific conditions.

Though there are various sources of tropospheric $O_3$, by comparing correlations between $O_3$ and other trace species, and considering the meteorological situation, one can often draw conclusions about the origin and transport of $O_3$ in the troposphere.

Carbon monoxide has its largest source in the PBL, from combustion of fossil fuels or biomass burning. In addition, CO is the end product in the oxidation chain of $CH_4$ and NMHCs. The primary loss mechanism for CO in the troposphere is reaction with the OH (Levy II, 1971; Condon et al., 1987). In mid-latitudes, the typical lifetime of CO is of the order of a few months (Thompson and Cicerone, 1986). CO was found to be a good tracer of PBL air (Fishman et al., 1980; Pickering et al., 1988a) so when CO and $O_3$ concentrations are simultaneously high, the source of the elevated $O_3$ is the PBL, or in-situ production in the free troposphere by PBL precursors (discussed below). CO concentration decreases sharply in the stratosphere, thus high $O_3$ with low CO indicates a stratospheric source of $O_3$.

Like CO, water vapor ($H_2O$) originates in the PBL, at the surface,

# ORIGIN OF TROPOSPHERIC OZONE

# OVER CENTRAL US

by

Donna P. McNamara

Thesis submitted to the Faculty of the Graduate School

of the University of Maryland in partial fulfillment

of the requirements for the degree of

Master of Science

1988

Advisory Committee:

Dr. Russell Dickerson
Dr. Robert Ellingson
Dr. George Huffman

## ACKNOWLEDGEMENTS

I would like to thank my husband, Brien, for his constant help and support throughout my time in graduate school. He also aided my research by calculating zenith angles and local times, and copying photographs.

I would also like to thank Dr. Russell Dickerson, my research advisor, for his help selecting a topic, and his constant support and encouragement. He showed great patience and persistence teaching chemistry to a meteorologist, and was always available when I needed help.

I also received much support from my fellow graduate students who collected the field data. Ken Pickering provided innumerable assistance, and was like a second research advisor. Winston Luke and Linda Nunnermacker helped open my eyes to analytical chemistry and explained the workings of the various trace gas measurement techniques. Brian Gockel prepared the framework for the numerical model used to estimate ozone production; He and Melody Owens helped me stay ahead in my many battles with the computer.

Dr. George Huffman provided very helpful support and ideas for the meteorological analysis in this research.

Jose Meitin, of NOAA/ERL, promptly provided much supporting data, such as rawinsondes, radar images, and satellite pictures.

Dr. Arlan Krueger, of NASA, provided the initial TOMS pictures which sparked my interest in the TOMS analysis. Dr. Jack Fishman, also of NASA, supplied the enhanced imagery and raw data used in the analysis. The analysis was aided by P.K. Bartia, of STX Corp., who explained the processing algorithms.

The Research Aviation Facility of the National Center for Atmospheric Research supported the aircraft measurements.

This research was supported by NSF Grants ATM-83-05843 and ATM-86-19491, and the PRECP and PRESTORM programs.

Finally, thanks must go to my father, Wallace Palmer, for his great help with the word processing and printing of this thesis.

TABLE OF CONTENTS

## LIST OF TABLES

## LIST OF FIGURES

# INTRODUCTION

Ozone ($O_3$) is a key species in the troposphere for several reasons. It is a key ingredient of "Los Angeles-type smog" as a result of photochemical reactions. Tropospheric $O_3$ also impacts the radiation budget and may cause climate change because it is a greenhouse gas with a strong absorption band centered at 9.6 μm in the atmospheric window region (Fishman et al., 1979). Also, photolysis of $O_3$ by radiation of wavelengths less than 318 nm is the primary source of hydroxyl (OH) radicals in the troposphere:

$$O_3 + h\nu \rightarrow O(^1D) + O_2 \quad (1)$$

$$O(^1D) + M \rightarrow O(^3P) + M \quad (2)$$

$$O(^1D) + H_2O \rightarrow 2 \cdot OH \quad (3)$$

$O(^1D)$ is an excited state of atomic oxygen; $O(^3P)$ is the ground state. OH radicals are important in the cleansing of the atmosphere through oxidation of pollutant species such as carbon monoxide (CO), methane ($CH_4$), non-methane hydrocarbons (NMHCs) and some halocarbons (Levy, 1971).

Sources of tropospheric $O_3$ have been under much debate in the past few years. $O_3$ is known to be photochemically active in the stratosphere where it strongly absorbs ultraviolet radiation, causing the reversal in lapse rate there. As explained by Fishman (1985), earliest studies considered $O_3$ inert in the troposphere; deposition at the surface was believed balanced by injection from the stratosphere (Junge, 1962). Photochemical production of $O_3$ in the troposphere was first considered after the discovery of $O_3$ as a key species in "Los

Angeles-type smog". In the early 1970's, the idea that significant amounts of $O_3$ may be produced outside the polluted planetary boundary layer (PBL) was proposed (Chameides and Walker, 1973; Crutzen, 1973). It is now quite clear that photochemistry and transport both effect the observed $O_3$ distribution in the troposphere. What remains is to determine the relative contributions of each process under specific conditions.

Though there are various sources of tropospheric $O_3$, by comparing correlations between $O_3$ and other trace species, and considering the meteorological situation, one can often draw conclusions about the origin and transport of $O_3$ in the troposphere.

Carbon monoxide has its largest source in the PBL, from combustion of fossil fuels or biomass burning. In addition, CO is the end product in the oxidation chain of $CH_4$ and NMHCs. The primary loss mechanism for CO in the troposphere is reaction with the OH (Levy II, 1971; Condon et al., 1987). In mid-latitudes, the typical lifetime of CO is of the order of a few months (Thompson and Cicerone, 1986). CO was found to be a good tracer of PBL air (Fishman et al., 1980; Pickering et al., 1988a) so when CO and $O_3$ concentrations are simultaneously high, the source of the elevated $O_3$ is the PBL, or in-situ production in the free troposphere by PBL precursors (discussed below). CO concentration decreases sharply in the stratosphere, thus high $O_3$ with low CO indicates a stratospheric source of $O_3$.

Like CO, water vapor ($H_2O$) originates in the PBL, at the surface,

but it is not an ideal tracer because precipitation is a sink for $H_2O$.

The sources of nitrogen oxides are more complex. The largest source of nitric oxide (NO) is combustion of fossil fuels and biomass burning. But another large source is lightning, and smaller amounts of NO come from soil exhalation, stratospheric intrusions, aircraft emissions, oxidation of ammonia ($NH_3$) and photolysis of marine $NO_2^-$ (Stedman and Shetter, 1983; Logan, 1983). Estimates of the relative contributions of each source vary dramatically. For example, Davis et al. (1987) estimate lightning to contribute from 2 to 20 Tg N/yr. Because the sources are numerous and variable, and only recently have effective measurement techniques been developed, the estimates of typical NO concentrations for specific situations are also highly uncertain. It is common to consider NO and nitrogen dioxide ($NO_2$) together as $NO_x$ and all odd nitrogen (NO, $NO_2$, $NO_3$, $N_2O_5$, $HNO_2$, $HNO_3$, $HO_2NO_2$, peroxyacetyl nitrate (PAN) and other organic nitrates) as $NO_y$. In the troposphere $NO_x$ and $O_3$ participate, in part, in the following reactions:

$$NO + O_3 \rightarrow NO_2 + O_2 \quad (4)$$

$$NO_2 + h\nu \rightarrow NO + O \quad (5)$$

$$O + O_2 + M \rightarrow O_3 + M. \quad (6)$$

These reactions approach a steady-state, called the photostationary state, when not disturbed by changes in light intensity, reactant concentrations, or competing reactions (Leighton, 1961). When $NO_2$ is photolyzed (by radiation of wavelengths less than 420 nm), $O_3$ will eventually be produced. If there is enough $NO_x$ in the presence of CO, $CH_4$, NMHCs and sunlight, the peroxy radicals ($HO_2$ and $RO_2$) formed will

convert NO to $NO_2$ without consuming $O_3$ (or O), resulting in an increase in $O_3$ (Chameides and Walker, 1973; Crutzen, 1973). Thus, production of $O_3$ is critically dependent on $NO_x$ concentration (e.g. Crutzen and Gidel, 1983; Liu et al., 1987). The concentration of $NO_x$ may vary by as much as 4 orders of magnitude from the remote marine atmosphere to the polluted continental PBL (Logan, 1983). $NO_x$ has a short lifetime, just one to two days in summer, before it is converted to one of the $NO_y$ species, such as nitric acid ($HNO_3$), which can act as a reservoir or be removed from the atmosphere. $NO_y$ is lost through wet deposition of soluble species such as $HNO_3$, and dry deposition of $NO_2$ and $HNO_3$ (Logan, 1983).

Tropospheric concentrations of a trace gas are in part a function of its lifetime and sources, as well as the meteorological conditions. Concentrations of trace gases such as oxides of nitrogen exhibit large variations in the troposphere because they react on the time scale of minutes to hours, their sources are not uniformly distributed, and they participate in chemical reactions before meteorological transport can uniformly distribute them throughout the troposphere. Chemistry as well as meteorology must be considered when analyzing the distribution of these species. In contrast, trace gases such as $CH_4$ have very long lifetimes, so transport has time to mix these species thoroughly, resulting in concentrations that are nearly constant throughout the troposphere. Intermediate to these are species such as CO, which do show variability in concentration in the troposphere, but have lifetimes long enough to be considered unreactive on a time scale of a few hours; location of sources and transport are then responsible for

most of the observed variations.

When pollutants remain in the PBL, they are generally short lived due to wet and dry deposition. Wind speeds are lower in the PBL, so transport is minimized. If the pollutants are transported to the free troposphere however, their lifetimes increase, and they can be transported much farther (Dickerson et al., 1987). Pollution now becomes a regional or national problem, rather than a local, primarily urban, problem. Recent research by Liu et al. (1987) suggests the efficiency of $O_3$ production increases as $NO_x$ concentration decreases; potentially more $O_3$ is produced than current estimates if more $NO_x$ escapes from the PBL and is diluted in the free troposphere. Generally the PBL is topped with a temperature inversion that inhibits mixing with the free troposphere, and tropospheric layers persist because mean vertical velocities on the synoptic scale are of the order of just a few centimeters per second (Holton, 1979). However, when instability allows cumulus convection, mesoscale vertical mixing may be large. Gidel (1983) and Chatfield and Crutzen (1984) developed photochemical models that included transport by cumulus clouds; their results suggest convective transport from the PBL plays a larger role in tropospheric chemistry than previously believed. Isaac et al. (1984) found evidence that precipitating and non-precipitating clouds transport pollutants out of the PBL. Chameides et al. (1987) found model-calculated OH concentrations were correlated with measured elevated NO concentrations from a thunderstorm source and concluded that, as the convection pumps PBL air to high altitudes, the anvil area of a thunderstorm should be a "photochemical hotspot".

During the summer of 1985, tropospheric trace gases and meteorological data were collected as part of a project to study trace gas profiles over rural North America. The project, "Trace Gas Profiles II" was sponsored by the National Science Foundation (NSF), and was conducted concurrently with two other projects, PRE-STORM (sponsored by the National Oceanic and Atmospheric Administration (NOAA), and NSF) and PRECP (sponsored by the US Dept. of Energy). Operations were based in Oklahoma City. The National Center for Atmospheric Research (NCAR) Sabreliner aircraft was fitted with detectors to measure the trace gases ozone, carbon monoxide, and nitrogen oxides; as well as many meteorological parameters. This thesis examines two Sabreliner flights on June 22, 1985. For analysis of other flights from this project see Dickerson et al. (1987), Pickering (1987), Pickering et al. (1988a), and Pickering et al. (1988b).

Dickerson et al. (1987) studied a thunderstorm and found elevated values of CO, NMHCs, $O_3$, $NO_x$ and $NO_y$ in the outflow region of the storm, suggesting thunderstorms are a mechanism for significant vertical transport from the PBL. In contrast, Pickering et al. (1988a), found a thunderstorm case where a cold front cut off the cell from PBL air, such that the cell could not mix PBL air with the free troposphere. Therefore, significant vertical transport cannot be assumed with all convective cells.

The two flights considered here investigated convection associated with a dissipating frontal system and fair weather in the region

later the same day. The purpose of this research is to present the observed trace gas distributions, account for the origin of gradients in tropospheric $O_3$, and quantify the $O_3$ production possible under the conditions observed. Vertical profiles and time series of trace gases are presented. Correlations between the various trace gases are analyzed. Total Ozone Mapping Spectrometer (TOMS) data from the NASA Nimbus 7 polar-orbiting satellite are presented to look for effects of tropospheric $O_3$ concentrations on column abundances. An estimate of the in-situ photochemical production of $O_3$ is made using a simple photochemical model.

# I. INSTRUMENTATION

Data were collected from the NCAR Sabreliner--a twin engine research jet with a flight altitude ceiling of about 11 km. In addition to its normal package of meteorological equipment (NCAR, 1984), the Sabreliner carried instruments to measure $O_3$, CO, NO, $NO_x$ and $NO_y$. Details of the trace gas data processing are described in Appendix A. Detailed one minute average data for both flights are given in Appendix B. For some missions, grab samples of NMHCs were collected for later analysis.

Nitrogen oxides were measured by $O_3$ chemiluminescence with a Thermo Electron Corporation Model 14B detector modified for greater sensitivity (Delany et al., 1982; Dickerson et al., 1984). Measurement of NO using chemiluminescence is based on reaction 4, above, of the photostationary state, in which NO and $O_3$ react to form $NO_2$ (Stedman et al. 1972). Approximately 10 percent of the $NO_2$ formed will be in an excited state and will emit light, which can be measured. Before oxides of nitrogen other than NO can be detected, they must first be converted to NO. The detector uses ferrous sulfate to convert $NO_x$ to NO and a molybdenum catalyst to convert $NO_y$. An equipment intercomparison by Fehsenfeld et al. (1987) determined there is a positive interference in the measured $NO_x$ due to PAN when using the ferrous sulfate converter. To obtain measurements, the sample flow is mixed with $O_3$. A background signal is obtained by sending sample air through a preconverter where the NO and $O_3$ react out of view of the photomultiplier tube. The detector mode was usually

changed every 3 minutes to measure NO, $NO_x$, $NO_y$ and background on a 12-minute cycle. A measurement was recorded every second and averaged over 10 second intervals; about 30 seconds of data were lost during each mode change. The instrument has a detection limit of about 20 ppt NO; the uncertainty of NO detection is $\pm$ 14 percent, and that of $NO_y$ is $\pm$ 20 percent at the 95 percent confidence level (Fehsenfeld et al. 1987).

Ozone was measured using a Dasibi Model 1003 detector, which measures $O_3$ absorption of 254 nm radiation. A reference signal is determined by passing the sample air first through a catalyst which destroys all the $O_3$. The sample and reference signals are subtracted to obtain the $O_3$ concentration every 7 seconds. The instrument has a detection limit and uncertainty of about $\pm$ 2 ppb (at 95 percent confidence level).

Carbon monoxide was measured using a modified Thermo Electron Corporation Model 48 gas correlation non-dispersive infrared detector. Gas filter correlation (GFC) analyzers operate by sensing the absorption from CO in the 4.67 $\mu$m fundamental vibration-rotation band. Radiation in this region is also absorbed by the wings of other trace gases, most significantly carbon dioxide ($CO_2$) and $H_2O$. GFC corrects for this by passing the source beam alternately through a filter of pure nitrogen ($N_2$) and a filter of pure CO, before passing through the sample cell. The $CO_2$ and $H_2O$ in the sample will attenuate both beams almost the same amount, but CO in the sample cell will change only the beam that passed through the $N_2$. The CO cell produces a reference

signal. The difference in the intensities of the two beams yields the concentration of CO in the sample cell. Modifications further eliminated the $H_2O$ interference by removing it from the sample with a drying tube, reduced the amount of zero drift by inserting a chemical zero, and increased the signal-to-noise ratio. The modified instrument has a detection limit of about 24 ppb (95 percent confidence level) with a 60 second signal average (Dickerson and Delany, 1988). Values were recorded every 10 seconds, and the instrument was usually in zero mode for 3 of every 12 minutes. Data used in this research are 30 second signal averages.

## II. Synoptic Situation

On 21 June 1985 an upper level trough was located in the mountain states, extending as far south as southern Colorado at 300mb. Associated with this trough was a strong cold front located north of Oklahoma, through central Nebraska and along the northern border of Colorado. Around 0200 GMT (2100 CDT) convection developed along a squall line east of Amarillo TX. By 0500 GMT a squall line also developed along the border of Kansas and Oklahoma. Throughout the night, the line pushed to the southeast. In Kansas, there were three reports of tornadoes; hail and severe wind gusts were reported in Oklahoma and Kansas (Meitin and Cunning, 1985).

By the morning of 22 June, the upper level trough (Figure 1) had become vertically stacked through the central US from Minnesota to Missouri, and continued to recede northward in the next 24 hours. The surface front at 1200 GMT (Figure 2) extended from Illinois to Texas, through central Oklahoma, and had weakened drastically. GOES IR (NOAA geostationary infrared) satellite imagery (Figure 3) showed high level clouds remaining from central Oklahoma to southern Illinois along the old front. Radar reports confirmed some convection remained, organized in a line that pushed slowly through central Arkansas during the flight periods. The first flight of the day took off from Oklahoma City at 1220 CDT (1720 GMT) and flew a nearly straight east-southeast out and back track through central Arkansas, turning around over northwest Mississippi (Figure 4). The Sabreliner ascended quickly to an altitude greater than 8 km, and spent much of the flight

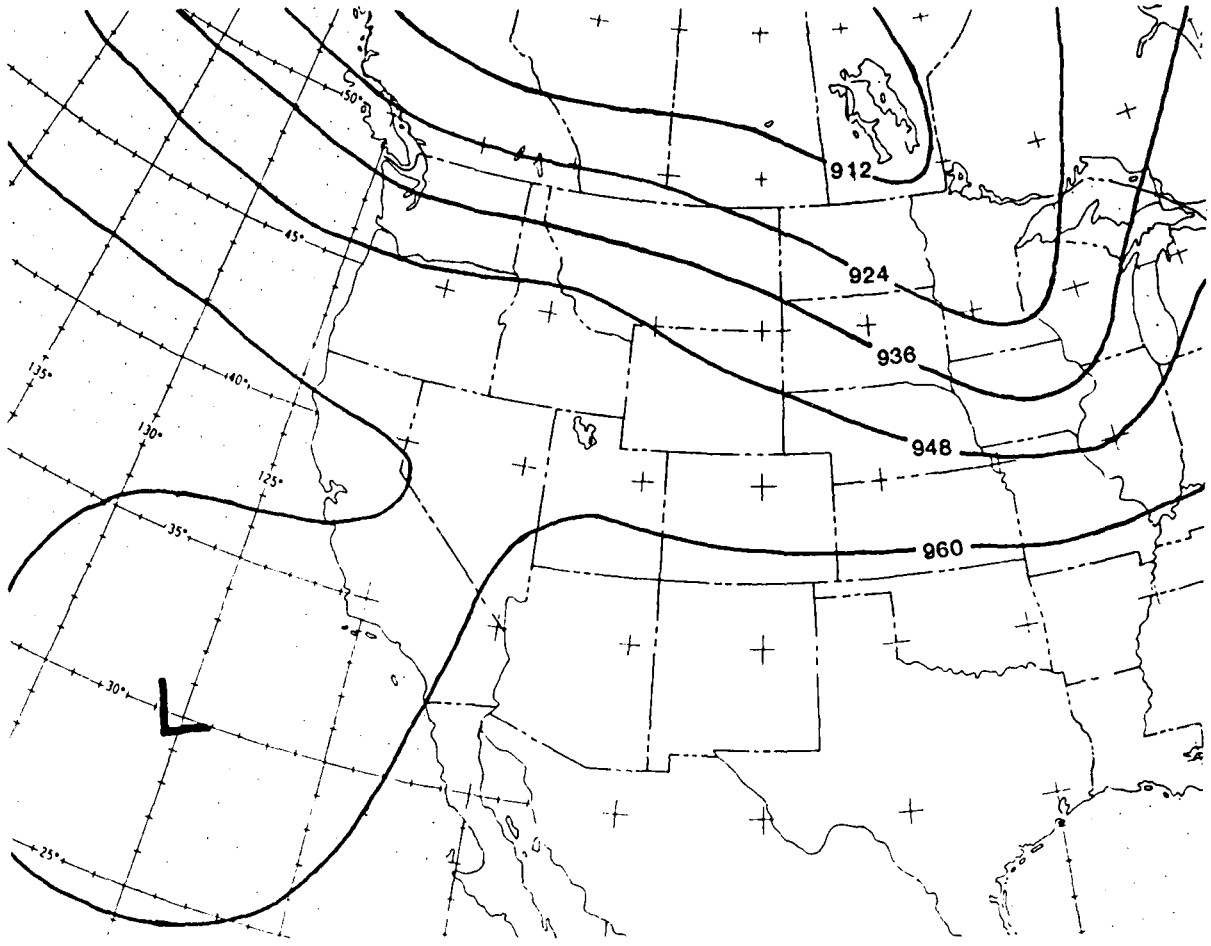


Fig. 1. 300 mb heights (in decameters) for 1200 GMT (0700 CDT), 22 June 1985.

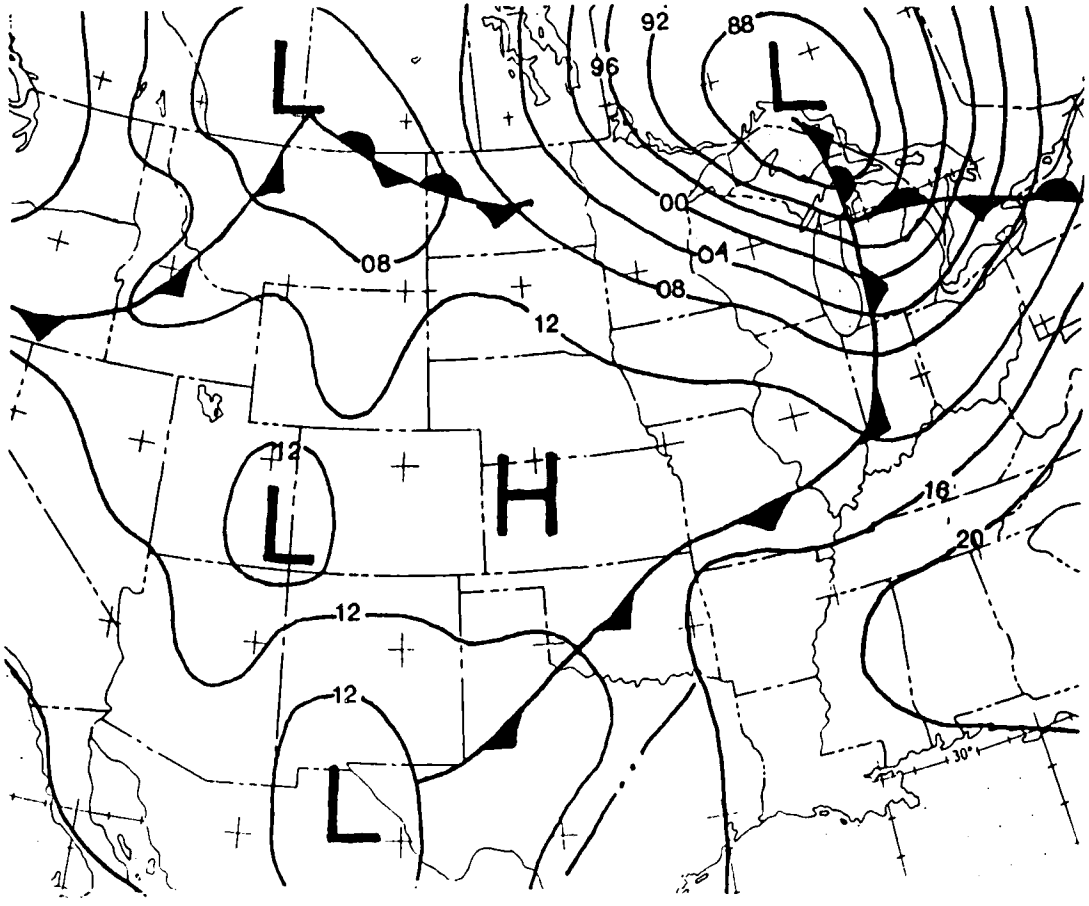


Fig. 2. Sea level pressure isobars (plus 900 or 1000 mb) and frontal positions for 1200 GMT (0700 CDT), 22 June 1985. The symbol in central Texas indicates a squall line.

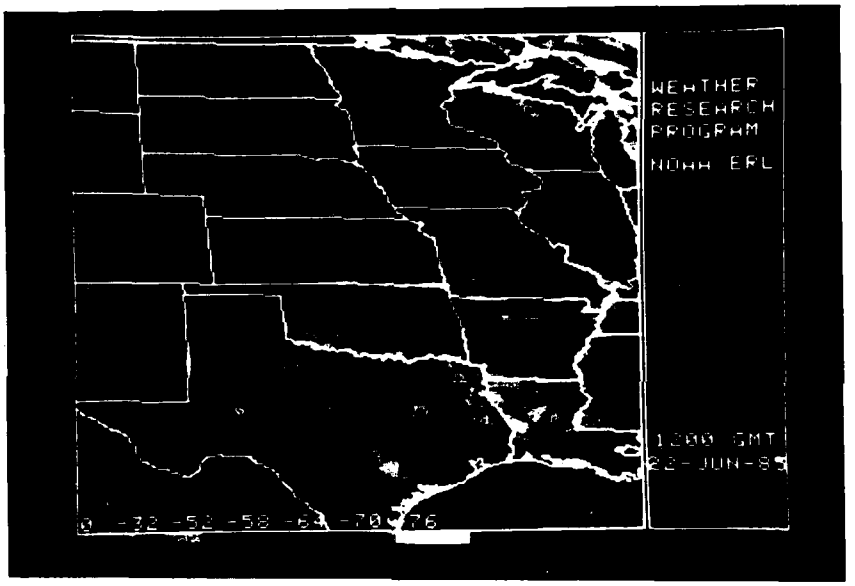


Fig. 3. GOES IR satellite imagery, 1200 GMT (0700 CDT), 22 June 1985.

Fig. 4. Flight track for the first mission.

in cloud (Figure 5). The return leg was in clear air after the descent to 5.5 km just before reaching the Arkansas-Oklahoma border. The flight sampled a vertically mixed troposphere, shortly after the peak in convective activity as determined by satellite imagery.

By 2300 GMT (1800 CDT), the remaining convection continued to decay (Figure 6). The surface front had dissipated just north of Oklahoma City. The second flight of the day left Oklahoma City at 1702 CDT and flew east, making several loops within Oklahoma (Figure 7). The Sabreliner spent much time in level flight at 7 km and 10.6 km, and made an extra penetration into the PBL (Figure 8). The only clouds were fair weather cumulus, built mostly to about 2 km, with some as high as 4.5 km.

All day, the area from Oklahoma City through eastern Arkansas stayed predominantly under southerly flow at the surface from the Gulf of Mexico, never experiencing an obvious frontal passage. At upper levels (above 700mb), the wind had a westerly component throughout the day.

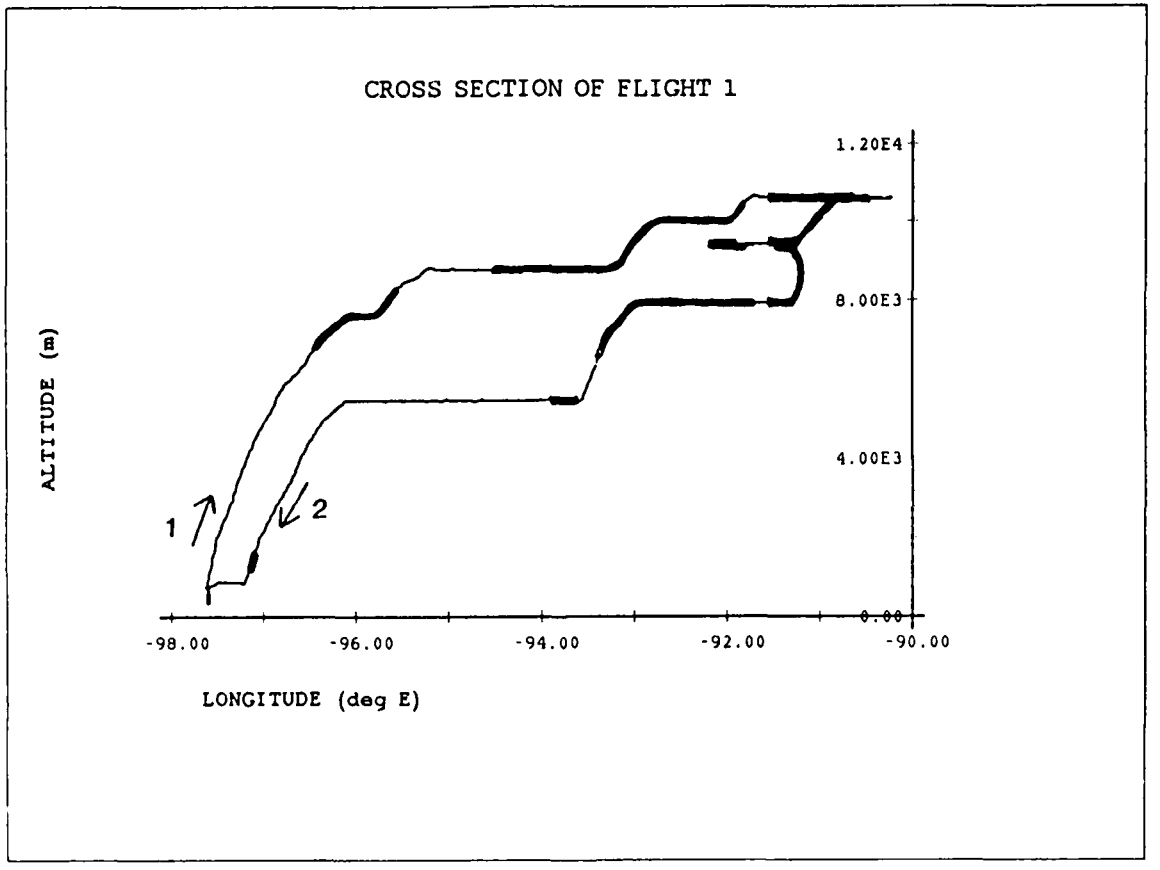


Fig. 5. Cross section of the first flight track. Heavy lines indicate when the Sabreliner was in cloud (determined from nose-camera film and the airborne liquid water sensor). Profiles are labelled 1 and 2.

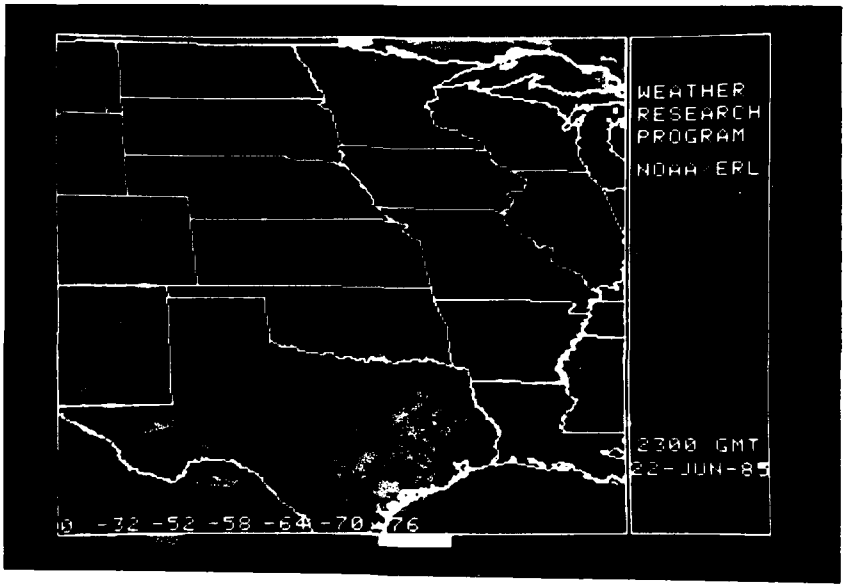


**Fig. 6. GOES IR satellite imagery, 2300 GMT (1800 CDT), 22 June 1985.**

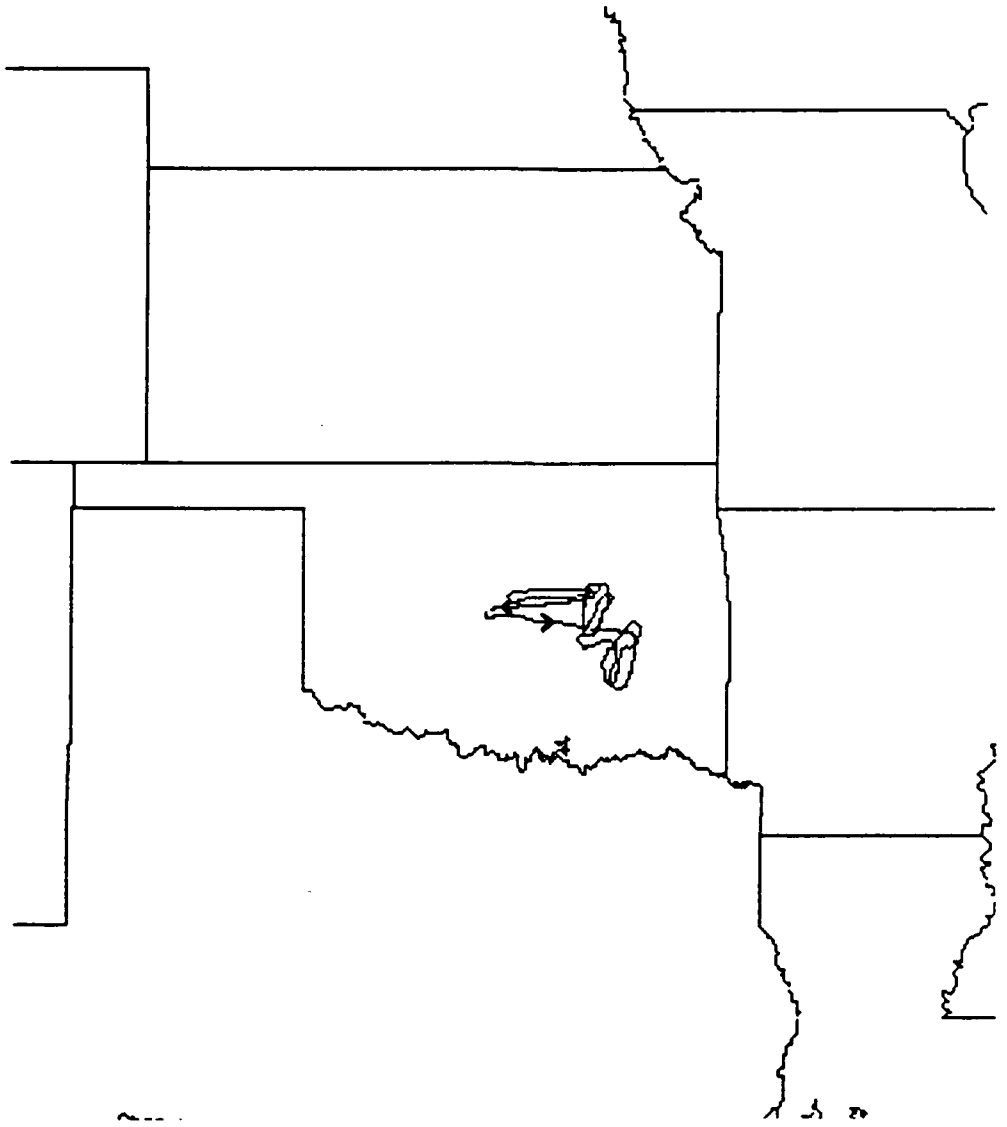

Fig. 7. Flight track for the second mission.

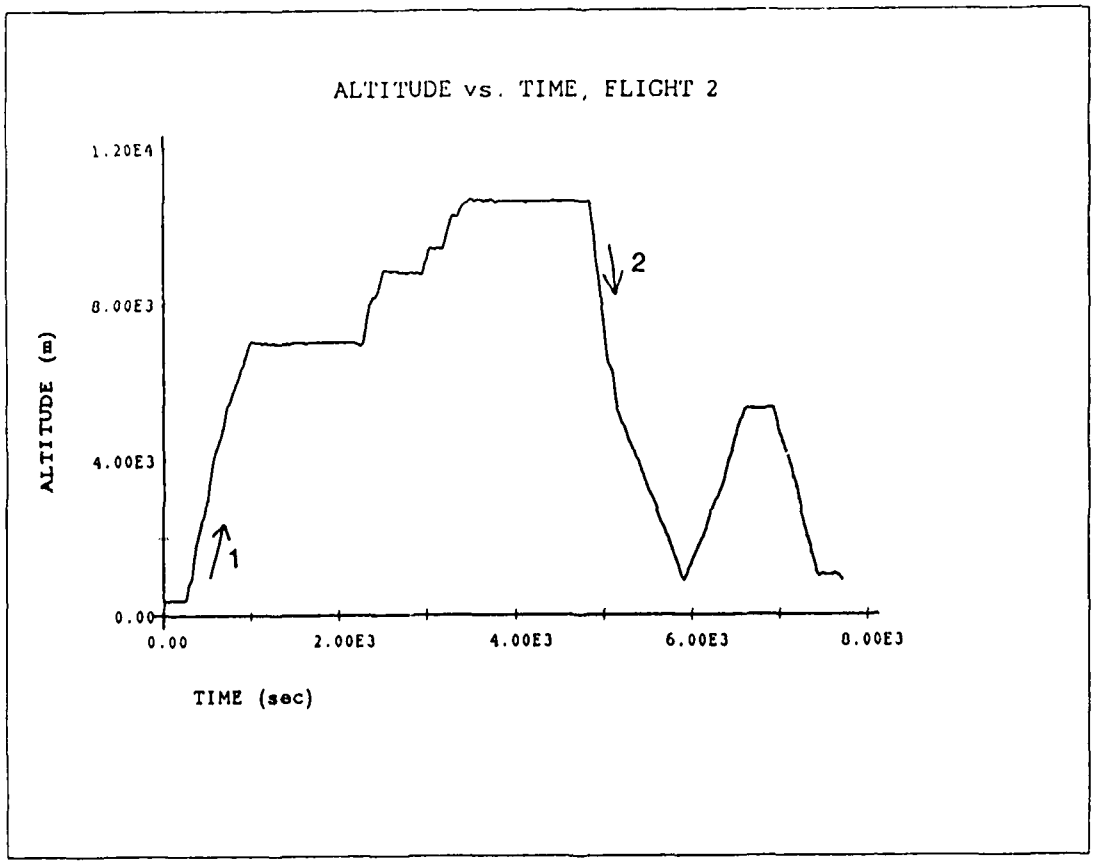


Fig. 8. Sabreliner altitude versus time for the second flight. Profile 1 is from surface to 10.6 km; profile 2 is from 10.6 km through first descent to 0.9 km.

# III. RESULTS

## A. Flight 1 (1215-1455 CDT)

Analysis of the trace gas data from the first flight shows strong evidence of vertical transport of pollution out of the PBL over large areas, possible in-situ photochemical production of ozone and strong vertical mixing throughout the troposphere.

### 1. Vertical Profiles

Vertical profiles of $O_3$ and CO concentration for the ascending (profile 1) and descending (profile 2) legs are presented in Figures 9 and 10. The profiles for flights 1 and 2 show high levels of $O_3$ and CO, and substantial variability when compared to remote clean air profiles (e.g. Danielson et al., 1987; Fishman et al., 1987) measured over the Pacific Ocean. Temperature and dew point are also plotted against altitude in Figures 11 and 12.

The intense solar radiation of early afternoon in summer produced conditions favorable for convection, making it hard to determine the exact height of the PBL. For this research, the PBL will be assumed to be capped by the slight temperature inversion at about 1.9 km on both ascent and descent, which best matches the first drop in CO that appears in profile 2 (this definition of PBL includes layers that could also be called the mixed and cumulus layers). Maximum CO concentration in the PBL was almost 160 ppb, which is relatively clean compared to the average nonurban surface value for that latitude of

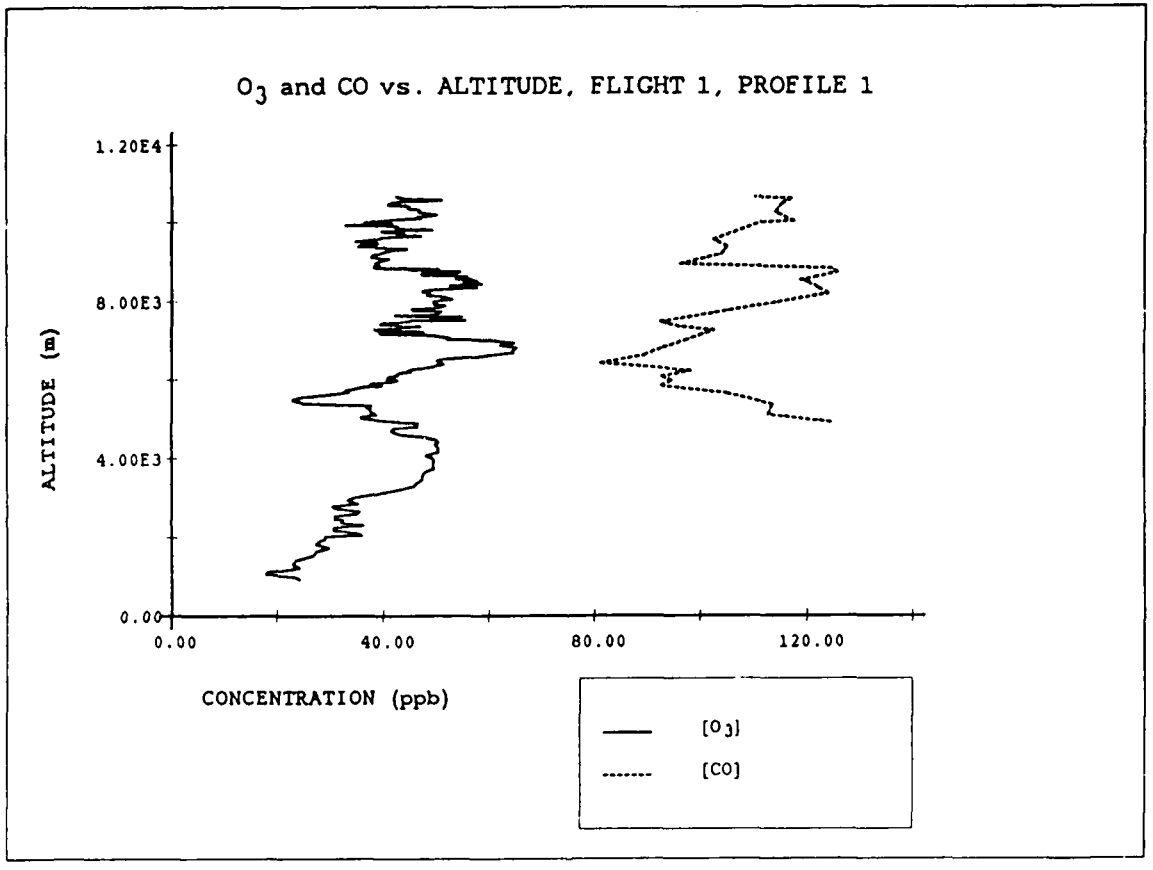


Fig. 9. Vertical profile of $O_3$ and CO for the ascending leg, flight 1. $O_3$ is 7 sec. data. CO is 30 sec. averages with breaks where the instrument was in background mode. Constant altitude data are not included.

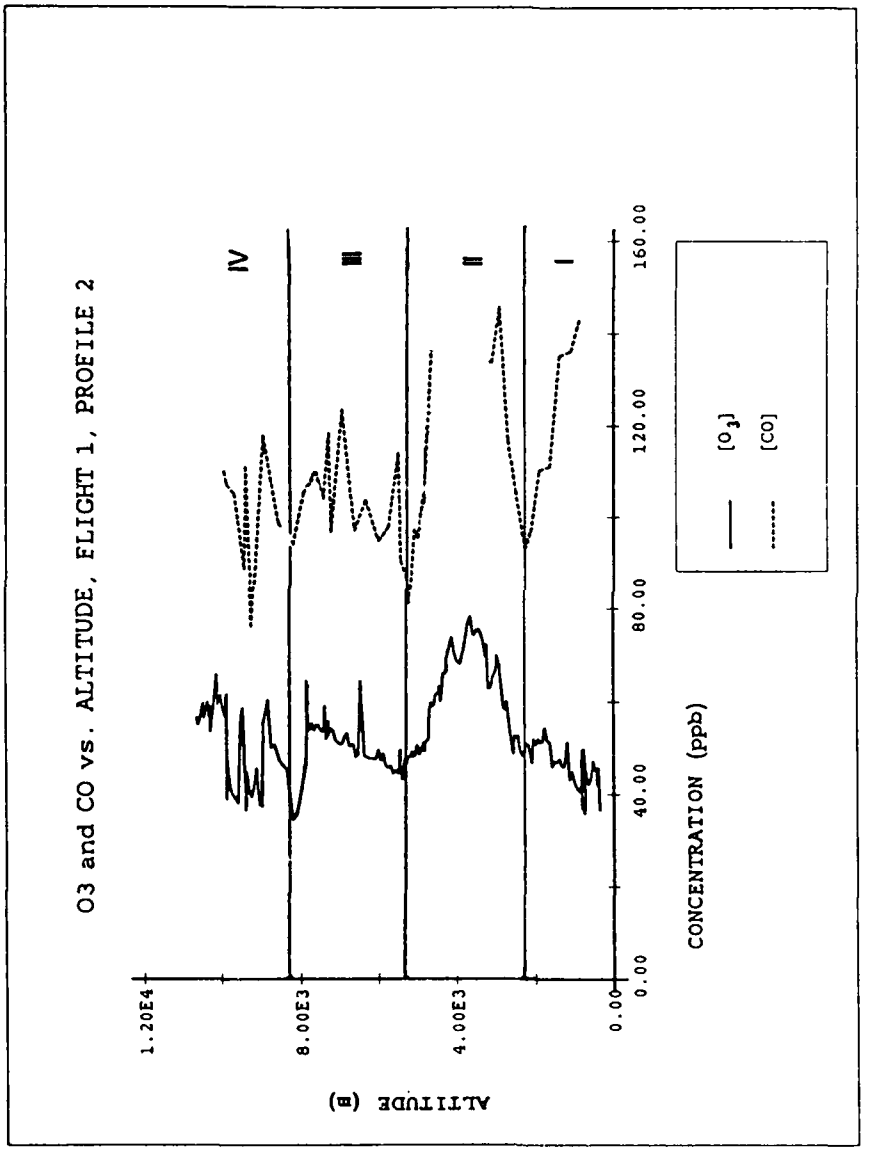


Fig. 10. Like Figure 9, vertical profile of $O_3$ and CO for the descending leg, flight 1. Layers are used in later calculations.

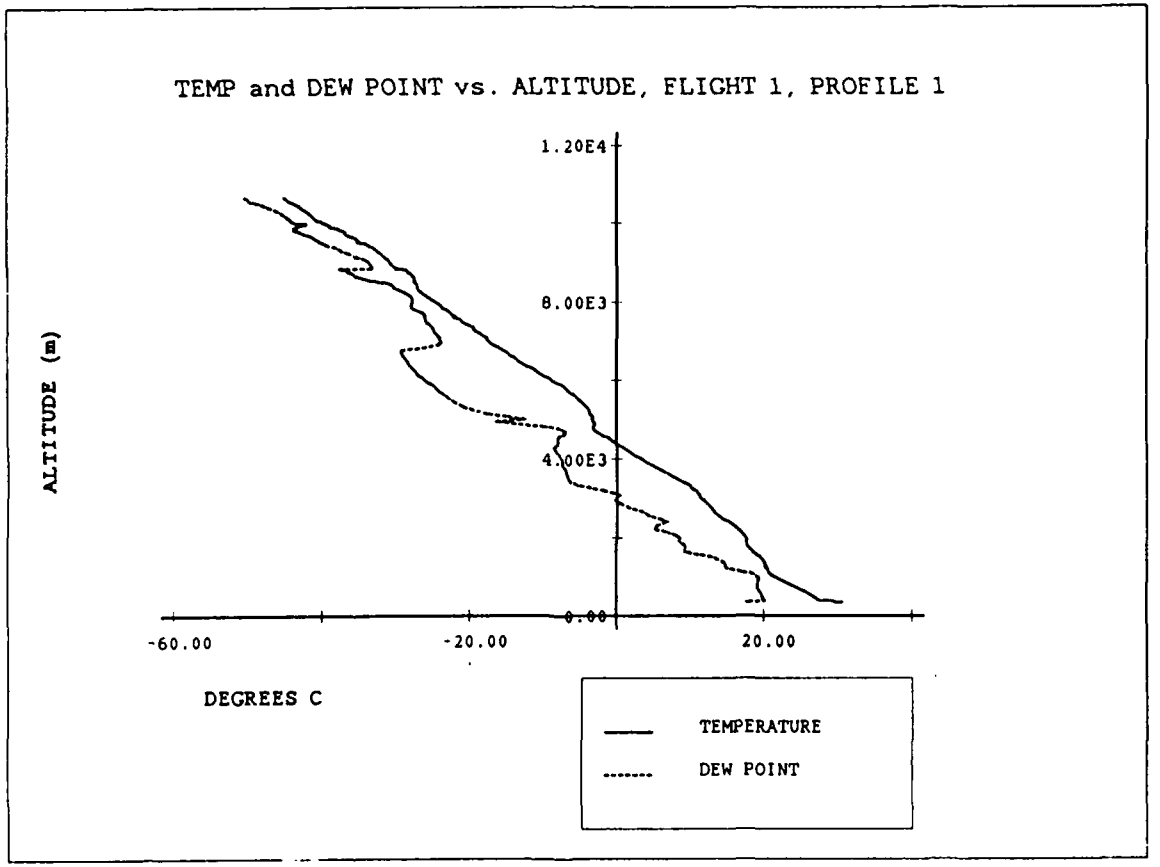


Fig. 11. Vertical profile of temperature and dew point for the ascending leg, flight 1. Constant altitude data are not included.

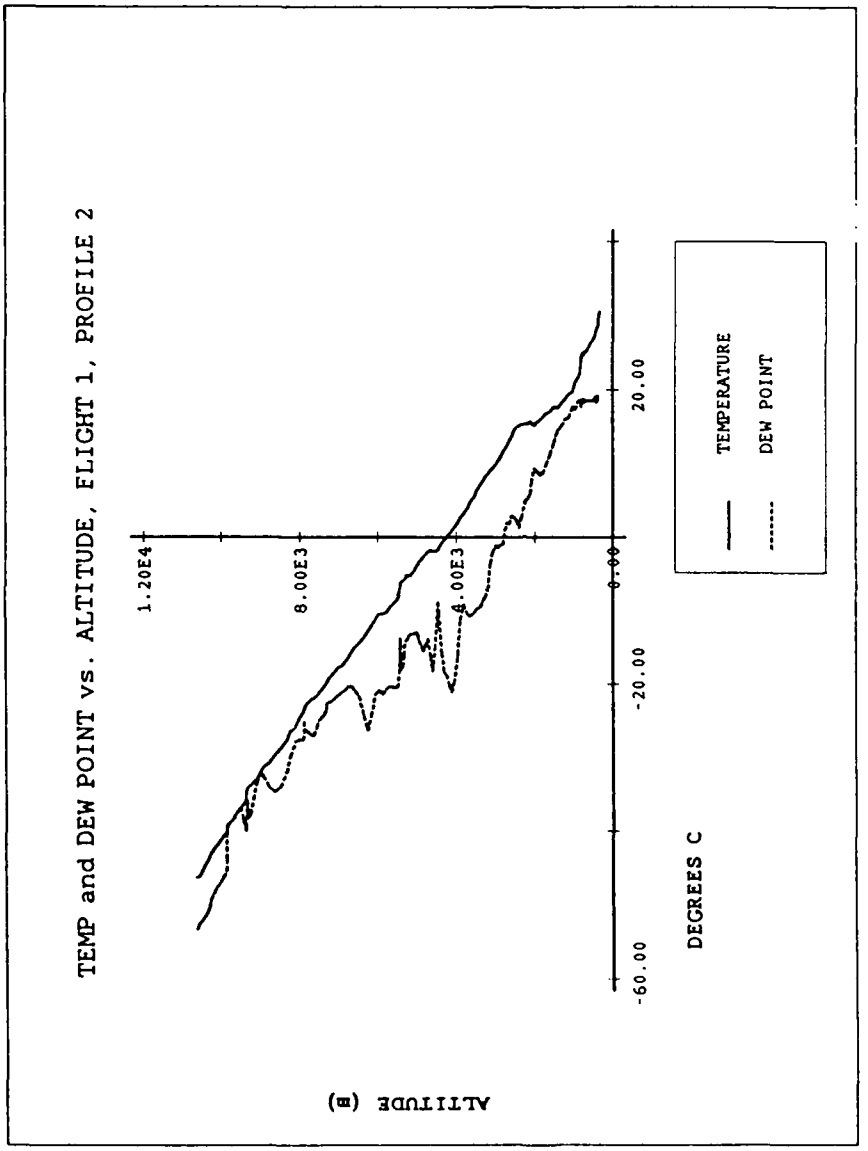


Fig. 12. Like Figure 11, vertical profile of temperature and dew point for the descending leg, flight 1.

about 200 ppb reported by Logan et al. 1981. $O_3$ concentration was fairly low in the PBL, ranging from about 20 ppb at take off to 40 ppb at the end of the flight.

A surprising feature is the strong increase in both $O_3$ and CO above the PBL up to about 5 km; this feature was also evident during the late afternoon flight. Concentration of both species began to decrease right above the temperature inversion at 4.7 km in profile 1 and 4.5 km in profile 2. The CO concentrations in this layer approached PBL values, $O_3$ concentrations were much higher than in the PBL, and the air was dry. Unfortunately, no NO data are available for this layer. Figure 13 shows odd nitrogen concentrations versus altitude measured for the entire flight. $NO_x$ values up to 1400 ppt were recorded in the PBL, but a secondary maximum (approximately 600 ppt) was evident just below 4 km. This indicates more than enough $NO_x$ to catalyze the photochemical production of $O_3$ (Crutzen and Gidel, 1983, estimate that greater than 5 ppt NO at the surface and 20 ppt aloft will result in $O_3$ production).

The $O_3$ concentrations, higher than those in the PBL, may have resulted from a combination of in-situ production and venting of PBL air. With a PBL 1.9 km thick, even with a dry deposition velocity of 1 cm/s (Droppo, 1985), the $O_3$ lifetime in the PBL would be more than 2 days; $O_3$ could escape the PBL before being lost at the surface. Alternatively, this layer could be the original PBL that was lifted and displaced by convection-induced downdrafts of cleaner mid-tropospheric air (e.g., Lyons et al., 1986a). It is important to note that

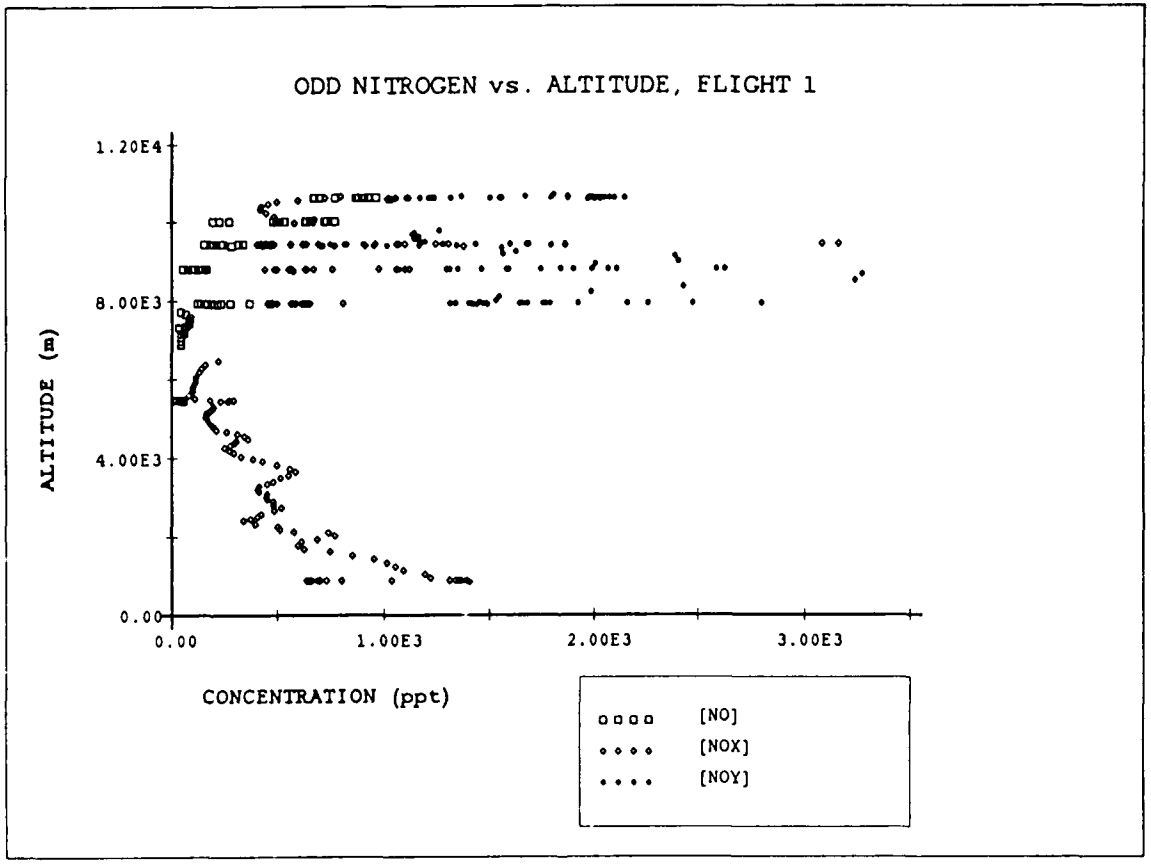


Fig. 13. Vertical profile of NO, $NO_x$, and $NO_y$ for the first flight; includes all data.

one can determine air of PBL origin (by its elevated CO, $NO_x$, NMHC or $H_2O$), but as the PBL was not sampled over large areas beneath the flight track and upstream, one can make no conclusions about the original geographic location of the PBL air. The air may have traveled long horizontal distances.

Above this layer, the vertical profiles indicate widely varying concentrations of $O_3$, CO and nitrogen oxides. There is some layering present, but it is not consistent between the ascending and descending profiles. The large variations in the horizontal probably resulted from the strong convective mixing on this day. These results are consistent with those of Lyons et al. (1986) and Lyons and Calby (1986), who describe large vertical transport by mesoscale systems ranging in size from single airmass thunderstorms to large (up to 2500 km wide) convective complexes. The Sabreliner was often in cloud at these higher altitudes (Figure 5). Analysis of radar reports, satellite imagery (Figure 14), and nose and side camera films indicate some regions of active convection and some regions of outflow cirrus. At 1700 GMT, National Weather Service (NWS) radar at Little Rock, Arkansas indicated a line of showers, about 50 km wide, extending east-northeast to west-southwest through central Arkansas. The showers were dissipating, but some remained as the Sabreliner crossed the line around 1800 GMT. Winds from the west aloft extended the cirrus outflow to the east. In general, above 5 km CO ranged from about 70 to 140 ppb, $O_3$ was between 30 and 70 ppb, and odd nitrogen showed large variation.

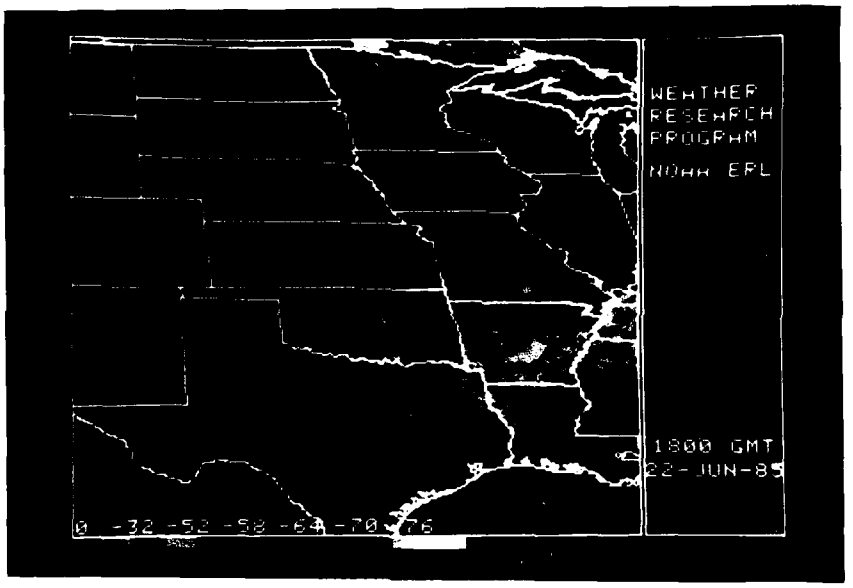


Fig. 14. GOES IR satellite imagery, 1801 GMT (1301 CDT), 22 June 1985.

## 2. Time Series

The Sabreliner spent a significant amount of time at constant altitude, so time series were prepared for the trace gas species. Figure 15 shows $O_3$ and CO versus time; Figures 16 and 17 show odd nitrogen and dew point depression versus time (dew point depression is the difference between the dew point and ambient temperature; it shows good variation at all altitudes, unlike other moisture parameters such as mixing ratio which drop to near zero out of the PBL). Only constant altitude data are included in these figures.

A very interesting feature shows up in the time series at 7000 sec (1418 CDT), lasting for a little more than 6 minutes (about 60 km of flight trajectory). The CO climbed to 150 ppb and the $O_3$ to its highest value of the flight, 93 ppb. The Sabreliner was in level flight at 5.5 km in clear air returning to Oklahoma City. The air was very dry, as indicated by the large dew point depression. Satellite imagery at 1800 GMT and 1900 GMT (Figures 14 and 18) show the convection was rapidly deteriorating in Arkansas and western Oklahoma before this time. The nose camera film showed nothing visibly different about the air as the concentrations increased; uniform cumulus cells topping below flight level were scattered in the foreground. Unfortunately, the nitrogen oxide detector was being calibrated at this time. The origin of this air is discussed later as Event 1.

Another surprising feature is seen in the time series for the odd nitrogen data. The NO concentrations generally run well below 500 ppt, except at 2500 sec. and 3200 sec. (about 1804 and 1816 GMT) where

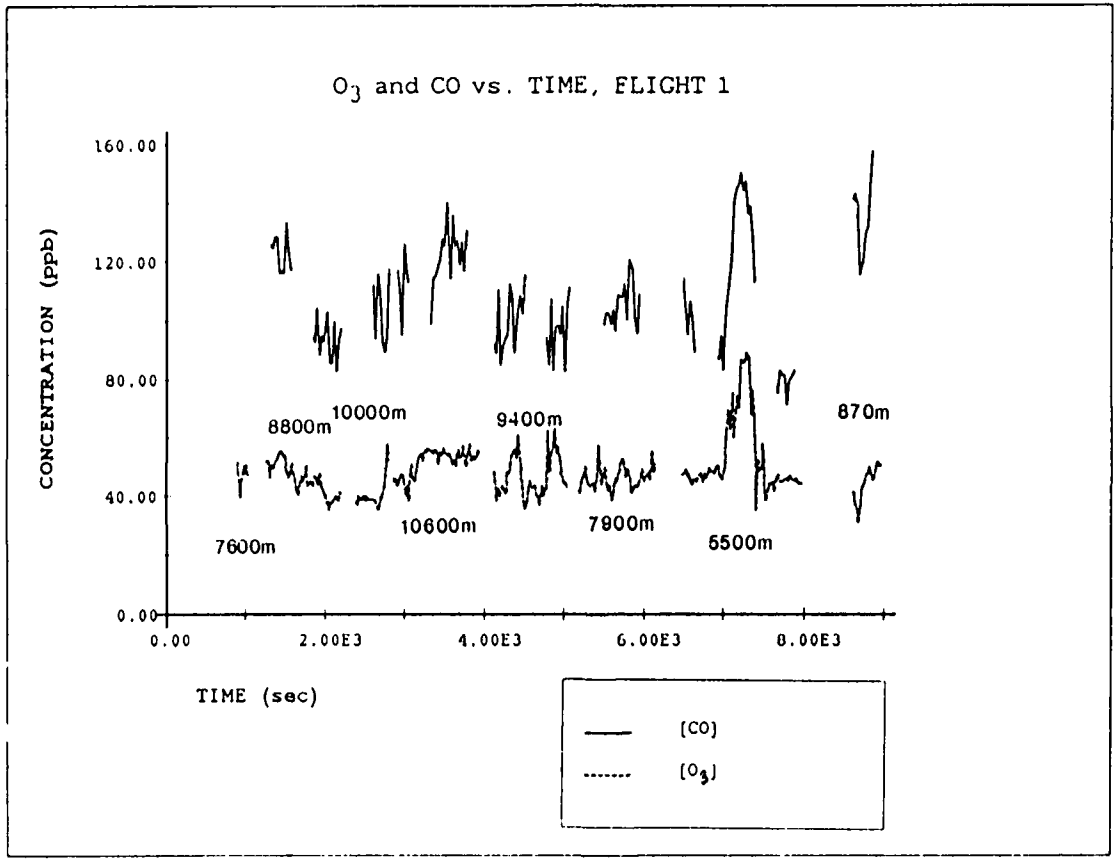


Fig. 15. Time series of $O_3$ and CO, flight 1, for segments of level flight (at altitudes labelled). 0 sec. corresponds to takeoff time. Four 7-second $O_3$ values were averaged to obtain 28 sec. data to show approximately the same amount of variation as the 30 sec. CO data.

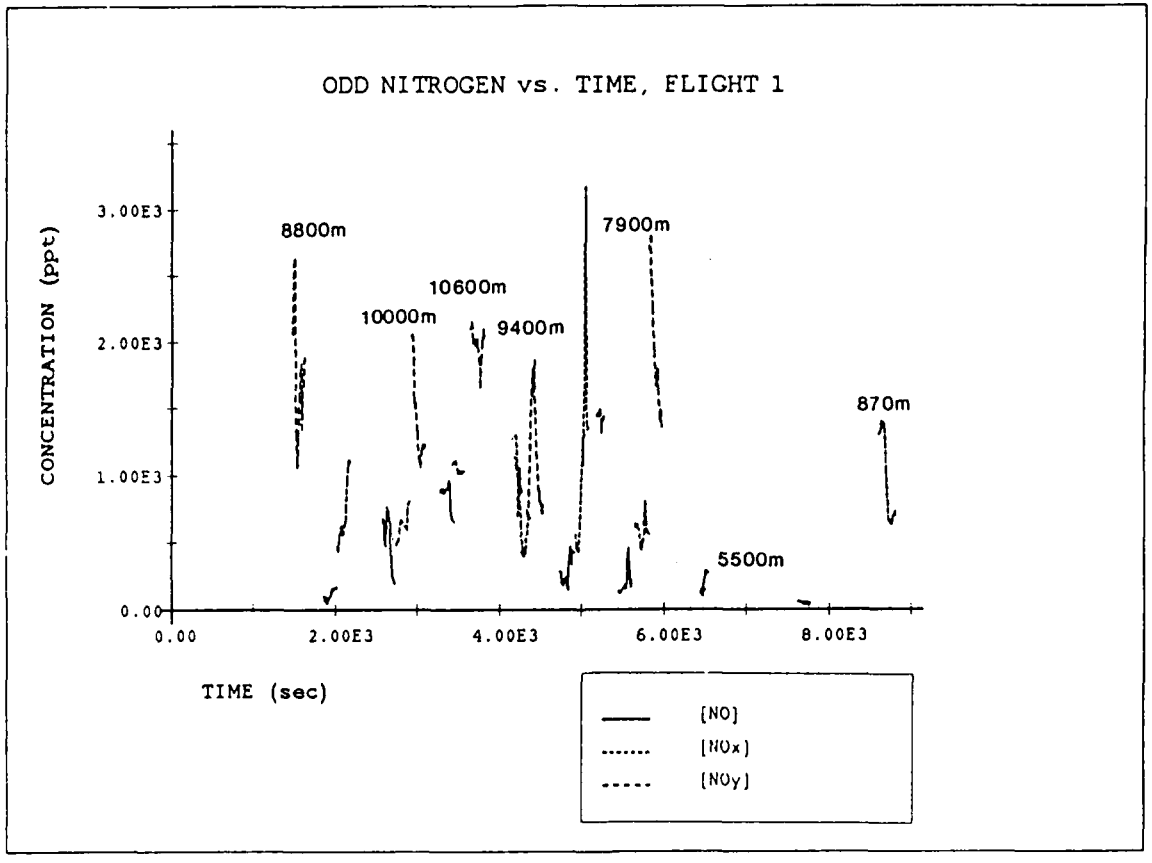


Fig. 16. Like Figure 15, time series for NO, $NO_x$ and $NO_y$ (10 sec. data) for segments of level flight, flight 1.

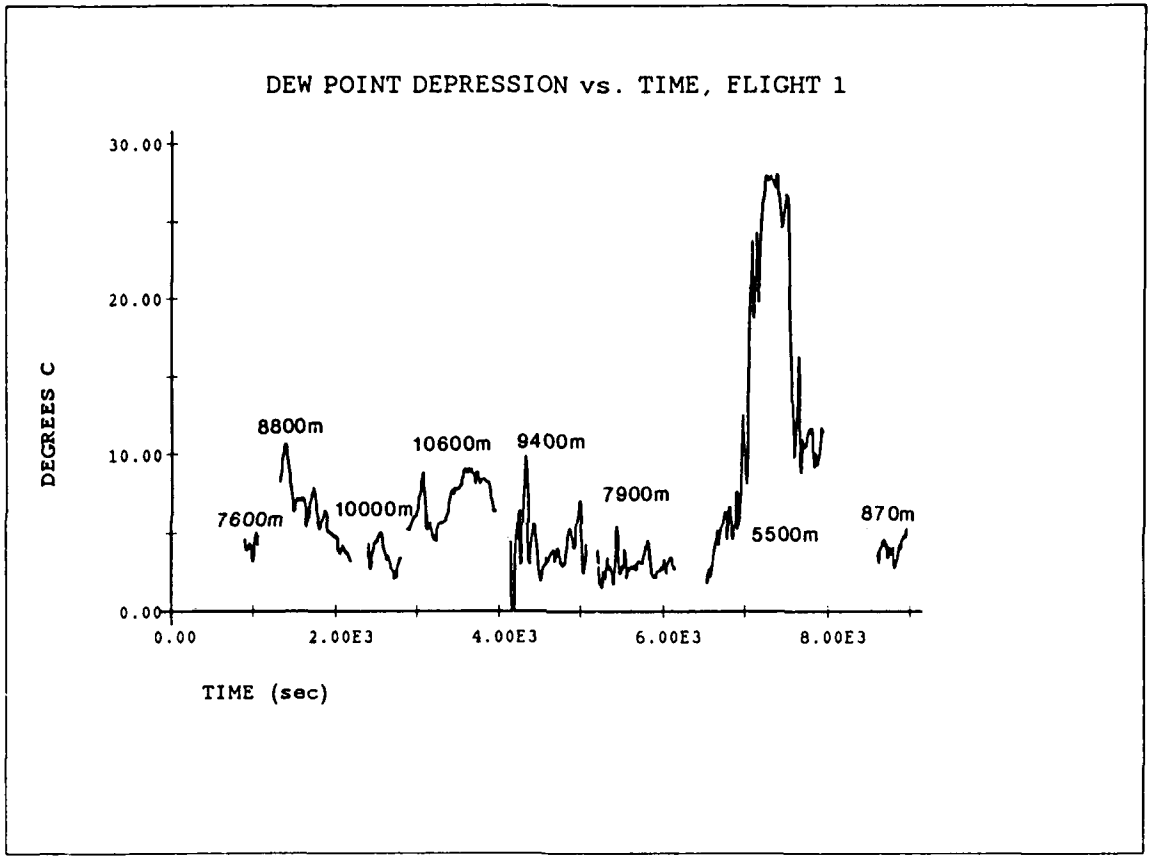


Fig. 17. Like Figure 15, time series of dew point depression (10 sec. data) for segments of level flight, flight 1.

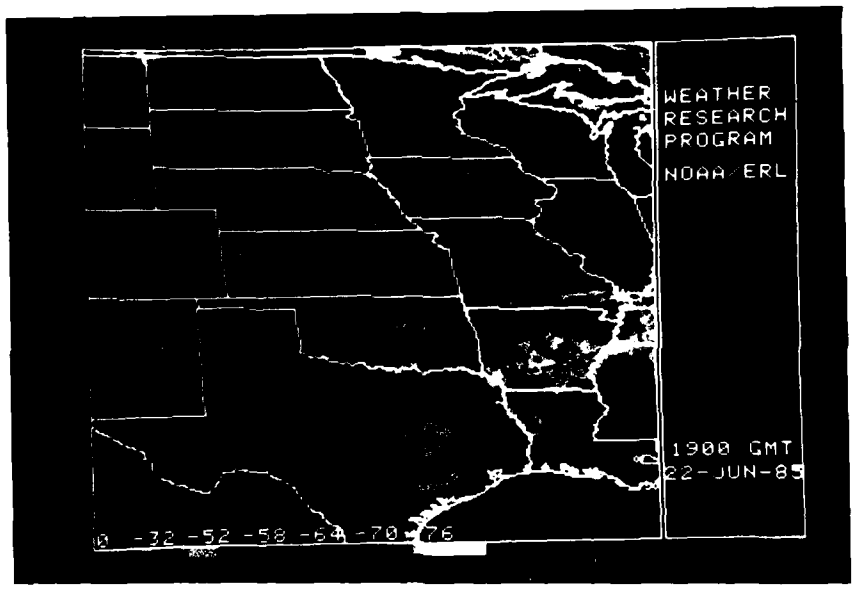


**Fig. 18. GOES IR satellite imagery, 1900 GMT (1400 CDT), 22 June 1985.**

they reach 760 and 960 ppt. The Sabreliner was in cloud at both times at flight levels above 10 km. The $NO_x$ and $NO_y$ values were not unusually high. The Sabreliner may have encountered NO from a recent lightning strike or a fresh aircraft plume; NO would be high, but may not have yet been substantially converted to $NO_2$ or the other $NO_y$ species. Radar screen images (plan position indicator, 250 nm) from the NWS at Little Rock at 1802 GMT confirm the existence of a line of thunderstorms over Little Rock extending east-northeast through west-southwest, moving southward. Winds aloft carried the cirrus shield toward the east. It is impossible to quantify exactly the distance from a cell because the Sabreliner was almost directly over Little Rock at 1804 GMT, and the antenna was set at an elevation angle which passed the radar beam under the convection close to the radar site. Nevertheless, lightning is possible within the anvil itself, even after the thunderstorm cell has decayed (US Air Force, 1982). Chameides et al. (1987) also attributed elevated NO concentrations above 500 ppt to lightning while near a storm anvil.

B. Flight 2 (17:02-19:12 CDT)

The mission flown in the afternoon, under fair skies, is an excellent contrast to the case described above. Analysis of trace gas data showed distinct layers immediately above the PBL and in the upper troposphere, with pollutant concentrations nearly as high as in the PBL.

## 1. Vertical Profiles

Satellite imagery near takeoff time (Figure 19) shows no remaining organized cumulus convection in eastern Oklahoma. Vertical profiles for $O_3$ and CO, which include all data, are shown in Figure 20. Except for small fluctuations, the $O_3$ profiles overlay each other quite well. Where CO data exist more than once at an altitude, the values are also quite similar. The atmosphere appears quite homogeneous in the horizontal and layered in the vertical. Therefore, it is reasonable to consider $O_3$ and CO profiles obtained by averaging all available data to 0.1 km layers (Figure 21). The temperature and dew point profiles (Figures 22 and 23) helped delineate the layers found in Figure 21. Odd nitrogen profiles are shown in Figure 24.

In the PBL (I) below 2.1 km, CO and $NO_x$ decrease with height and $O_3$ increases with height. CO ranges from about 130 to 175 ppb, $NO_x$ from about 500 to 1500 ppt, and $O_3$ from about 20 to 50 ppb. Above the PBL up to about 4.1 km is once again a very dirty layer (II) characterized by drier conditions, and $O_3$, CO and $NO_x$ concentrations reaching as high as 75 ppb, 172ppb, and 1200 ppt, respectively. Nose and side camera footage show scattered fair weather cumulus mostly to about 2 km, but some penetrating the lowest temperature inversion and reaching about 4.5 km. The dirty air in layer II may be the top of an old PBL that was well-mixed to the higher level and cut off from the surface when a new inversion formed near the surface at night (Vukovich et al., 1985). Concentrations in layer II could then increase from in-situ photochemical $O_3$ production and further venting of PBL air.

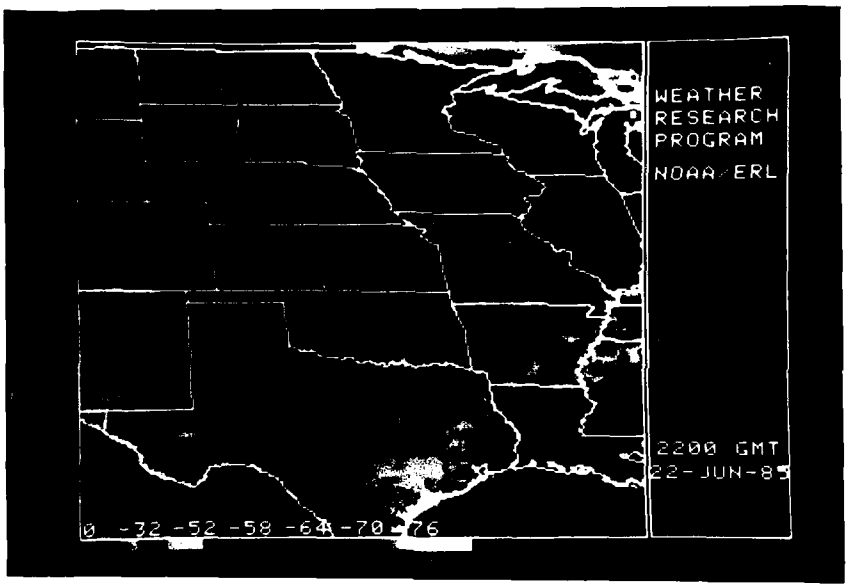


**Fig. 19. GOES IR satellite imagery, 2200 GMT (1700 CDT), 22 June 1985.**

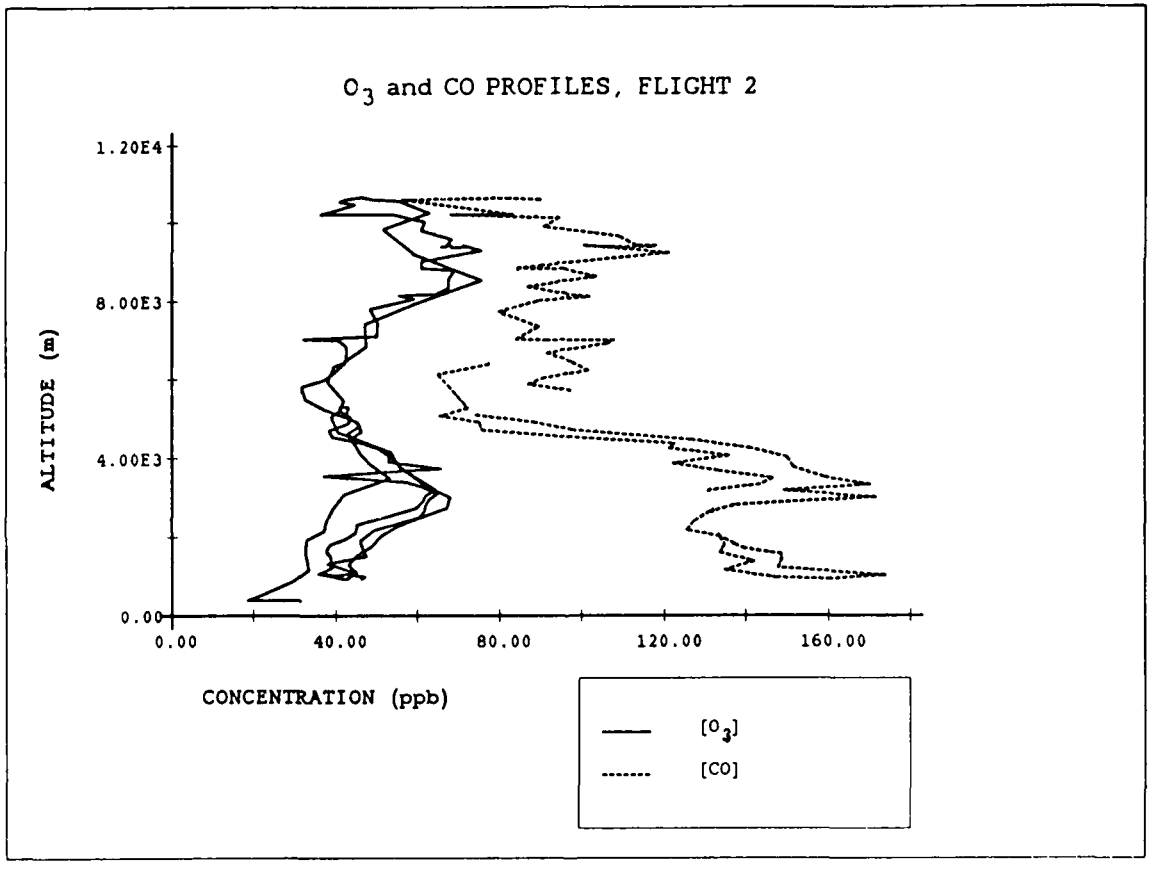


Fig. 20. Vertical profiles of $O_3$ and CO, all data, flight 2. $O_3$ is 7 sec. data. CO is 30 sec. averages, with breaks in data where the instrument was in background mode. Constant altitude data are not included.

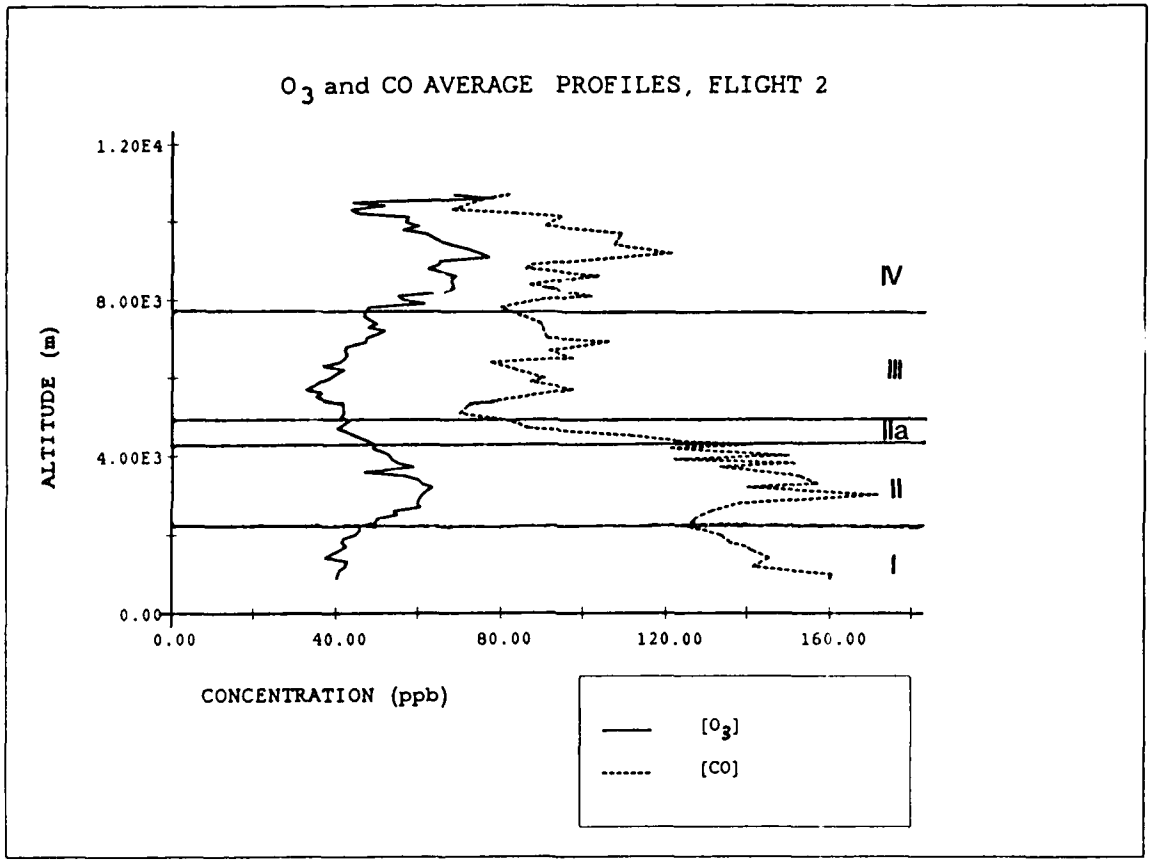


Fig. 21. Average vertical profiles of $O_3$ and CO for flight 2. All available data were averaged in 0.1 km layers.

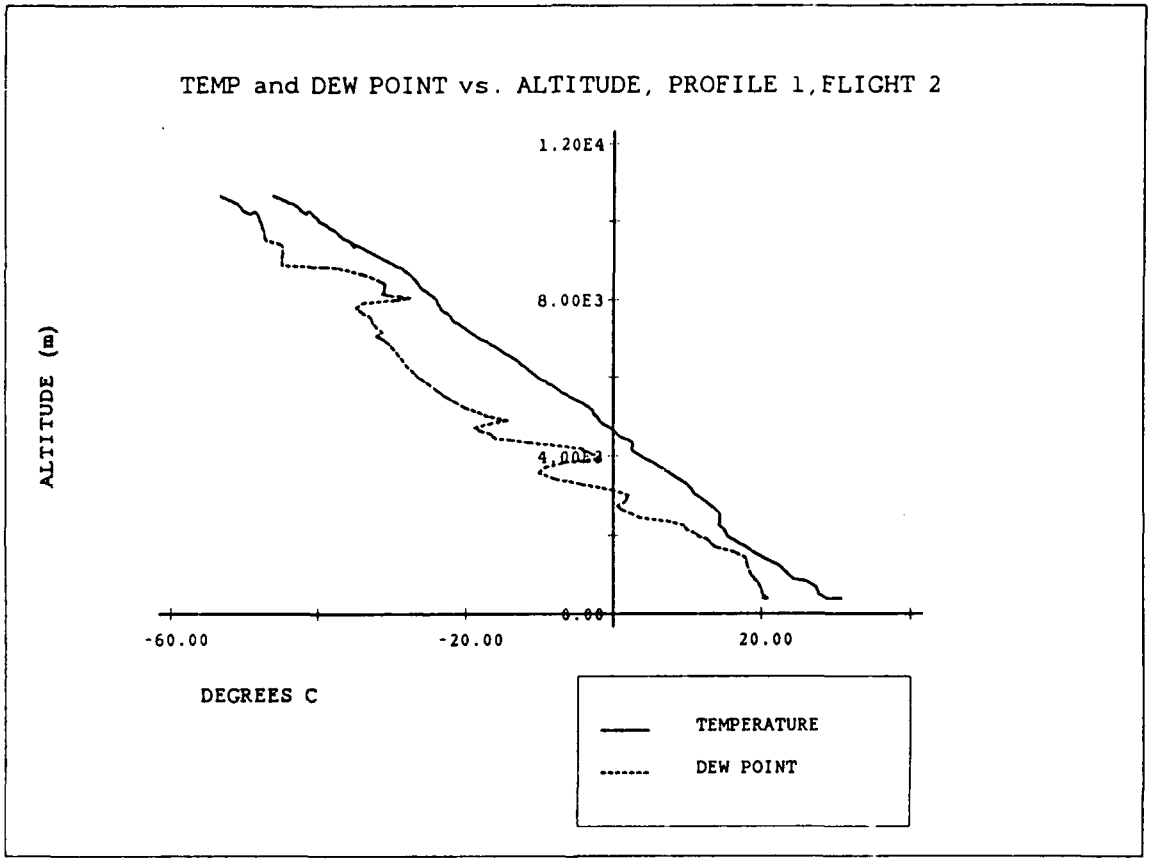


Fig. 22. Vertical profile of temperature and dew point for the ascending leg, flight 2. Constant altitude data are not included.

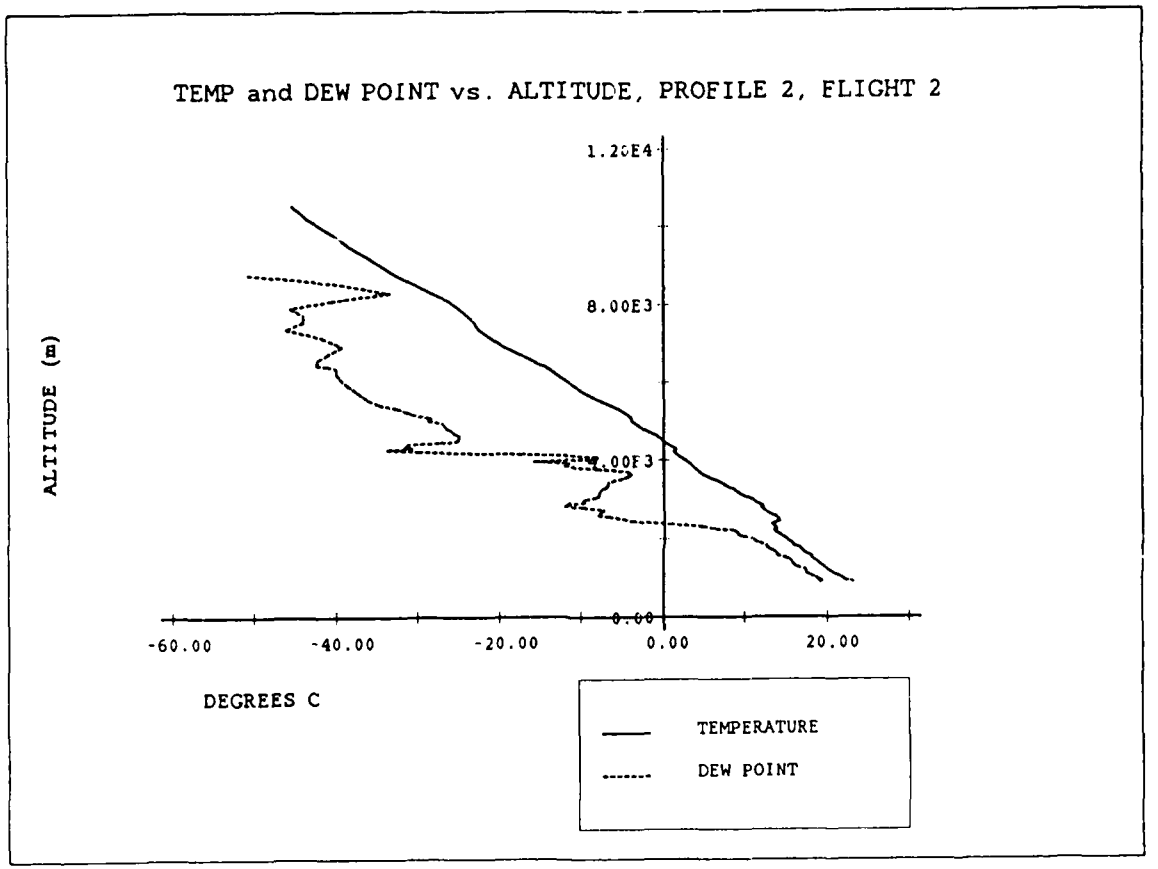


Fig. 23. Like Figure 22, vertical profile of temperature and dew point for the descending leg, flight 2.

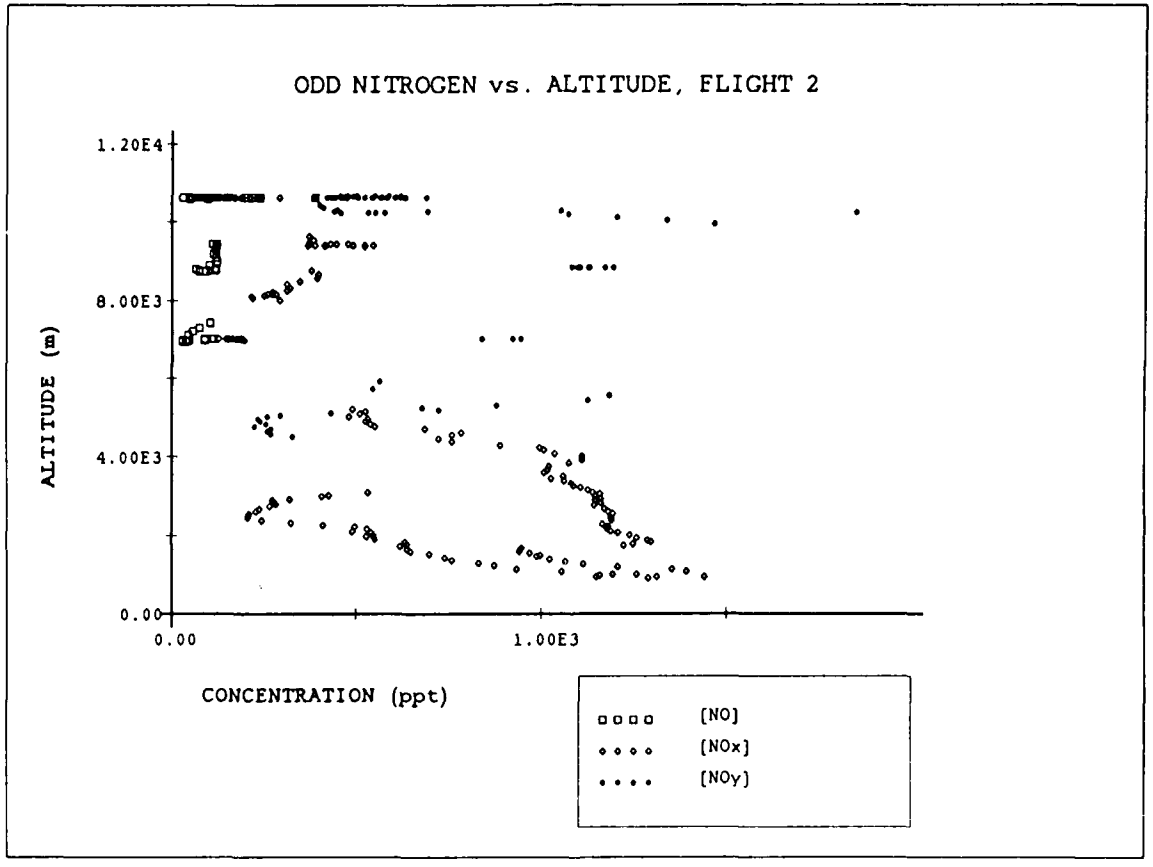


Fig. 24. Vertical profile of NO, $NO_x$, and $NO_y$ for flight 2; includes all data.

Stull (1984) parameterized cumulus clouds as forced clouds and active clouds. Forced clouds resemble the shallow clouds described above, which only mix air within the PBL and provide conditions for aqueous-phase chemical reactions. Active clouds, such as the taller clouds mentioned above which penetrate the temperature inversion capping the PBL, vent PBL air to higher altitudes and increase pollutant levels aloft. Layer II is also topped by a temperature inversion beginning at about 4.2 km, which prevents further upward mixing and allows pollutant levels to accumulate. Pollutant levels decrease rapidly above the inversion up to 4.6 km (layer IIa).

Layer III, between 4.6 and 7.8 km, contains the cleanest air sampled during the mission. The layer was dry and none of the fair weather cumulus were seen penetrating to this layer. CO concentrations were as low as 65 ppb, $O_3$ concentrations decreased to 28 ppb (the only lower concentration was found near the surface), and $NO_x$ concentrations were mostly less than 500 ppt. Above 7.8 km (layer IV), pollutant levels were variable but generally higher than in layer III. $O_3$ concentrations exceeded 70 ppb (as high as 141 ppb in level flight at 10.6 km), CO concentrations reached 120 ppb, and $NO_x$ concentrations were variable. Back (constant level) trajectory analysis of the air at 9.1 km (30,000 ft) placed this air in north Texas and northeast New Mexico when convection was occurring in that region. As summertime convection to the upper troposphere is common, and probably carries $O_3$ or $O_3$ precursors to the upper troposphere, we might expect this layer of the atmosphere to show elevated concen-

trations of CO and $NO_x$.

## 2. Time Series

Time series were prepared for data from this flight as well, again including data only from level flight segments. Figure 25 shows CO and $O_3$, Figure 26 shows odd nitrogen, and Figure 27 shows dew point depression versus time.

The most striking feature of all the time series is in the $O_3$ time series at 10.6 km (beginning at 3400 sec.). The first jump in $O_3$, from less than 40 ppb to more than 110 ppb, was such a surprise that the onboard scientist requested the pilot fly a loop and reinvestigate the same location again. The existence of the feature was confirmed, and $O_3$ concentration this time reached more than 140 ppb. Although at other levels many smaller peaks in $O_3$ match peaks in CO (1500 sec., 2300 sec., 2900 sec., and 6200 sec.), these two peaks at 10.6 km are independent of changes in CO. The origin of this sharp gradient is discussed later as Event 2.

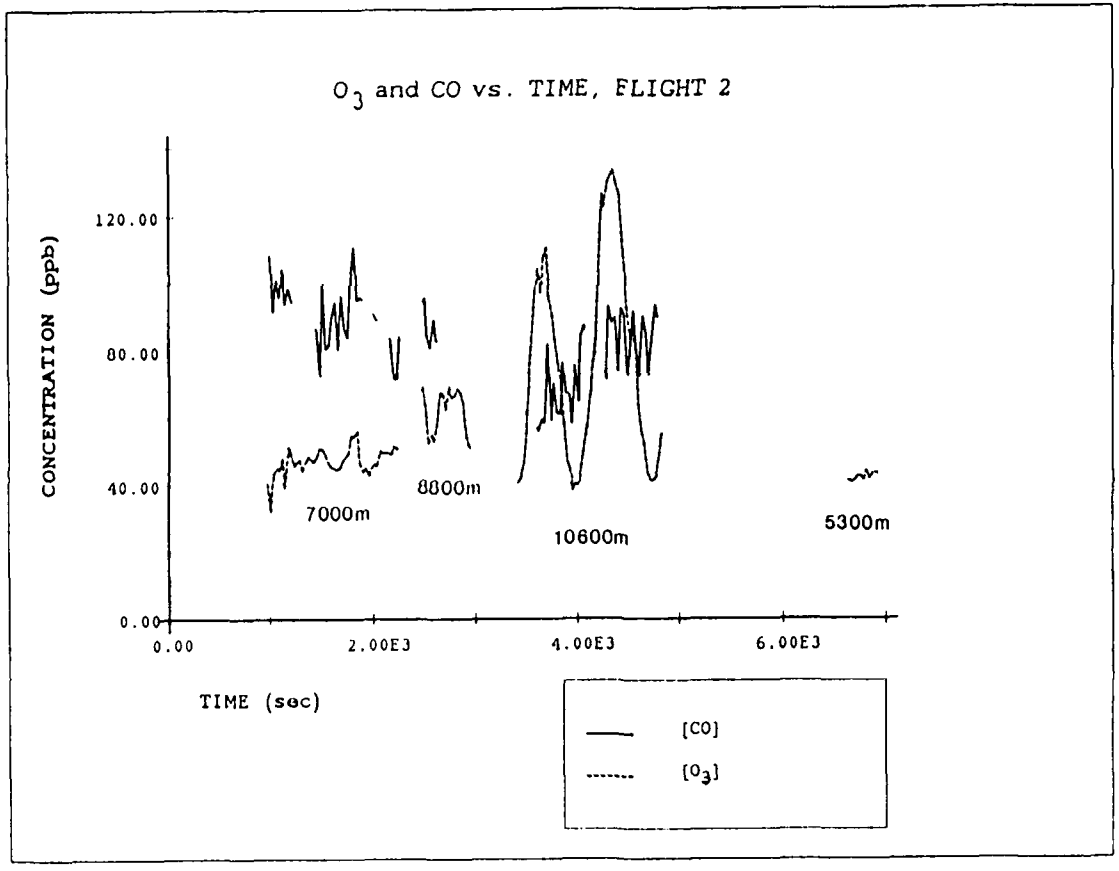


Fig. 25. Time series of $O_3$ and CO, flight 2, for segments of level flight (at altitudes labelled). 0 sec. corresponds to takeoff time. Four 7-second $O_3$ values were averaged to obtain 28 sec. data to show approximately the same amount of variation as the 30 sec. CO data.

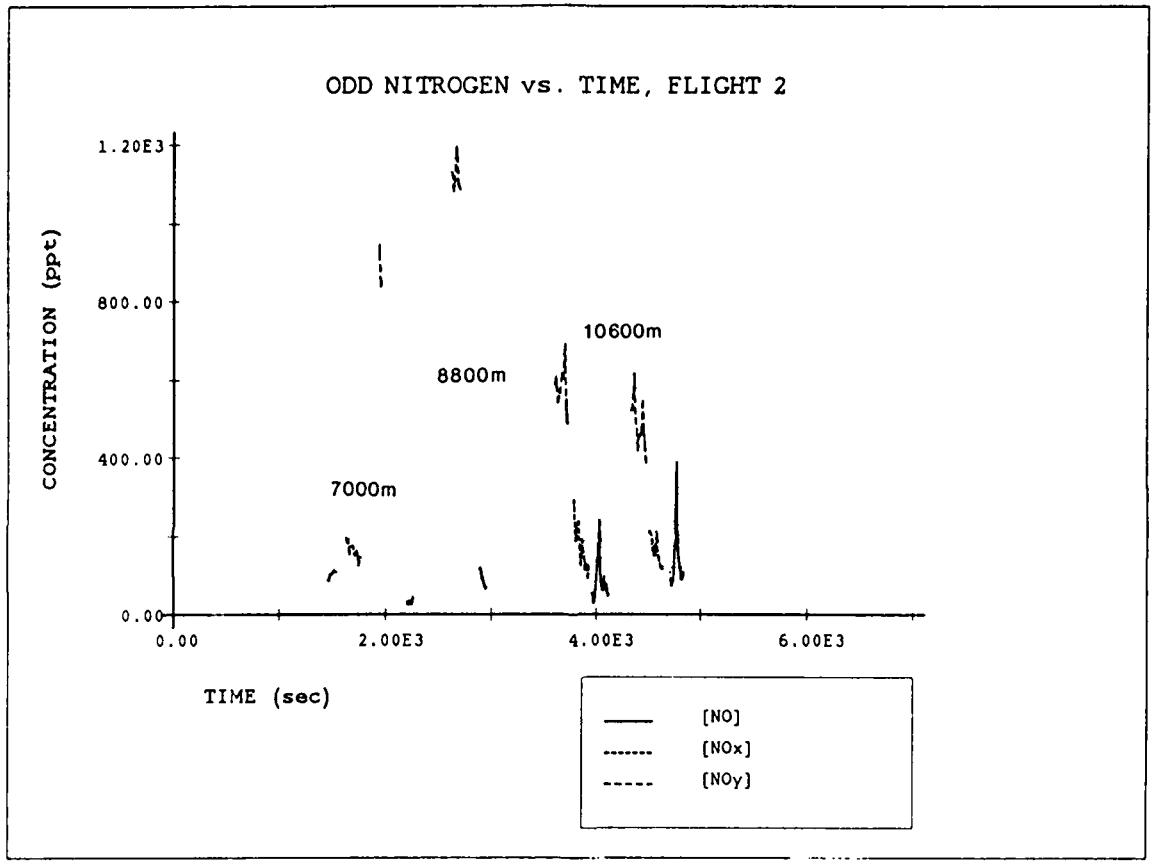


Fig. 26. Like Figure 15, time series for NO, $NO_x$ and $NO_y$ (10 sec. data) for segments of level flight, flight 2.

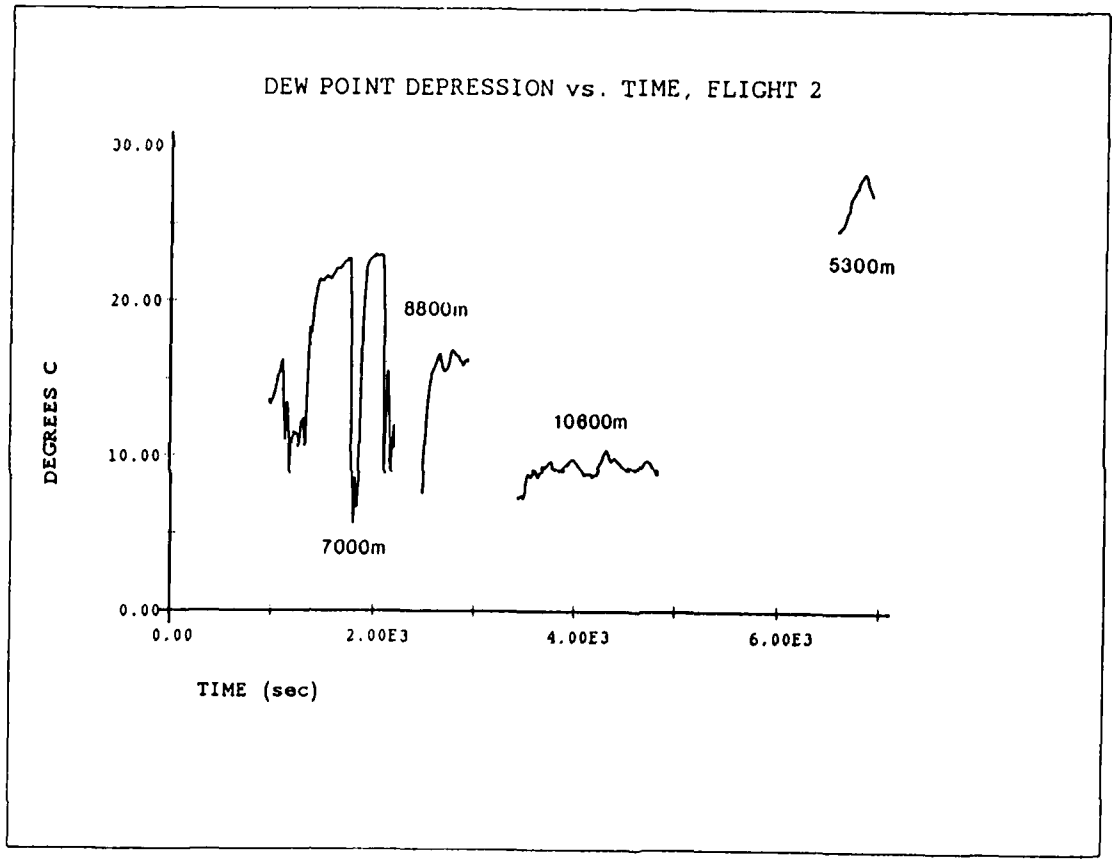


Fig. 27. Like Figure 15, time series of dew point depression (10 sec. data) for segments of level flight, flight 2.

# IV. DISCUSSION

## 1. Correlations - Flight 1

To understand further the relative importance of tropospheric $O_3$ production versus stratospheric injection, one must make a more detailed assessment of the correlations between the various trace gas species (Fishman et al. 1987). One way to do this is to prepare scatter diagrams between the individual measurements of two species, but this technique has problems. The average or background profiles of the different species vary significantly and will overpower the small-scale correlations between the species. For example, water vapor tends to be very large in the PBL and becomes very small above; CO is also largest in the PBL, but shows a much more gradual decrease aloft; $O_3$ tends to be large in the upper troposphere due to its stratospheric source; and odd nitrogen tends to show two maxima, in the PBL and upper troposphere. In addition, it is very hard to prove a statistical correlation between the two species because each measurement in a time series is not independent and the degrees of freedom are much less than the total number of measurements.

The effective degrees of freedom (N') for a time series can be computed according to the following formula:

$$N' = N / (1 + r_1 r_1' + r_2 r_2' + r_3 r_3' + r_4 r_4' + r_5 r_5')$$

N is the number of data pairs; $r_1$, $r_2$, etc. are autocorrelation coefficients for the first variable in the series; $r_1'$,$r_2'$, etc. are autocorrelation coefficients for the second variable in the series (Quenouille, 1952). Prior to computing the correlations, the data

were paired and times were matched by taking the species with the longest measurement interval and averaging all measurements of the second species occurring more than half in the longer time interval (for example, a CO 30 second average could match up with as many as five $O_3$ 7 second averages). The correlations using all data from the flight are listed in Table 1. Most of the regression coefficients are small, and all are statistically insignificant using the effective degrees of freedom. However, scatter plots of some subsets suggest relationships between the trace gases.

CO versus $O_3$ (Figure 28) appear positively correlated with a slope of 0.24 (units ppb/ppb), but this relationship is not quite significant at the 95 percent confidence level ($R^2$ of 0.199). The small number of points with high CO and $O_3$ suggest there may be at least places where the two species are well correlated. Including only data above the PBL (Figure 29) eliminates the known level of poor correlation right at the surface (where $O_3$ has its shortest lifetime due to removal by dry deposition and chemical reactions). This analysis produces a slope of 0.32, and $R^2$ of 0.312 meets the significance test at the 95 percent confidence level (Panofsky and Brier, 1968).

Most scatter plots between $O_3$ and the various nitrogen oxides do not demonstrate clear relationships because odd nitrogen concentrations show large variations; the more interesting plots are shown here. Figure 30 shows $NO_x$ versus $O_3$; linear regression produces only a weak, non-significant slope of -0.0081 (units ppb/ppt, $R^2$ of 0.130),

TABLE 1

OVERALL TRACE GAS CORRELATIONS

| Flight 1 | Slope | $R^2$ | Significant slope |
|---|---|---|---|
| $CO/O_3$ | 0.24 | 0.20 | no |
| CO/DPdep.* | 0.095 | 0.080 | no |
| $O_3$/DPdep. | 0.60 | 0.0074 | no |
| $NO/O_3$ | 0.0060 | 0.062 | no |
| $NO_x/O_3$ | -0.0081 | 0.13 | no |
| $NO_y/O_3$ | 0.0044 | 0.12 | no |
| Flight 2 | | | |
| $CO/O_3$ | -0.17 | 0.050 | no |
| CO/DPdep. | -0.041 | 0.029 | no |
| $O_3$/DPdep. | -0.34 | 0.016 | no |
| $NO/O_3$ | -0.0028 | 0.00028 | no |
| $NO_x/O_3$ | -0.012 | 0.17 | no |
| $NO_y/O_3$ | -0.016 | 0.026 | no |

*DPdep - dew point depression

All correlations were calculated using all data from the flight.

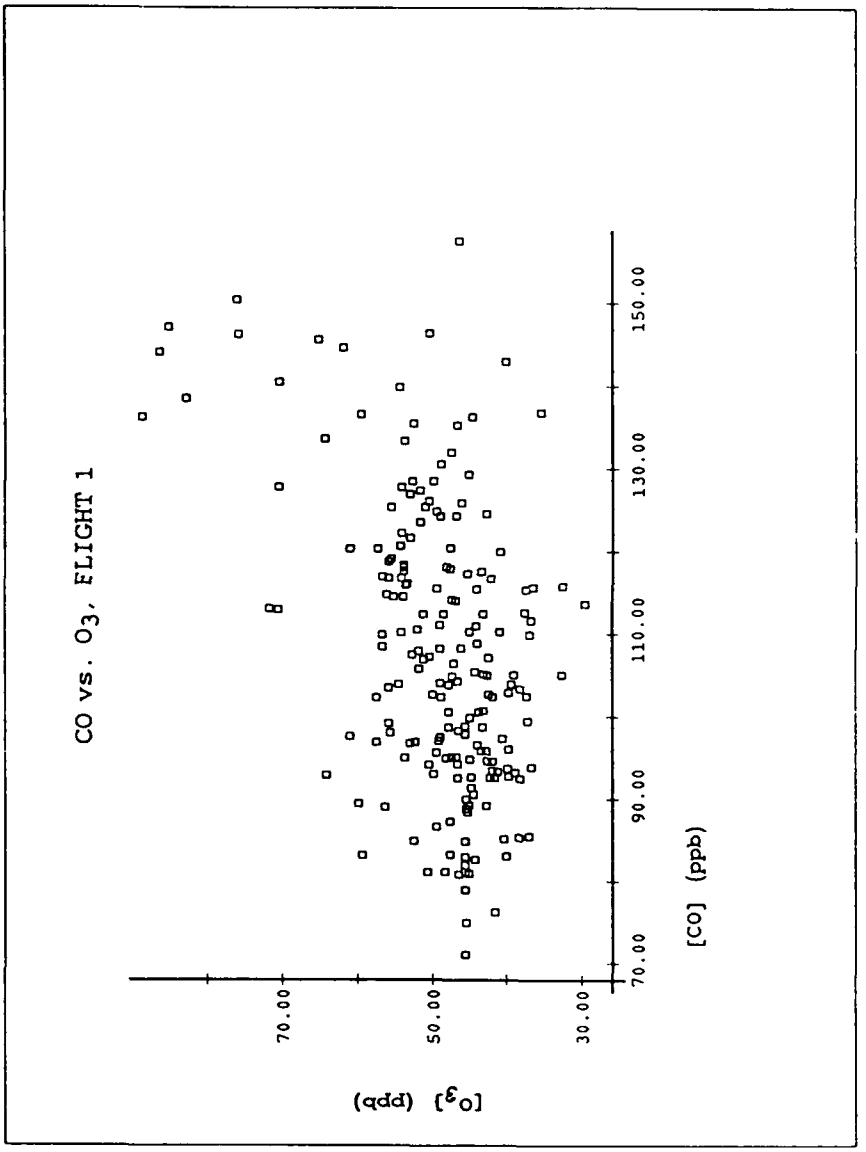


Fig. 28. Scatter plot of CO versus $O_3$, all data, flight 1.

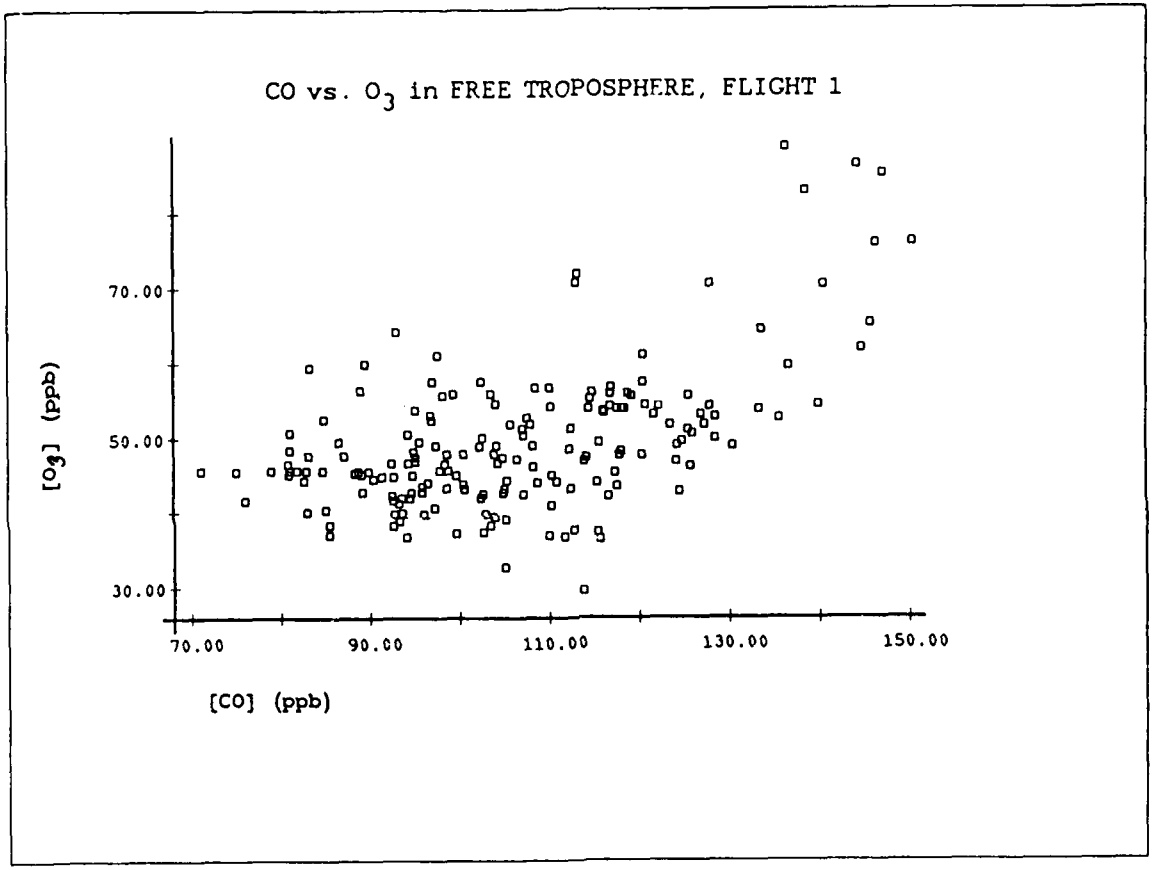


Fig. 29. Scatter plot of CO versus $O_3$ in the free troposphere, flight 1. Same as Figure 27, but without data in the boundary layer, below 1.9 km.

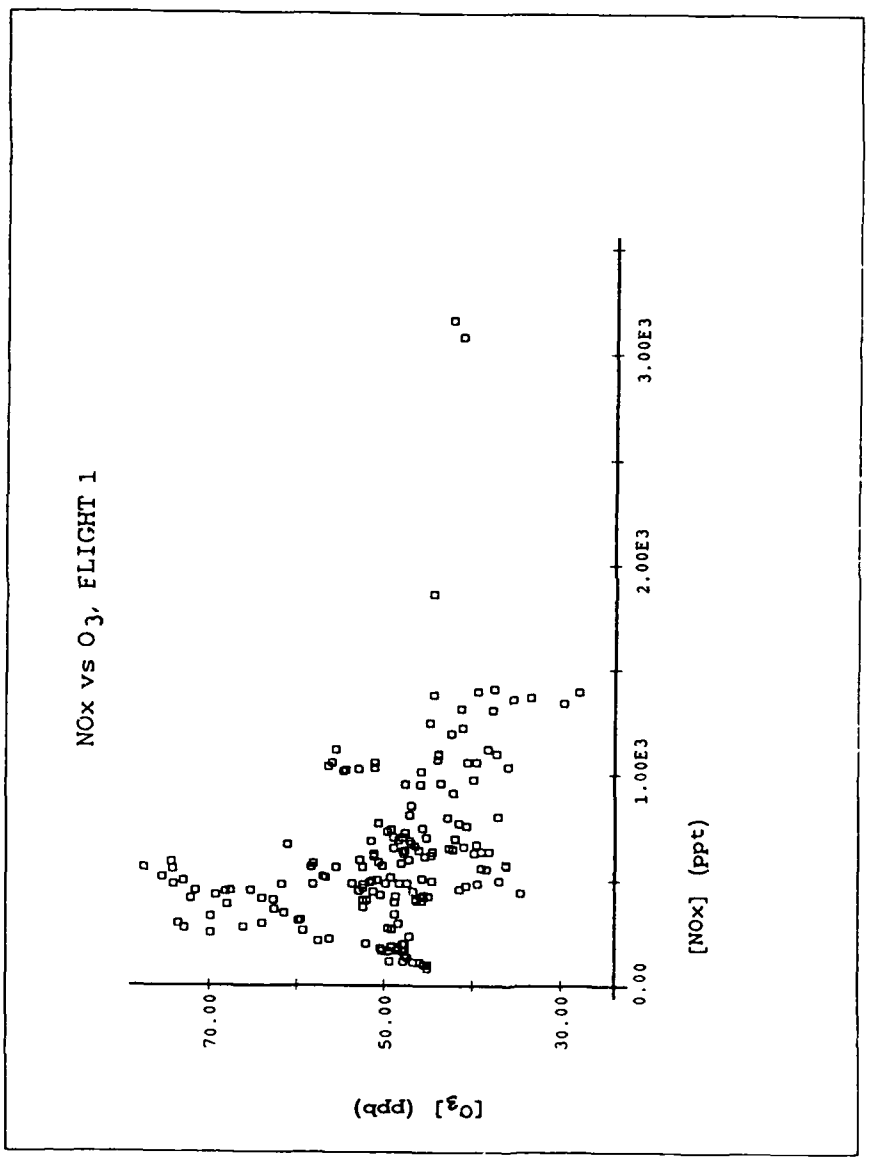


Fig. 30. Scatter plot of $NO_x$ versus $O_3$, all data, flight 1.

some regions of the graph show positive correlation and some appear to show slightly negative or no correlation. Some of the positively correlated points are between about 3 and 4.2 km in the inferred upper boundary layer, and the negatively correlated points include points from the PBL and upper troposphere. Figure 31, a plot of NO versus $O_3$, shows no correlation, which is not surprising as the points to the far right include the NO spikes possibly attributable to lightning and the points with low NO are near the instrument detection limit. The plot of $NO_y$ versus $O_3$ (Figure 32) includes only data above 7.9 km; the slight positive slope of 0.0044 (still insignificant with $R^2$ just 0.122) is expected because both have sources in the polluted PBL air and the stratosphere. These results differ from those reported by Pickering (1987), for another fair weather case from the same project, where $NO_x$ and $O_3$ were always positively correlated.

Fishman and Seiler (1983) devised a technique to quantitatively measure the correlation between the vertical fine structure of two species and overcome the problem of their average profile variations overshadowing their small scale variations. Looking at concurrent vertical profiles of two species, they find the best linear fit line for each profile and subtract this line from the data averaged for every 0.1 km layer. They then compute the product of the residuals at each level where data exist for both species. The species are positively correlated in layers in which the product is positive, and negatively correlated where the product is negative. The products are summed over the entire profile and normalized by dividing by the sum of the products of the absolute values of the residuals. If this

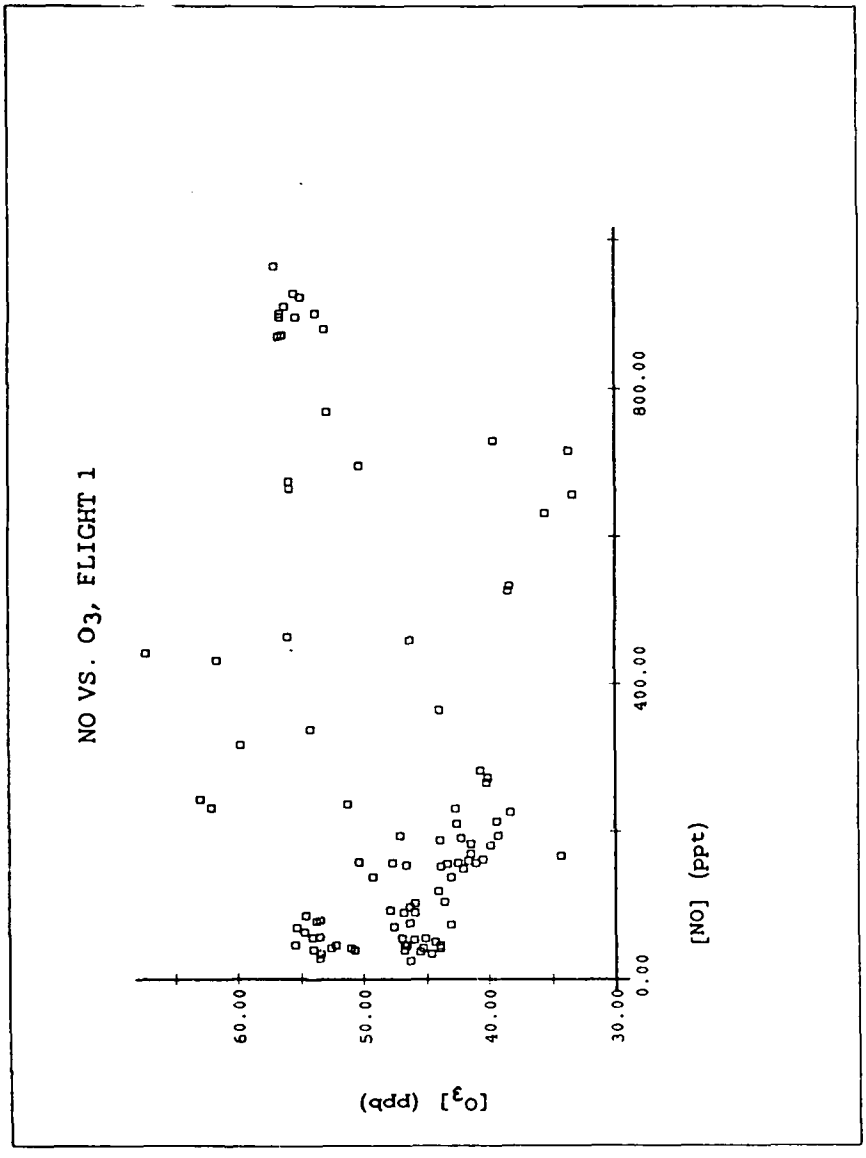


Fig. 31. Scatter plot of NO versus $O_3$, all data, flight 1.

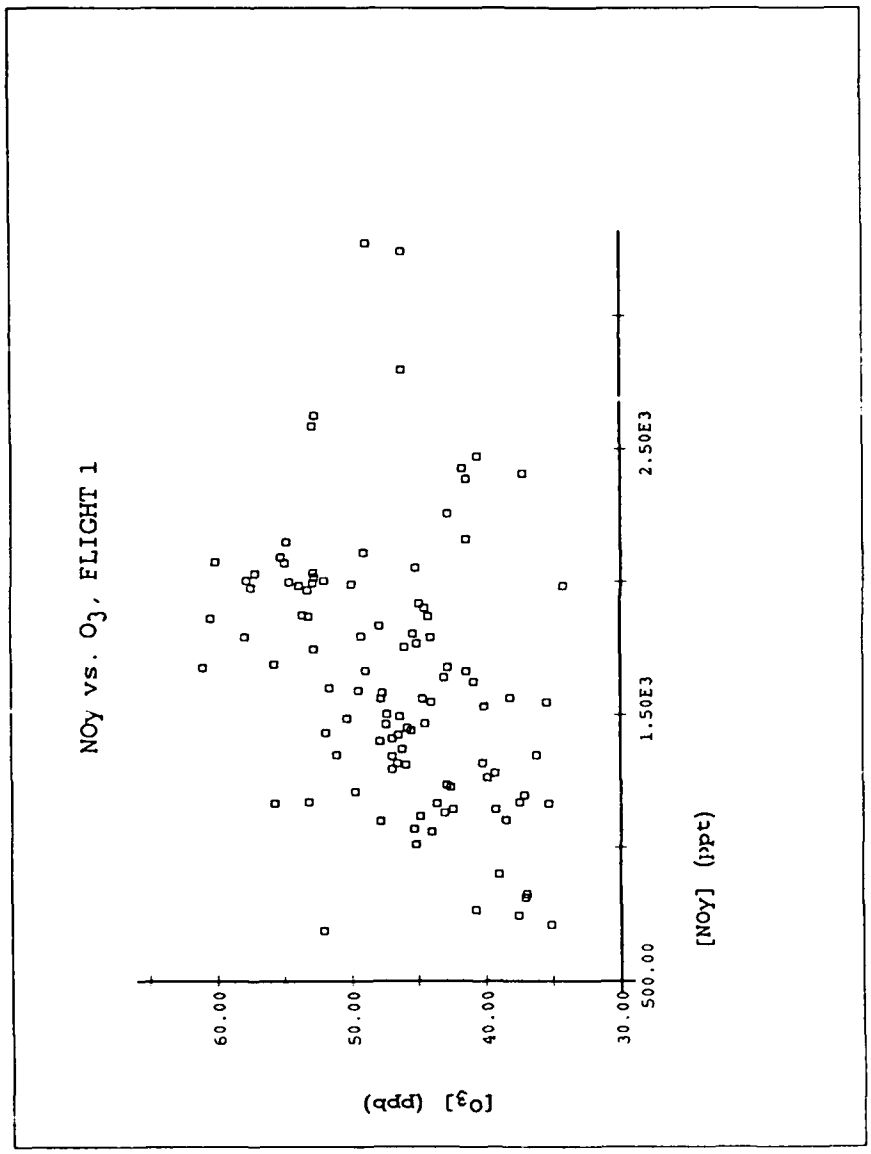


Fig. 32. Scatter plot of $NO_y$ versus $O_3$, all data, flight 1.

quotient is + 1.0 the species are perfectly positively correlated, if - 1.0 they are perfectly negatively correlated; a result of zero indicates no correlation. Fishman and Seiler (1983) arbitrarily chose 0.5 to be the lower limit for significance, and conclude that bands of elevated $O_3$ and CO, which occur with elevated $NO_x$ and NMHCs, strongly suggest in-situ photochemical production of $O_3$ is occurring.

Fine structure correlations from this data set, between the possible combinations of $O_3$, CO and dew point temperature (TD) for each profile, are summarized in Table 2. The profiles are averaged for each 0.1 km layer and the best fit lines are shown in Figures 33 and 34. The net positive slope for CO in profile 1, although it only contains data above about 5 km, suggests how strongly the recent convection disturbed the troposphere. Correlations with TD must be interpreted with caution because the lag time of dew pointer on the Sabreliner varies significantly with altitude, and is different for ascent and descent. The lyman alpha instrument has almost immediate response, but the values of all moisture parameters except TD drop off so abruptly above the PBL that they cannot be reasonably fit by a linear regression. (An algorithm exists from NCAR to calculate absolute humidity from the lyman alpha voltages, but the correction of the lag is not perfect as the algorithm uses absolute humidity measured with the dew pointer to calibrate the voltages.) In addition, in this case there was a sink for water vapor in the recent rainfall (2.2 cm in the 24 hours ending at 23 June 1200 GMT was reported at Little Rock, for example) which explains how CO could be poorly correlated with TD when both have sources in the PBL.

TABLE 2

TRACE GAS PROFILE CORRELATIONS

| Flight | Profile | Species | Normalized Corr. Coeff. | Significant |
|---|---|---|---|---|
| 1 | 1 | $O_3$/CO | 0.0022 | no |
| 1 | 1 | CO/TD | 0.29 | no |
| 1 | 1 | $O_3$/TD | -0.26 | no |
| 1 | 2 | $O_3$/CO | 0.48 | no |
| 1 | 2 | CO/TD | 0.063 | no |
| 1 | 2 | $O_3$/TD | -0.82 | yes |
| 2 | All | $O_3$/CO | 0.90 | yes |
| 2 | All | CO/TD | 0.61 | yes |
| 2 | All | $O_3$/TD | 0.35 | no |

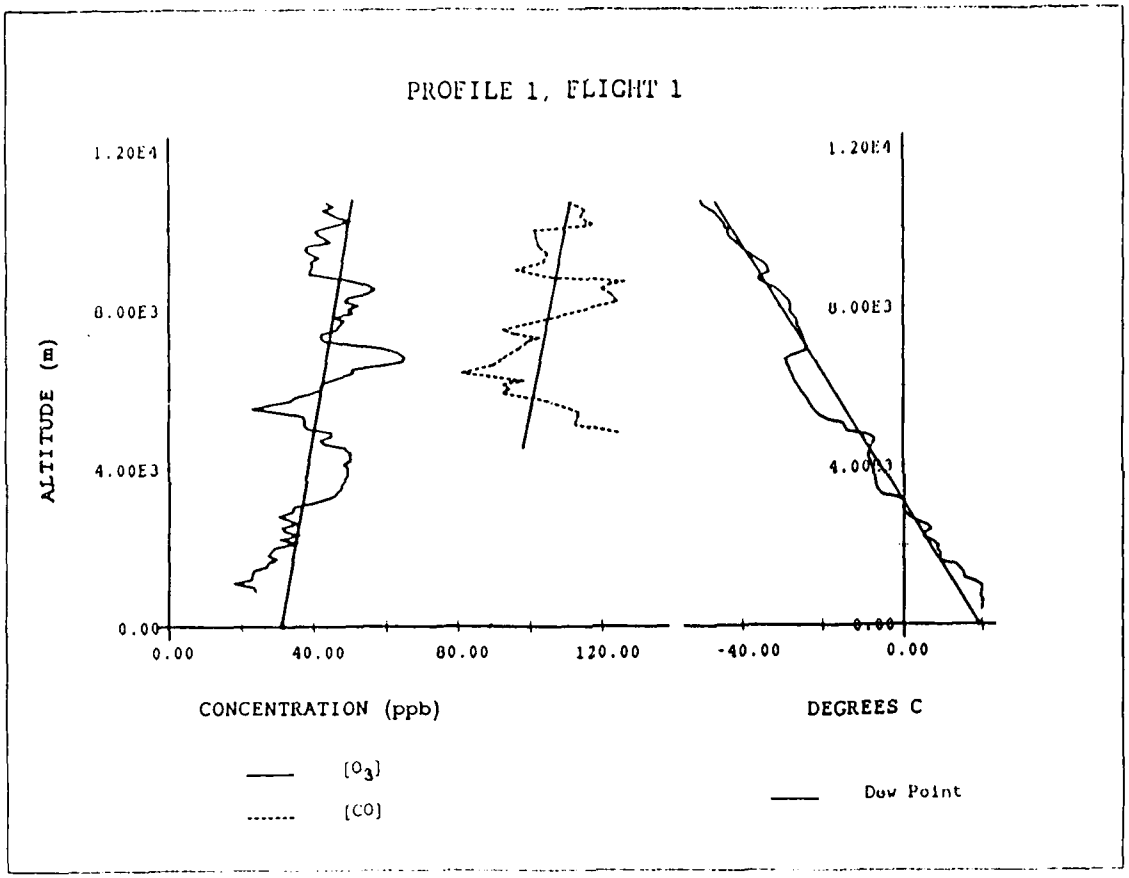


Fig. 33. Vertical profiles of $O_3$, CO and TD for the ascending leg, flight 1. Profiles were drawn using all data averaged over 0.1 km layers. The lines through the profiles represent the best fit lines from linear regression.

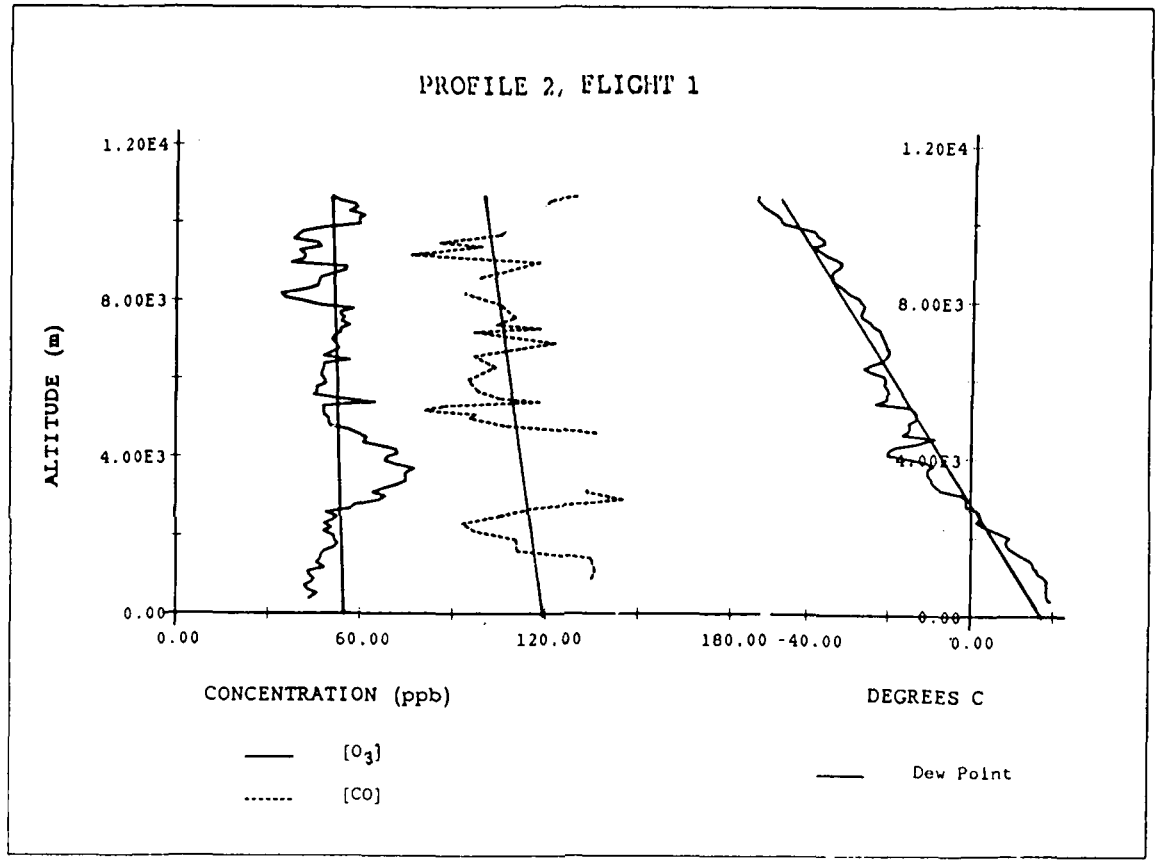


Fig. 34. Like Figure 32, vertical profiles of $O_3$, CO and TD for the descending leg, flight 1.

CO and $O_3$ are not highly correlated; their correlation in profile 1 is near zero and for profile 2 is 0.48, positive but not significant. Profile 1 shows high CO/low $O_3$ above 10 km and at 5 km; high $O_3$/low CO at 6.5 km. The high CO/low $O_3$ regions could be air recently brought up by convection from the PBL which would have low $O_3$ due to surface deposition, and low photochemical $O_3$ production due to the cloudy conditions. The high $O_3$/low CO layer could be the result of some stratospheric or upper tropospheric air mixing downward and being diluted. It is important to remember (as Chameides et al., 1987 point out) high $O_3$/low CO does not automatically eliminate the possibility of in-situ $O_3$ production; the production of $O_3$ is critically dependent on NO concentration, which has sources different from CO. Profile 2 has several spikes above 8 km with high CO/low $O_3$, and has high $O_3$/low CO between 5.7 and 7.6 km, which lowered its positive correlation. Certainly broad areas of the atmosphere were highly disturbed by mesoscale convective mixing during this flight. This is an area in which photochemistry is almost certain to produce substantial amounts of $O_3$, but the photochemical production has not yet had time show up in the vertical profiles. In Profile 2, the Sabreliner encountered less disturbed air that moved in behind the convection, so correlation between $O_3$ and CO was higher.

2. Correlations - Flight 2

As with the first flight, correlations were computed between the trace gases to further understand the various concentrations observed (see Table 1). In Figure 35, a plot of CO versus $O_3$ (all data), data

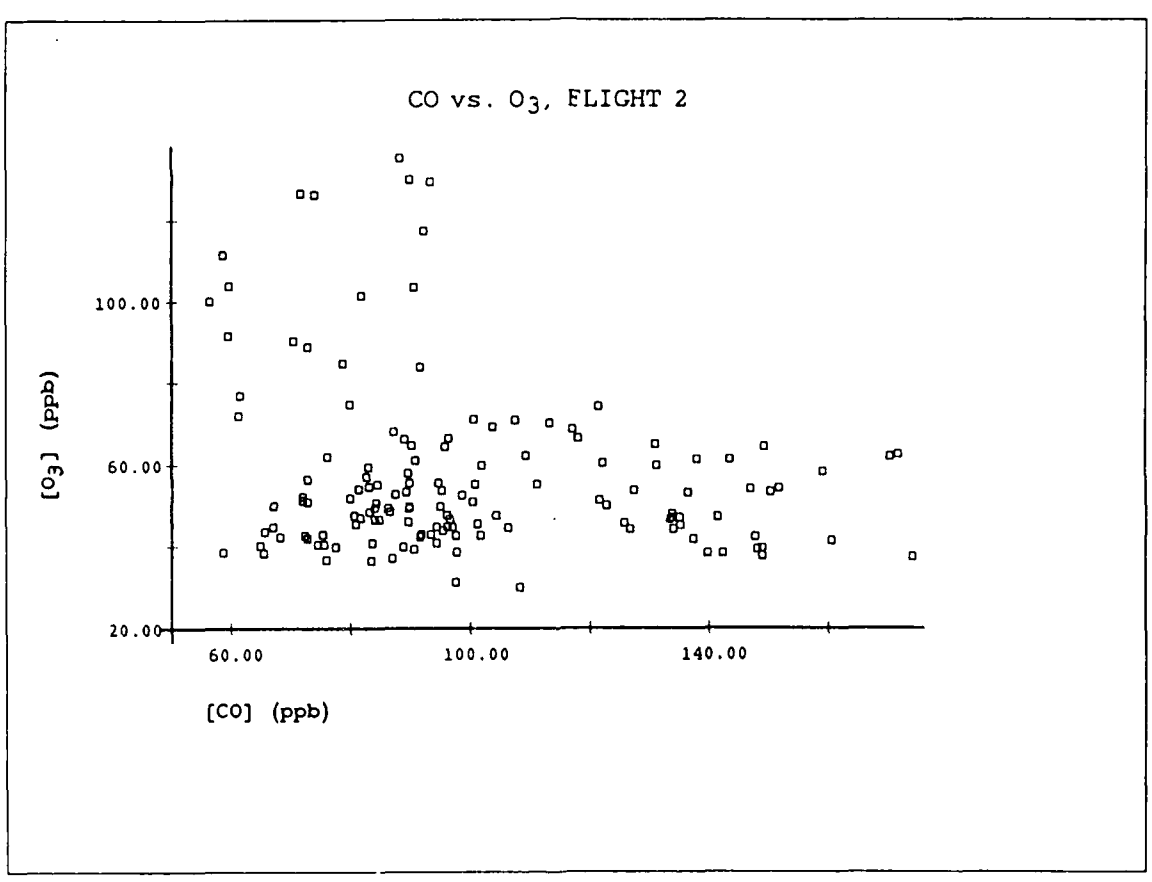


Fig. 35. Scatter plot of CO versus $O_3$, all data, flight 2.

from 10.6 km account for the points with high $O_3$ and little variation in CO; and most of the data with high CO and little variation in $O_3$ come from the PBL. Looking at subsets of the data is more informative. CO versus $O_3$ in just layers II and IIa (Figure 36) yields a positive slope of 0.24 (ppb/ppb), but is not significant with $R^2$ of 0.4631 because this data subset has only 2.8 effective degrees of freedom. In layer III, (Figure 37) the slope is only 0.014 (also not significant with $R^2$ only 0.000526). In layer IV, (Figure 38) without the data at 10.6 km (which is dominated by the strong $O_3$ peaks), $O_3$ and CO show a higher positive correlation with slope 0.49 (though $R^2$ of 0.546 is insignificant due to only 2.8 effective degrees of freedom), suggesting that some enhanced $O_3$ in the upper troposphere may indeed be the result of tropospheric production.

A few subsets of odd nitrogen versus $O_3$ suggest some correlation. At 10.6 km (Figure 39), $O_3$ appears slightly positively correlated with NO, $NO_x$ and $NO_y$ when one ignores the large spikes in NO and $NO_y$; indeed, $O_3$ versus $NO_x$ versus $O_3$ at 10.6 km (Figure 40) has a positive slope of 0.206 (ppb/ppt) (though insignificant with $R^2$ 0.647 and effective degrees of freedom 3.3). $O_3$ with all NO would be correlated if one ignores the strong NO spike (Figure 41).

When profile correlations were done using the technique of Fishman and Seiler (1983) discussed above, the results were much more straightforward than those for the first flight. The air sampled above about 700 mb on this flight had not been involved in convection for 12 hours or more, and strata of $O_3$ had time to develop. Average

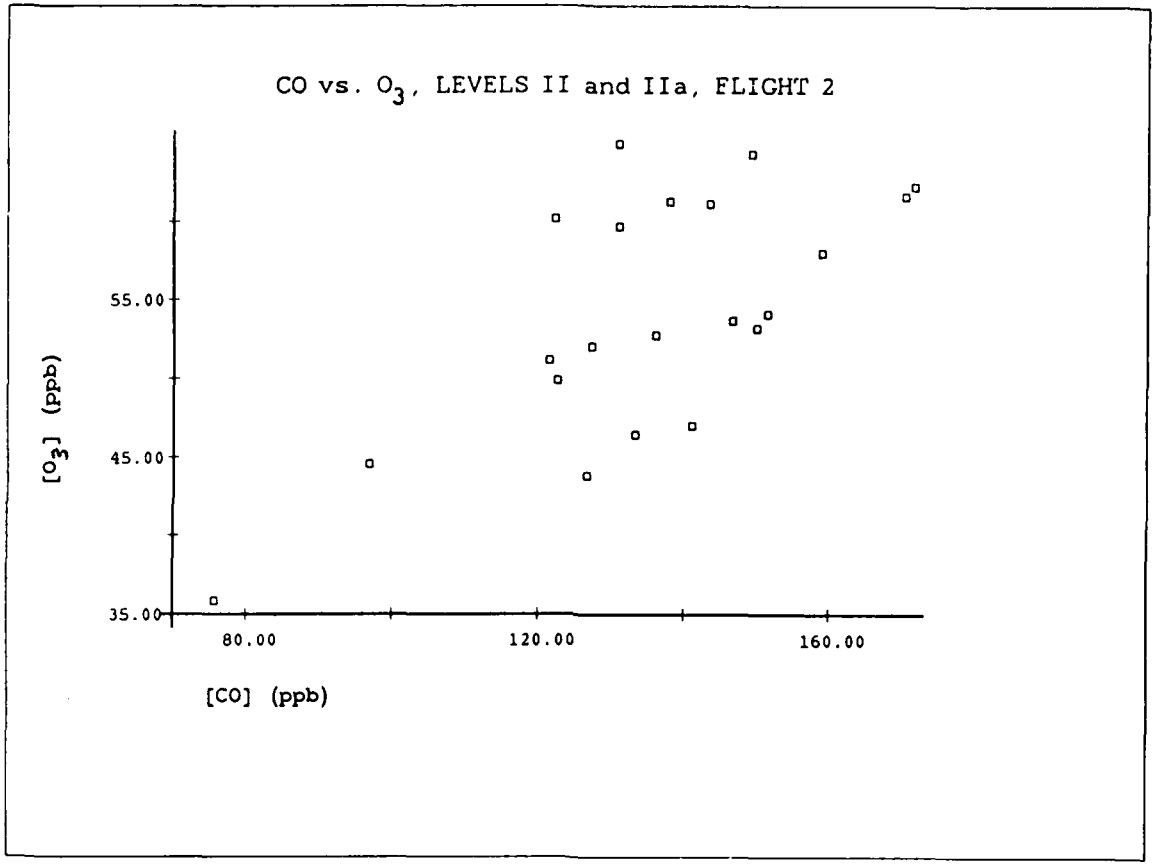


Fig. 36. Scatter plot of CO versus $O_3$ in levels II and IIa, flight 2.

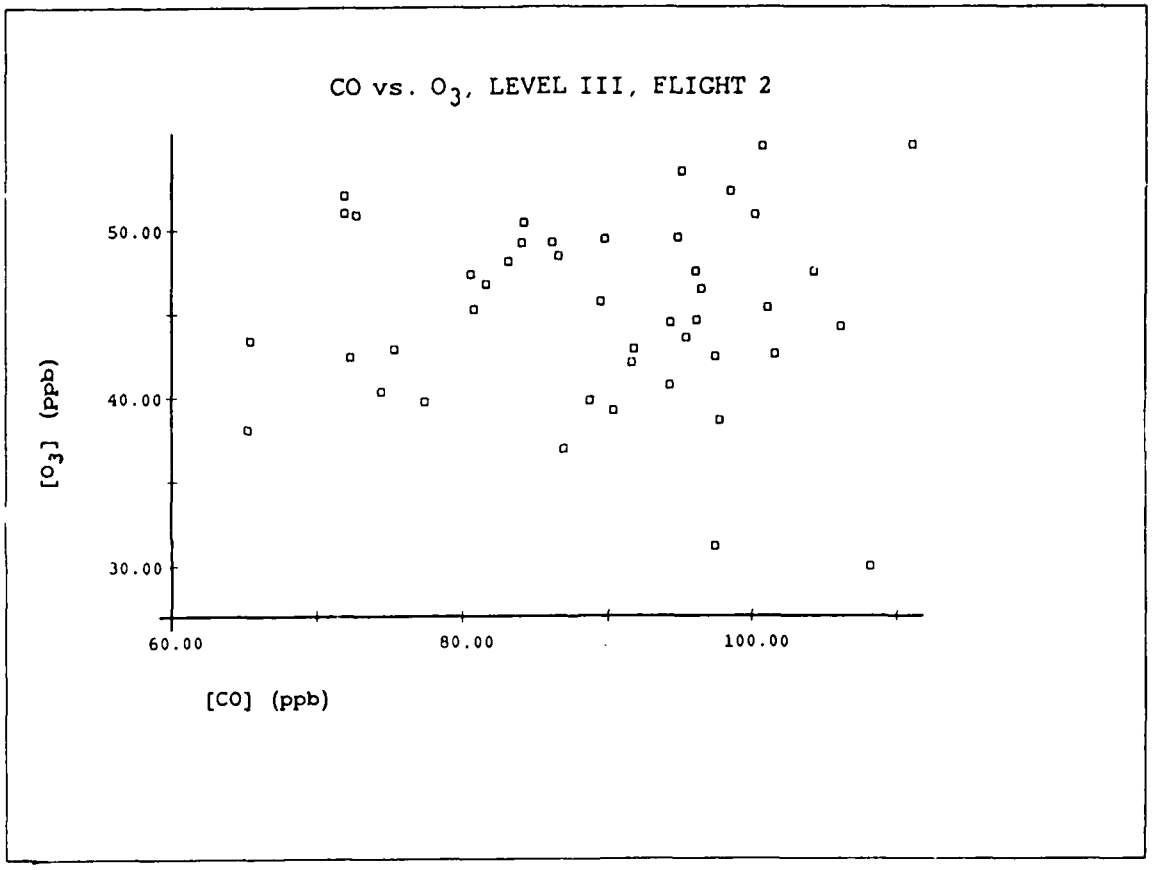


Fig. 37. Scatter plot of CO versus $O_3$ in level III, flight 2.

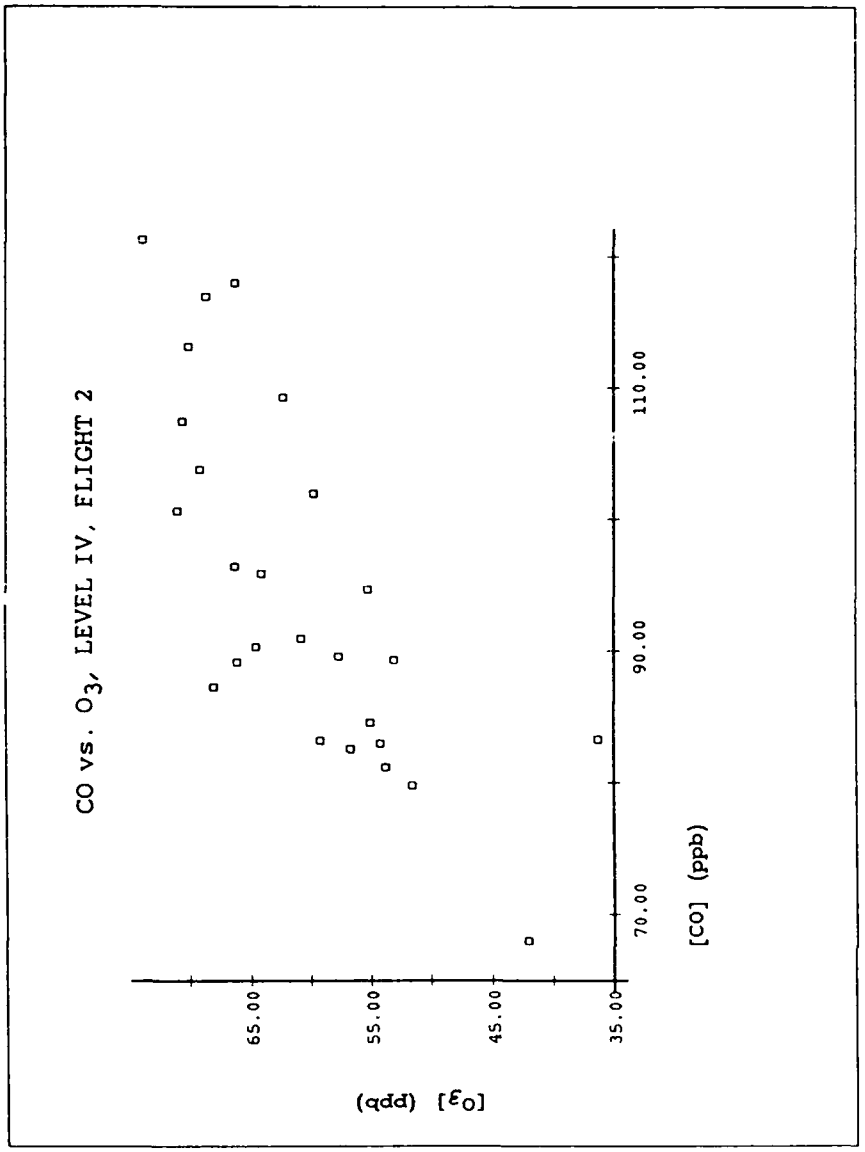


Fig. 38. Scatter plot of CO versus $O_3$ in level IV, flight 2.

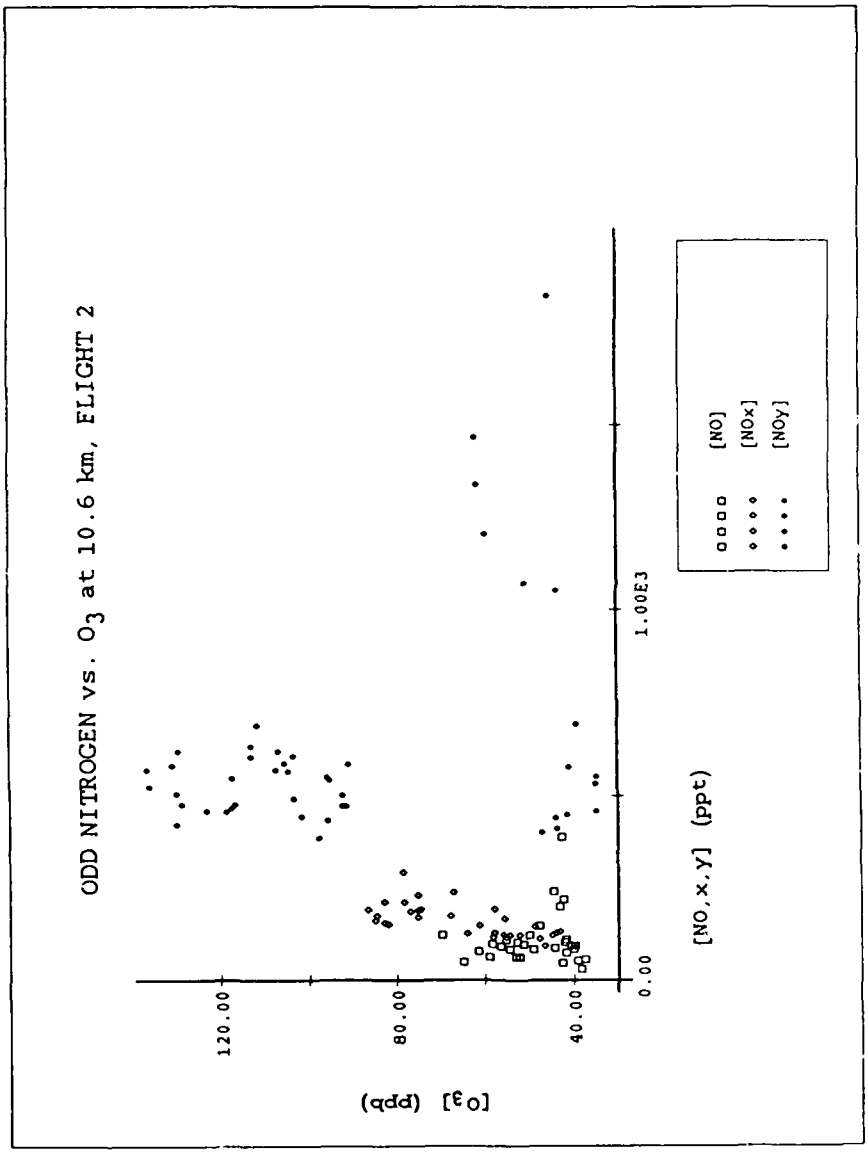


Fig. 39. Scatter plot of NO, $NO_x$ and $NO_y$ versus $O_3$ at 10.6 km, flight 2.

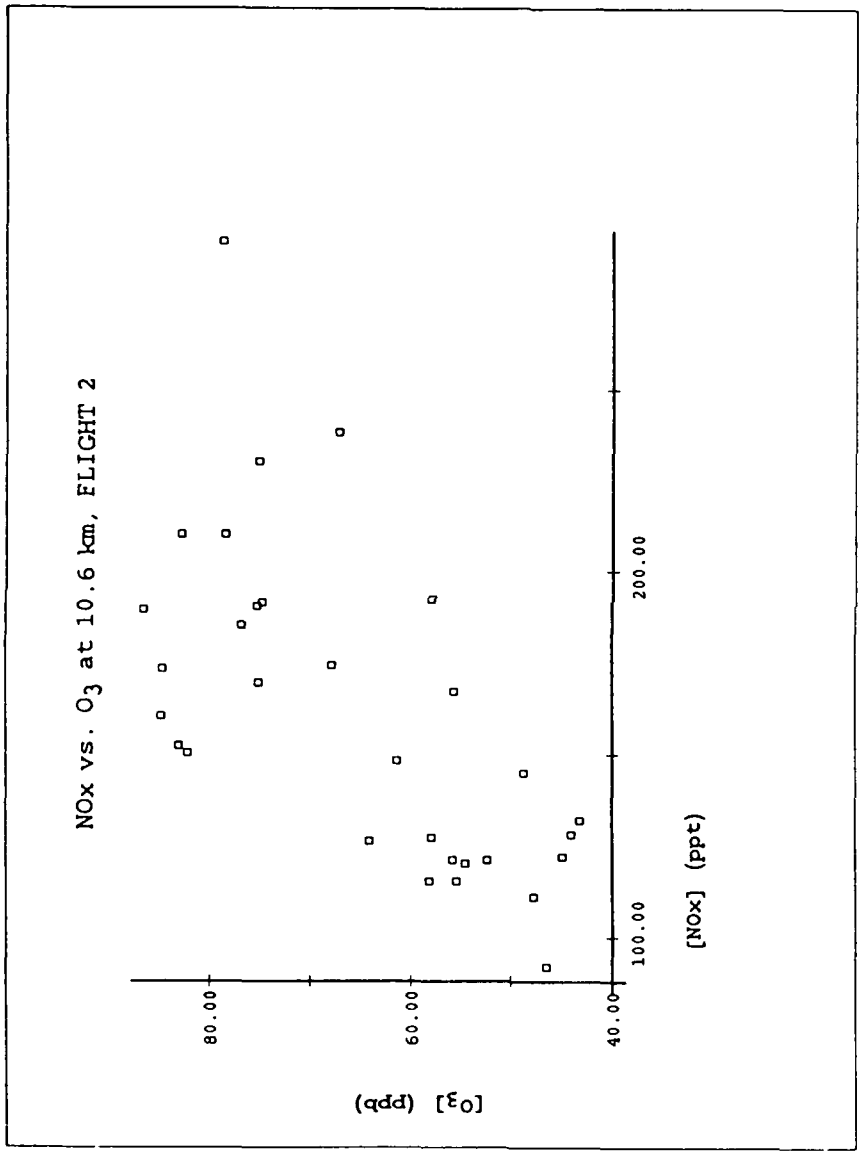


Fig. 40. Same as Figure 39, but only $NO_x$ versus $O_3$.

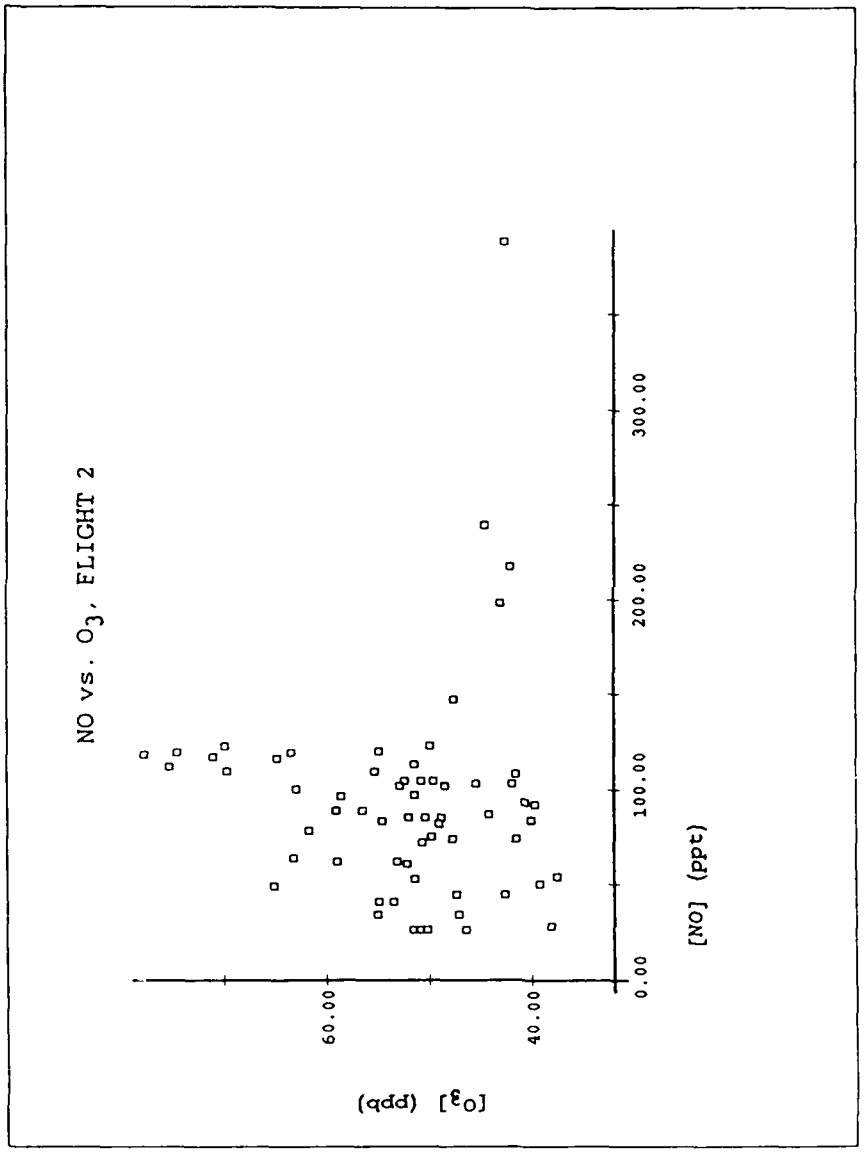


Fig. 41. Scatter plot of NO versus $O_3$, all data, flight 2.

profiles of $O_3$, CO, and TD are shown in Figure 42 with the best fit line for each, and the correlations are shown in Table 2. The TD profile is a bit jagged above 5 km as the descending profile was drier than the ascending one and some 0.1 km layer averages contain more points from the ascent or descent. However, the levels of saturation were the same on ascent and descent. $O_3$ and CO were strongly correlated with a profile correlation coefficient of 0.90. Without precipitation to act as a sink for water vapor, CO and TD were also positively correlated (0.61). $O_3$ and TD were also positively correlated (0.35), though not at a significant level. This strongly suggests that much of the enhanced $O_3$ is of tropospheric origin, and that it takes hours or days after $O_3$ precursors are released to the free troposphere to produce correlations with $O_3$.

3. Event 1 - High $O_3$ and CO at 5.5 km (flight 1)

When the Sabreliner was returning to Oklahoma City, it encountered an area of dry air with elevated $O_3$ (93ppb) and CO (150 ppb) concentrations about 60 km wide (see the sharp peaks at 5.5 km in Figures 15 and 17). Convection in Arkansas and western Oklahoma had been rapidly deteriorating, and only scattered cumulus cells topping below flight level remained. Air with this much CO must have come from the PBL, and the dryness indicates the air must have recently subsided nearly 3 km (determined simply from the dry adiabatic lapse rate of about 10 degrees per km and a dew point depression of almost 30 degrees). Potential temperature increased only about a degree in this air over the surrounding values; equivalent potential temperature (which is a function of the parcels temperature and moisture, and

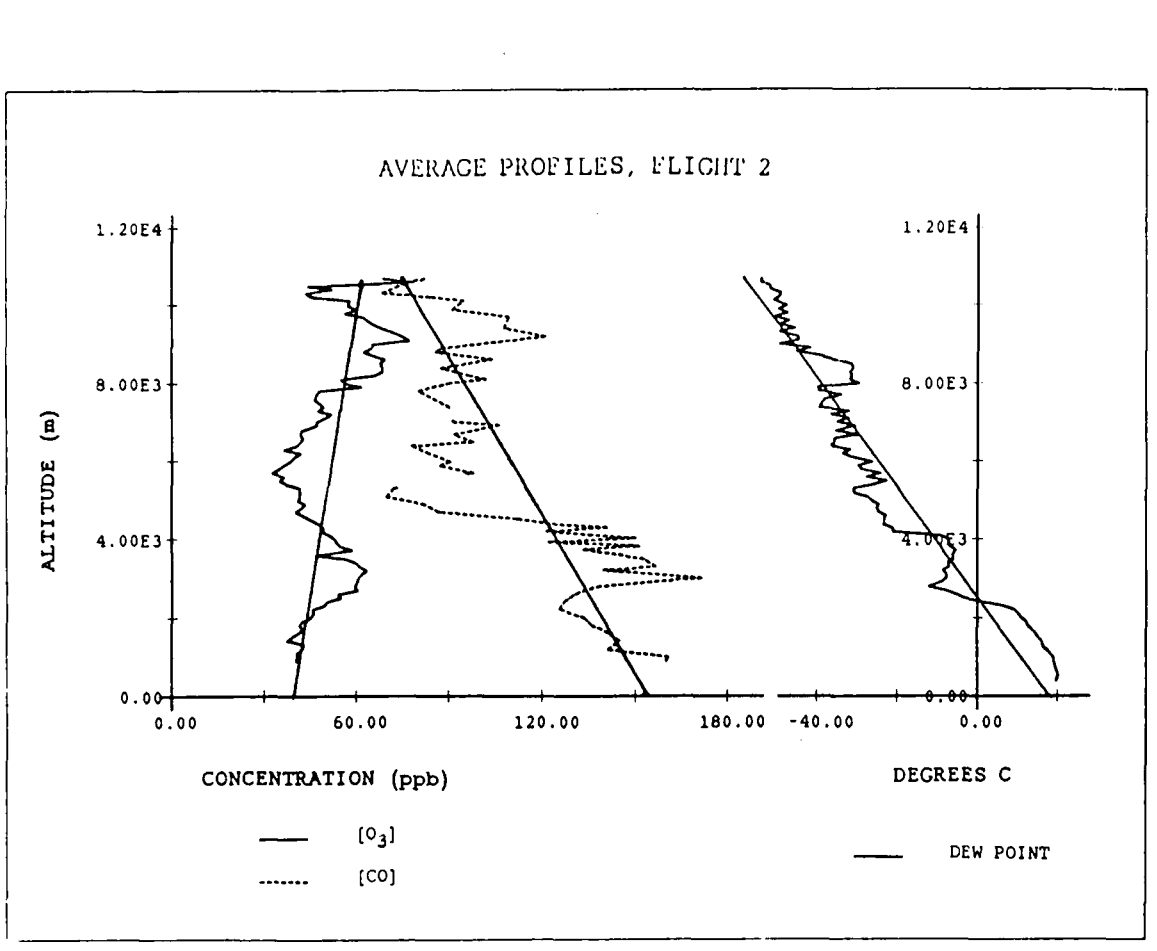


Fig. 42. Average vertical profiles of $O_3$, CO and TD for flight 2. Profiles were drawn using data averaged to the nearest .1 km. The lines through the profiles represent the best fit lines from linear regression.

accounts for the latent heat added if all moisture were condensed out) decreased about 4°C in the dirty air. Vertical wind velocity measured by the Sabreliner showed that on the average the air was sinking at 0.15 m/s (with a large standard deviation of $\pm$ 0.28 m/s). The $O_3$ values are not inconsistent with air from the upper troposphere, but alone give little information on the air's origin because the elevated values could have come from PBL air transported to this altitude by convection, from a stratospheric intrusion, or from in-situ production by ozone precursors. The strong correlation between $O_3$ and CO indicates the $O_3$ could not have come from the stratosphere (Fishman et al., 1980). Because of the recent convection, isentropic back trajectories are not reliable in this case.

A likely scenario is the air containing elevated CO was brought out of the PBL by a thunderstorm earlier that day, and during the rapid decay of the convection some mesoscale effect forced air to rapidly sink in that small area. $O_3$ was likely increasing in this air parcel because PBL air contains the necessary precursors for in-situ photochemical production. The concentration gradients would slowly disappear due to eddy diffusion with the surrounding air, but the temperature gradients would disappear much more rapidly, by a mechanism such as gravity waves, until the air was in thermal equilibrium with the surroundings. This suggests that chemical tracers of atmospheric motion remain discernible longer than the more traditional tracer--potential temperature.

4. Event 2 - Large $O_3$ Gradient at 10.6 km (flight 2)

The Sabreliner twice encountered a sharp gradient in $O_3$ while in level flight at 10.6 km (Figure 25). Figure 43 shows the Sabreliner flight track at 10.6 km. Maximum $O_3$ was found to the north and minimum $O_3$ was found to the south.

Immediately, a PBL source or photochemical production source for the $O_3$ gradient had to be eliminated because the $O_3$ concentrations were completely uncorrelated with CO, which showed only relatively small fluctuations (about $\pm$ 10 ppb) at 10.6 km. There was no discernible change in moisture ($H_2O$ was below the detection limit of the dew pointer and lyman alpha sensor). There was a decreasing trend in the odd nitrogen data as it cycled from $NO_y$ to $NO_x$ and NO as the $O_3$ decreased after each peak. Plots of the $NO_x$ and $NO_y$ versus $O_3$ after the first peak are shown in Figure 44. Positive correlation between $O_3$ and odd nitrogen with no correlation with CO point to a stratospheric source, but why the sharp gradient?

Potential temperature did not show much change at 10.6 km (less than 2° C), and was uncorrelated with the $O_3$ change, so there was no evidence the Sabreliner had found the edge of a tropopause fold from an abrupt intrusion of stratospheric air. The synoptic situation precluded a tropopause fold because the upper level trough was too far to the northeast, and in a fold one would expect anticorrelation between $O_3$ and CO (Danielson et al., 1987; Hipskind et al., 1987), which was not found in this case.

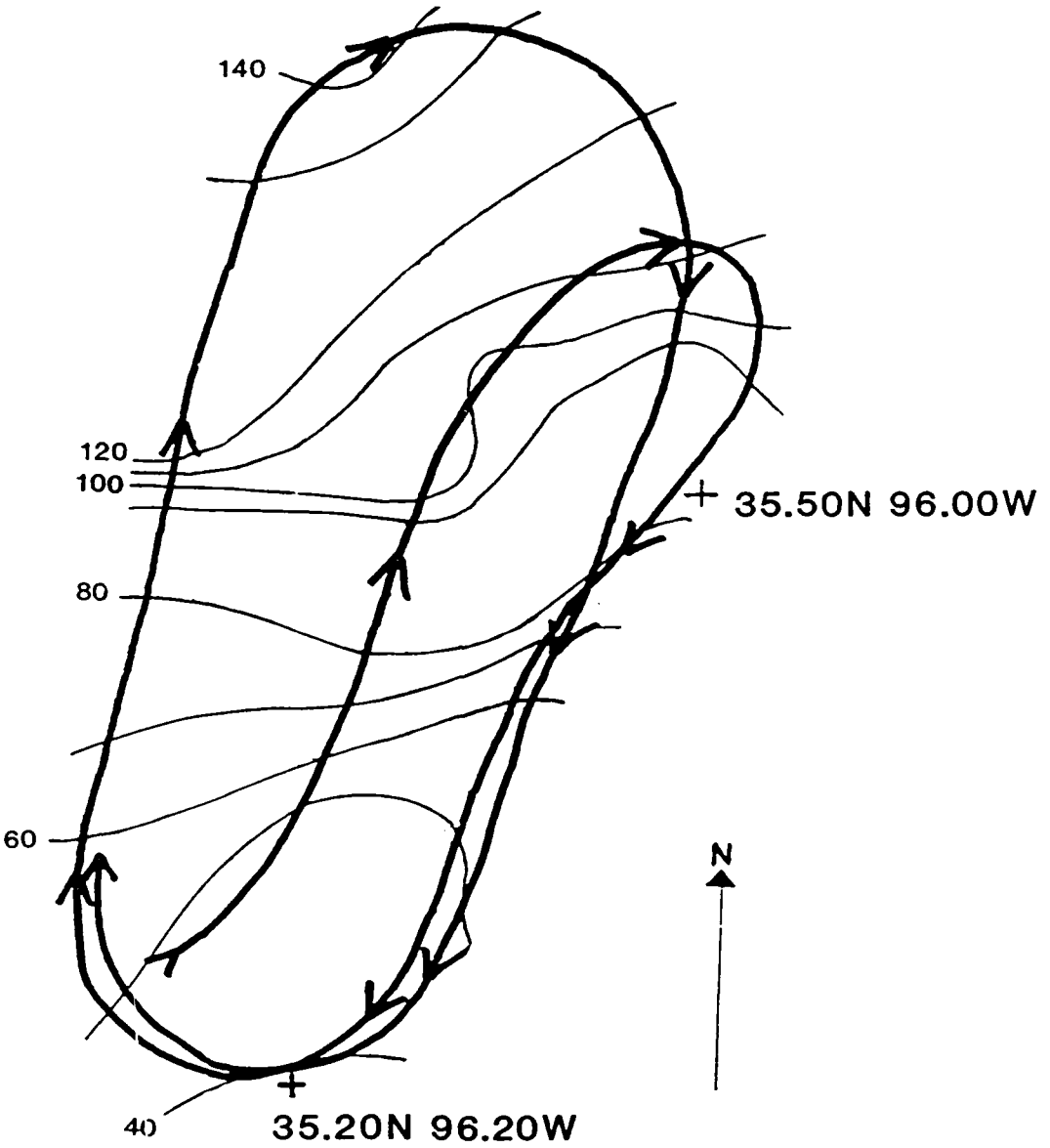


Fig. 43. Flight track of Sabreliner at 10.6 km on flight 2, with contours of $O_3$ concentration drawn from 7 sec. data.

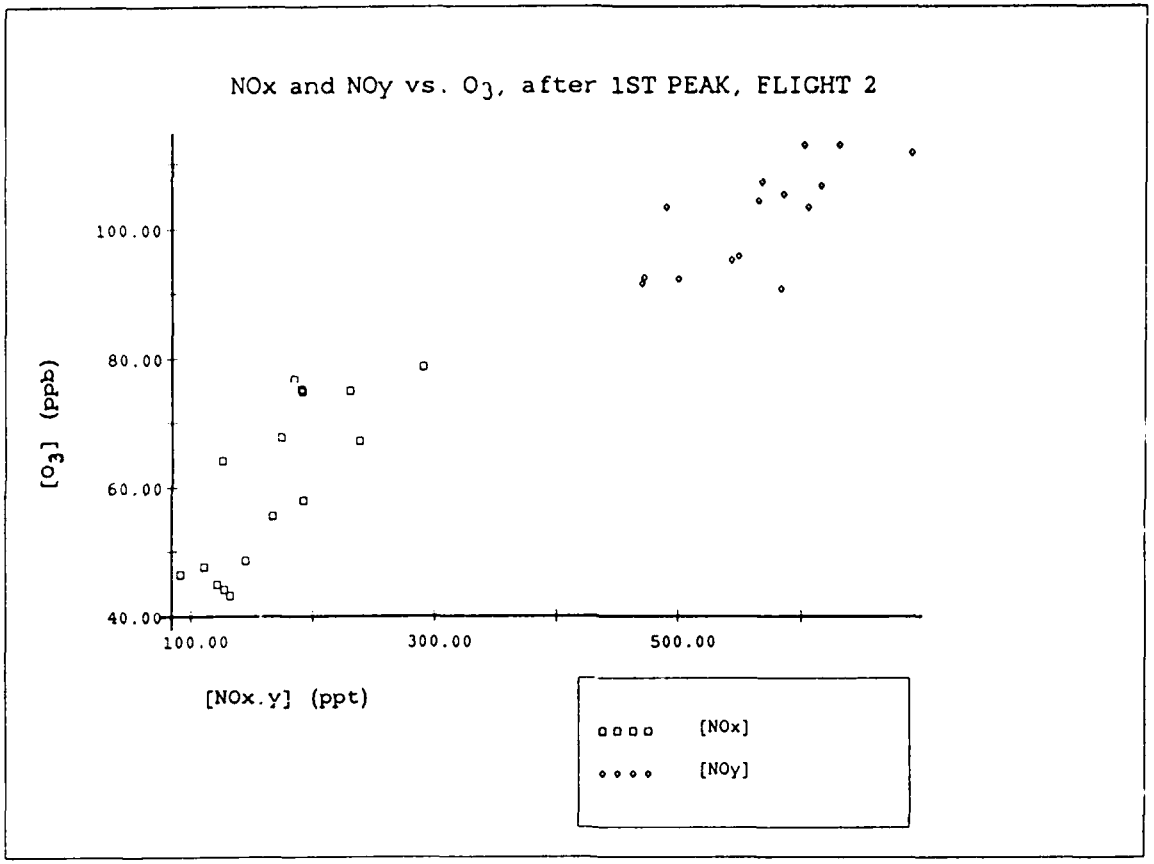


Fig. 44. $NO_x$ and $NO_y$ versus $O_3$, after the first peak in $O_3$ at 10.6 km, flight 2.

The only measured variable that had a time series matching the change in $O_3$ was wind. Winds were higher with a slightly more southerly, component where $O_3$ was lowest (Figure 45). In fact, the correlation between $O_3$ concentration and wind speed is significant at the 99 percent level, using the effective degrees of freedom for a time series as discussed above. An isentropic back trajectory, initialized using the Oklahoma City rawinsonde winds, showed the air at 10.6 km had come from the west in the vicinity of the upper level cut off low. As suggested by the $O_3$-wind correlation, the trajectories were repeated for two parcels (Figure 46), one from the northern (high $O_3$) part of the track and one from the southern (low $O_3$) part of track, initialized with the actual winds measured by the Sabreliner for each parcel for 6 hours (255 degrees at 11 m/s for the northern parcel and 245 degrees at 15 m/s for the southern parcel). The two parcels quickly diverged. The trajectories showed very little change in altitude and no interaction with convection. The air with higher $O_3$ concentrations had come north of the low from near the jet, while the air with low $O_3$ had come from around the southern side of the low where the tropopause was much higher. It appears the Sabreliner had flown through a confluence zone between air originating near the jet, where the parcel had a greater chance of encountering high $O_3$ concentrations, and air originating several kilometers below the tropopause in a more tropical location, where $O_3$ concentrations would be expected to be lower.

The isentropic trajectories were constructed by hand using all available upper air data. Before the last 6 hours, winds for the

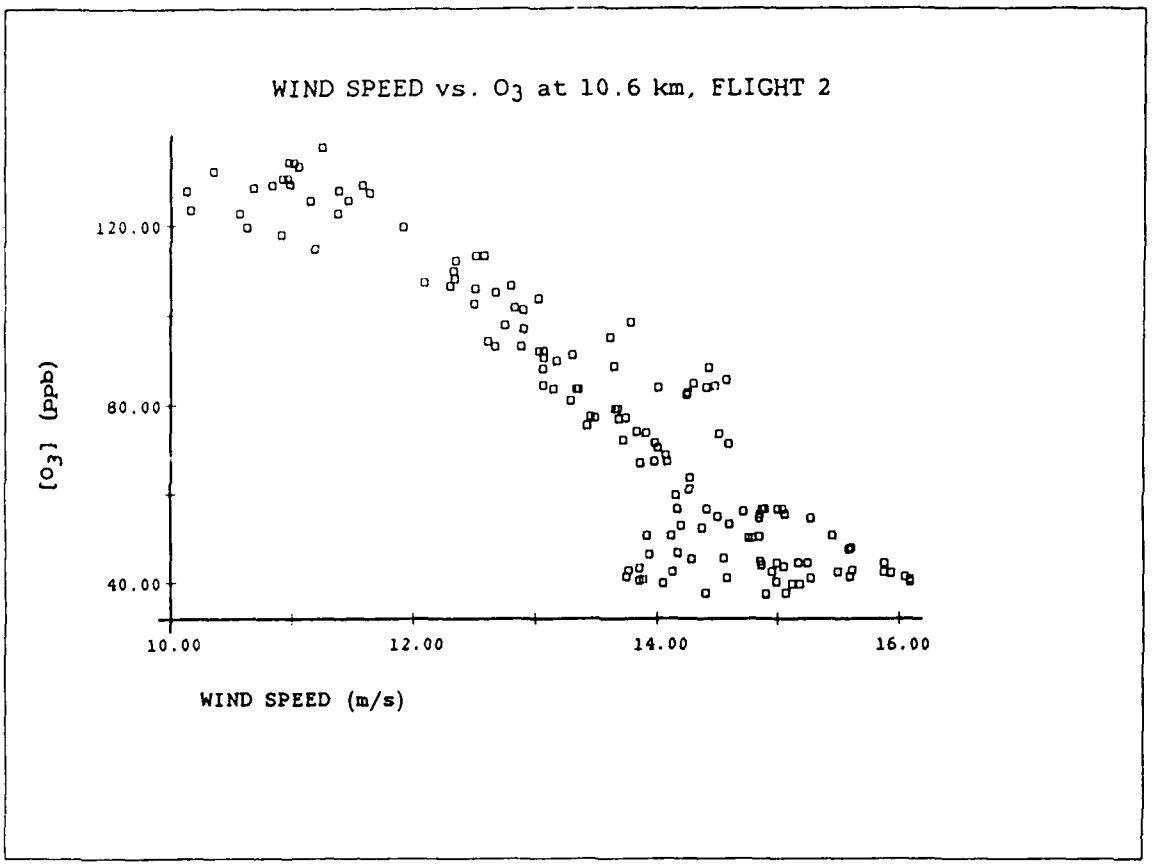


Fig. 45. Wind speed versus $O_3$ at 10.6 km, flight 2.

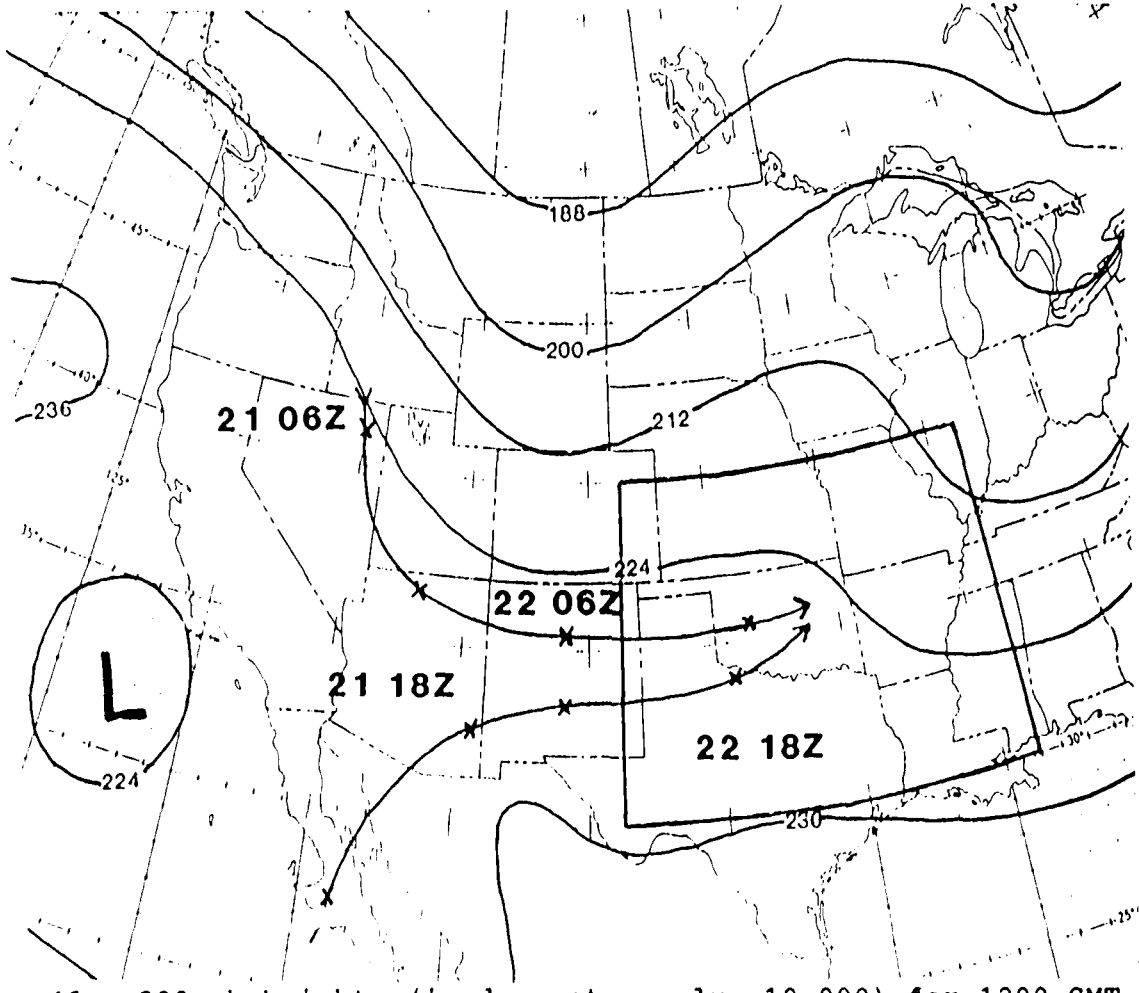


Fig. 46. 200 mb heights (in decameters plus 10,000) for 1200 GMT (0700 CDT), 21 June 1985. Isentropic back trajectories of air sampled at 10.6 km on flight 2 are shown, initialized with aircraft winds from the north and south of the flight track for six hours. Box designates geographic extent of gridded TOMS data discussed in a later section.

appropriate potential temperature surface were determined for each upper air station using linear interpolation between winds observed at 200 and 250 mb. Careful streamline analyses were done for each synoptic observation time, and the parcel was moved back along a streamline using the average horizontal wind from the surrounding stations. For example, streamlines at 1200 GMT were used to moved the parcel from 0600 to 1800 GMT.

5. TOMS Data

The TOMS sensor onboard the NASA Nimbus 7 satellite provides total column $O_3$ ($TC_{O_3}$) over the entire earth once a day. Fishman et al. (1986) have shown that in the tropics many of the features in $TC_{O_3}$ are from tropospheric $O_3$ variability, even though tropospheric $O_3$ accounts for only 5 to 15 percent of the column. Figure 47 shows data from June 21, and Figure 48 shows data from June 22 (flight day); the time of the data is close to local noon at any location (the equatorial crossing time is 11:50 am, in an ascending orbit). These data were analyzed to determine if the tropospheric features found by aircraft, in particular the high $O_3$ sampled at 5.5 km near the Oklahoma-Arkansas border on the first flight or the sharp $O_3$ gradient at 10.6 km on the second flight, were detectable in the $TC_{O_3}$ values. The data are in Dobson units (Du), where one Du equals 0.01 mm of $O_3$ if all the $O_3$ in the atmosphere were compressed to standard temperature and pressure. The thickness corresponding to a typical $TC_{O_3}$ amount of 300 Du is 0.3 cm.

A preliminary look at Figure 48 was encouraging. The $TC_{O_3}$

Fig. 47. TOMS imagery from the Nimbus 7 satellite for 21 June 1985.

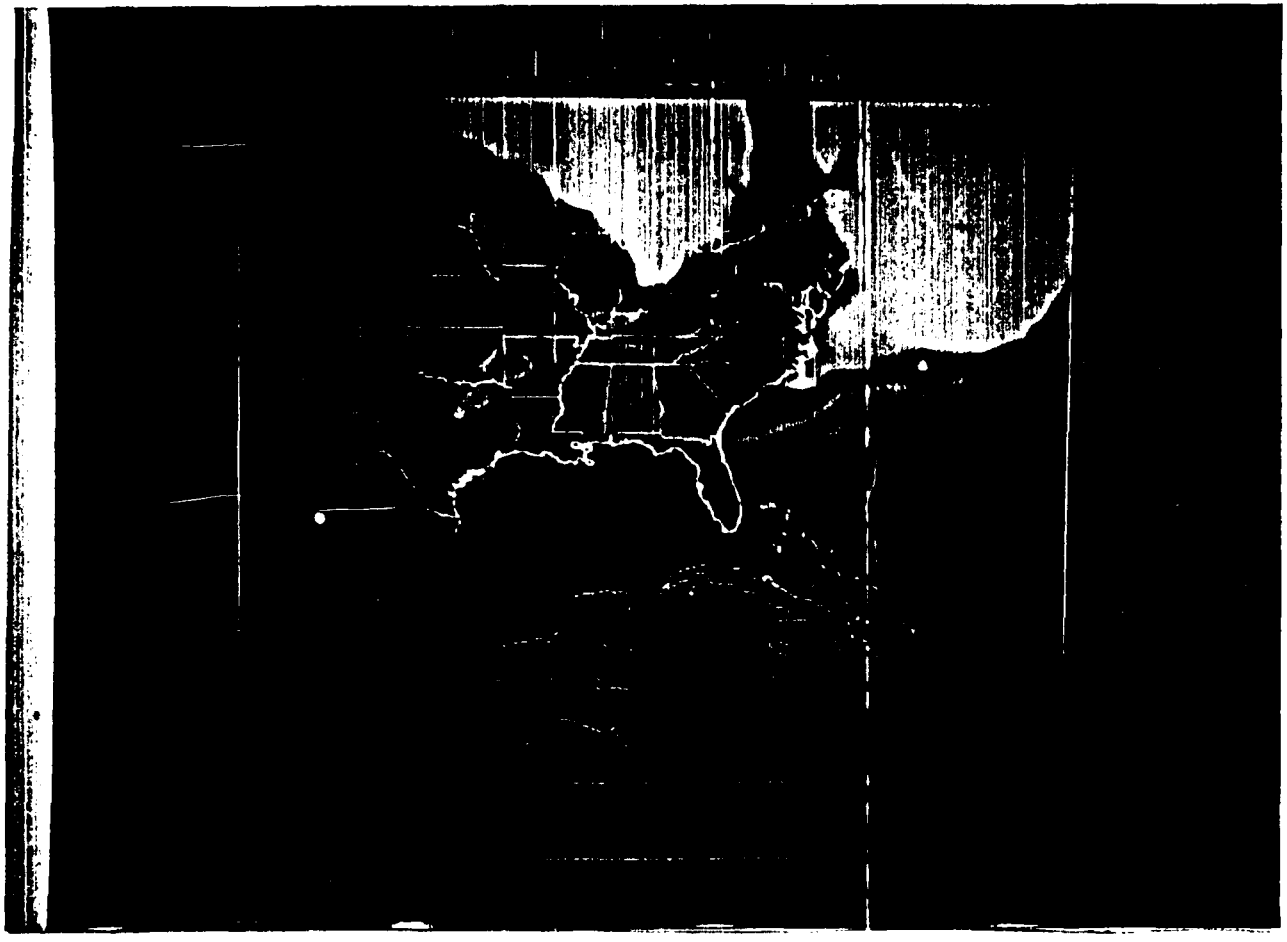

Fig. 48. TOMS imagery from the Nimbus 7 satellite for 22 June 1985.

maximum (15 Du above the surrounding area) near the Oklahoma-Arkansas border was exactly where the high $O_3$ on the first flight was sampled, and flight time was very close to the time of the satellite observation. A simple calculation using the ideal gas law explains that a 40 ppb increase in $O_3$ concentration (which was measured as the Sabreliner entered the dirty air), if the layer were 4 to 6 km thick, would account for an increase of 15 Du in $TCo_3$. In addition, the small spot of low $TCo_3$ in east central Oklahoma may be evidence of the gradient measured later in the day at 10.6 km. The picture shows vividly the large increase in $TCo_3$ north of the jet stream resulting from the lower tropopause height.

The TOMS sensor measures ultraviolet (UV) radiation and thus cannot see below clouds. Before any conclusion could be drawn, the effect of clouds had to be considered. Comparison between the TOMS imagery and infrared (IR) imagery from the NOAA GOES satellite for nearly the same time showed not only that the maximum in $TCo_3$ discussed above was near the clear air sampled, but that wherever there was strong convection, TOMS imagery gave lower $TCo_3$. NASA uses a simple climatological algorithm to correct for clouds in the continuous TOMS database. Was the variation really so well correlated to the tropospheric features, and a result of convection pushing up the tropopause, or was it merely an anomaly from the cloud correction routine?

The algorithm assumes cloud height is 300 mb in the tropics and 600 mb at the poles; at intermediate latitudes, cloud height (in mb)

is given as:

$$300 + (1 - \cos(2 \times \text{latitude}) \times 150). \quad (1)$$

The lowest 700 mb of the troposphere is assumed to contribute 19 Du (from climatology), distributed linearly with pressure (for a cloud at 300 mb one would add 19 Du, for a cloud at 650 mb one would add 9.5 Du). If ultraviolet (UV) reflectance measured by the sensor is less than 20 percent, it assumes clear skies; greater than 60 percent, it assumes a cloud at the climatological height; and in between 20 and 60 percent, the correction is linearly adjusted between zero and the total adjustment (P.K. Bartia, personal communication, 1988). TOMS data for some periods is available from NASA corrected using measured IR cloud heights and climatological tropospheric $O_3$.

Taking the grid of climatologically-corrected data (provided by J. Fishman, personal communication, 1988), I used the UV reflectance from each pixel to subtract the NASA correction and retrieve the raw $TCo_3$. Horizontal resolution is coarse, with just 8 pixels in every 10 degrees longitude, and 1 pixel for every degree latitude. The raw data was then corrected with a new algorithm.

Our algorithm uses better estimates of tropopause height, cloud height and tropospheric $O_3$. The Little Rock and Oklahoma City soundings showed the tropopause at 13 km. Comparing the coldest temperatures on the GOES imagery with the soundings showed the convection close to, but not penetrating, the tropopause. The strongest UV reflectance closely matched the coldest IR cloud tops. For the strongest convection at the time of the TOMS data, UV reflec-

tance was 88 percent. Therefore, an altitude of 13 km was set to correspond to 90 percent reflectance, and 0 km (no cloud) was set to correspond to 20 percent reflectance. Average tropospheric column $O_3$ was calculated by averaging the three best fit lines from the $O_3$ profile correlations; two lines had a small positive slope and one a small negative slope. The lines were extended to 13 km and the values at each 0.1 km were averaged over the three profiles. No correction was made for surface elevation, which was generally below 1 km, and the expected sharp increase in $O_3$ near the tropopause was not measured or included (these errors should partially offset each other). The resulting average was 49 ppb, or 33.4 Du from the surface to 13 km. The appropriate amount of tropospheric $O_3$ was added to the raw $TCo_3$ by linear interpolation based on the measured reflectance. No attempt was made to try to improve on a linear fit as reflectance from a thin high cloud may look similar to a solid low cloud, with the former letting through some radiation from below and the latter completely blocking radiation from the lowest levels. One really does not know what levels are being missed by the TOMS sensor.

The original values with the NASA cloud correction and the newly corrected $TCo_3$ values are shown in Figure 49. The new algorithm increased the $TCo_3$ where there were solid, high clouds. While high $TCo_3$ values remain on the Oklahoma-Arkansas border, it is no longer an isolated maximum, but a thin band of elevated $TCo_3$ extending from the high $TCo_3$ to the northeast. The small clean spot just northwest of this band remains.

**GRIDDED TOMS DATA**

(Unit Du minus 200)

INITIAL

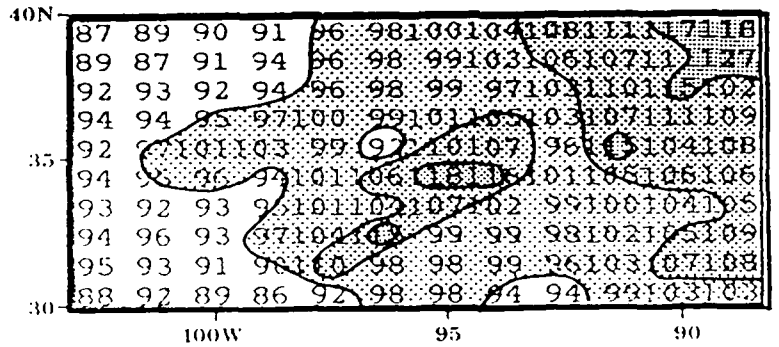


CORRECTED

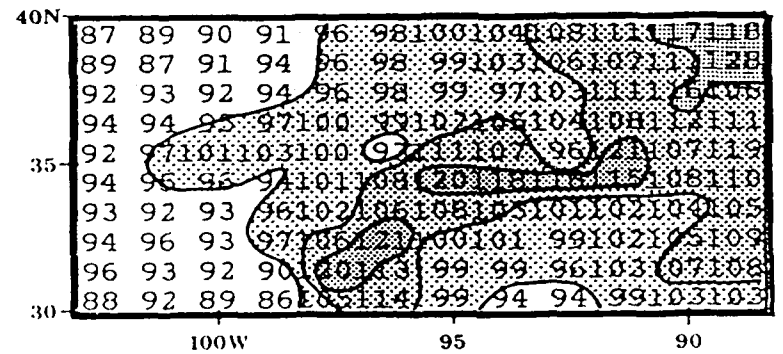


**Fig. 49. Gridded TOMS data from 22 June 1985. The initial data was derived using the NASA standard correction for tropospheric $O_3$. For the corrected data, the NASA standard correction was removed and a new correction was made based on the observed tropospheric conditions as described in the text. The box drawn in Figure 46 indicates the geographical extent of the gridded data.**

AD-A196 540 ORIGIN OF TROPOSPHERIC OZONE OVER CENTRAL UNITED STATES 2/2
(U) AIR FORCE INST OF TECH WRIGHT-PATTERSON AFB OH
D P MCNAMARA 1988 AFIT/CI/NR-88-25

UNCLASSIFIED F/G 4/1 NL

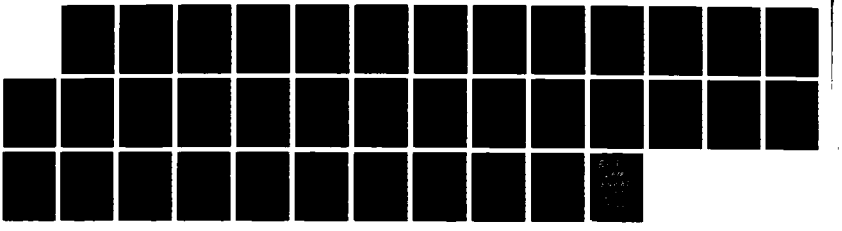

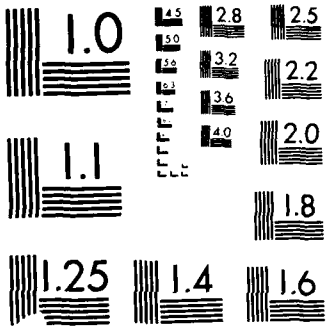


UTION TEST CHART

While the corrected TOMS data do not contradict the ideas proposed about the origin of the tropospheric $O_3$ gradients, they fail to provide any conclusive support, even when considered along with aircraft data, synoptic data, and IR (GOES) satellite imagery. The TOMS and synoptic data are on a very coarse scale compared to the small scale features sampled by the Sabreliner. The clean spot in east central Oklahoma is only one pixel, and the dirty area on the Oklahoma-Arkansas border is only 2 pixels; the synoptic network consists of at most a few stations per state. Upper air synoptic data are taken twice a day; TOMS data are available only once per day, and not at synoptic observation times. In addition, the TOMS instrument measured UV reflectance greater than 20 percent wherever there was a hint of cloud on the IR imagery; the tropospheric part of the $TC_{O_3}$ we are comparing with the aircraft observations was often partially blocked by clouds and corrections based on average tropospheric $O_3$ further obscure real tropospheric gradients.

The coarse time resolution of the TOMS data makes interpretation of the movement of the features between Figures 47 and 48 ambiguous. This ambiguity is not cleared up by the synoptic data close to the time midway between the two TOMS analyses. In the equivalent barotropic assumption, which assumes a linear increase in winds from the surface to the tropopause, synoptic patterns are assumed to propagate at the mean tropospheric flow, estimated by the 500 mb winds. But in this case the flow is strongly non-barotropic in the vicinity of Oklahoma, Arkansas and Texas because of the vertical wind shear (surface winds from the south and southeast shifted to west and north-

west by 300 mb). In this case waves may move faster than the parcels, or remain stationary with many parcels flowing through. Assuming the feature extending from the Arkansas-Oklahoma border southwest to east central Texas in Figure 48 is associated with a trough in the troposphere, causing a depressed tropopause as evidenced by the high $TCo_3$, it could correspond to several features in Figure 47, 24 hours earlier. The trough could be the feature in Figure 47 extending from western Arkansas to central Texas, which remained stationary and deepened slightly. Or, the trough could have pushed south from northern Kansas. Finally, the trough could have broken off from the larger scale trough in Figure 47, which at that time extended south to northern Colorado. GOES satellite imagery confirms that this larger trough pushed south to central Oklahoma, and is seen receding northward in Figure 48. The wave movement occurs independently from the individual air parcels.

Analysis of all the available data suggests the following possible interpretation of the trace gas observations. At 1200 GMT on 22 June, the upper level trough was moving out to the northeast. Winds over Oklahoma were light, cutoff from the faster flow to the north (Figure 1). The air at 5.5 km was subsiding, as evidenced by its vertical motion and large dew point depression. Although the Sabreliner flew near the band of high $TCo_3$ through central Arkansas, it only sampled high local $O_3$ in the small area near the Oklahoma border. The tropopause was depressed, and the tropospheric air below was sinking along this band. But the entire band was not pushed down uniformly; some mesoscale forcing pushed down air which happened to be

outgassed from a thunderstorm (as evidenced by the high CO concentration).

As for the large gradient sampled at 10.6 km, TOMS data confirms the difference in $TCo_3$ at the origins of the two parcels (Figures 46 and 47). The air at 10.6 km moved fast enough to have originated from behind the convection that affected the region earlier in the day, while the air slightly lower was involved in the recent convection. The fine structure at 10.6 km was caused by a dynamic process which caused confluence of the parcels; the parcels then became trapped in the slow moving flow over Oklahoma.

# V. TROPOSPHERIC OZONE PRODUCTION

Results from the two flights on 22 June suggest some of the $O_3$ sampled is of tropospheric origin, either produced in the PBL and brought by convection into the free troposphere, or produced in-situ in the free troposphere from ozone precursors (CO or hydrocarbons in the presence of $NO_x$ and sunlight). This section estimates the tropospheric $O_3$ production with a simple photochemical model.

A rough estimation can be made of whether net $O_3$ production is occurring by assuming the following simple reaction scheme (rate constants from NASA, 1985):

(4) $O_3 + NO \rightarrow NO_2 + O_2$ $\quad k_4 = 1.8(10^{-12})\exp(-1370/T)$

(5) $NO_2 + h\nu + O_2 \rightarrow NO + O_3$ $\quad j_5$

(7) $CO + OH + O_2 \rightarrow CO_2 + HO_2$ $\quad k_7 = 1.5(10^{-13})(1+0.6P)$

(8) $HO_2 + NO \rightarrow NO_2 + OH$ $\quad k_8 = 3.7(10^{-12})\exp(240/T)$

(9) $O_3 + HO_2 \rightarrow OH + 2O_2$ $\quad k_9 = 1.4(10^{-14})\exp(-580/T)$

The change in $O_3$ with time is found from reactions 4, 5, and 9:

$$d[O_3]/dt = j_5[NO_2] - k_4[O_3][NO] - k_9[O_3][HO_2] \qquad (2)$$

And the change in $NO_2$ with time is found from reactions 4, 5, and 8:

$$d[NO_2]/dt = k_8[NO][HO_2] + k_4[NO][O_3] - j_5[NO_2] \qquad (3)$$

Assuming steady state in $NO_2$ yields:

$$[NO_2]ss = (k_8[NO][HO_2] + k_4[NO][O_3])/j_5 \qquad (4)$$

This simplifies equation 2 above:

$$d[O_3]/dt = [HO_2] \times (k_8[NO] - k_9[O_3]) \qquad (5)$$

If the expression in parentheses is positive, $O_3$ will be produced, and if negative $O_3$ will be destroyed. This expression is a function of

temperature, NO concentration and $O_3$ concentration, and explains how one can define a critical NO concentration for $O_3$ production (e.g. Ridley et al., 1987).

To see if $O_3$ production was likely in the regions sampled on the two flights, calculations were done for the altitudes of level flight where NO was measured (Table 3). All concentration and temperature data at a level were averaged. At all levels where NO data existed, $O_3$ production was possible. In most cases, as altitude increased, $O_3$ production increased.

Liu et al. (1987) estimated the total column production of $O_3$ over the United States in summer from anthropogenic $NO_x$ to be about $1(10^{12})$ $cm^{-2}$ $s^{-1}$; somewhat greater than that estimated from natural $NO_x$, which they estimate to range from $1.9(10^{11})$ to $12(10^{11})$ $cm^{-2}$ $s^{-1}$. They made the estimate using surface measurements from the rural site at Niwot Ridge, Colorado. Average NMHC concentrations were derived from measurements by Greenberg and Zimmerman (1984). Above the PBL, trace gas concentrations were set at values representative of clean continental air, and NMHC concentrations were considered negligible. To compute a similar estimation with this data set required a more detailed model than reactions 4-9, to consider oxidation of both CO and hydrocarbons. What follows is an order of magnitude estimation of the column $O_3$ production under the conditions found on each flight, and an explanation of the approximations made.

Table 4 lists 26 reactions involved in tropospheric $O_3$ production

TABLE 3

OZONE PRODUCTION AT ALTITUDES OF LEVEL FLIGHT

$$\frac{dO_3}{dt} = [HO_2]\,(k_8[NO] - k_9[O_3]) = [HO_2]\,X$$

If $X > 0$, $O_3$ produced. If $X < 0$, $O_3$ destroyed.

Flight 1

| Altitude (m) | $X$ ($\times 10^{-2}$) |
|---|---|
| 8800 | 0.95 |
| 10000 | 4.8 |
| 10600 | 6.9 |
| 9400 | 2.4 |
| 7900 | 2.0 |
| 5500 | 0.44 |

Flight 2

| Altitude (m) | $X$ ($\times 10^{-2}$) |
|---|---|
| 7000 | 0.63 |
| 8800 | 0.87 |
| 9400 | 0.98 |
| 10600 | 0.82 |

$k_8 = 3.7(10^{-12})\exp(240/T)$ ; $k_9 = 1.1(10^{-14})\exp(-580/T)$

## TABLE 4

## REACTIONS INVOLVED IN OZONE PRODUCTION

| | |
|---|---|
| (1) $HO_2 + NO \rightarrow NO_2 + OH$ | $k_1=3.7(10^{-12})\exp(240/T)$ |
| (2) $O_3 + HO_2 \rightarrow OH + 2O_2$ | $k_2=1.4(10^{-14})\exp(-580/T)$ |
| (3) $OH + O_3 \rightarrow HO_2 + O_2$ | $k_3=1.6(10^{-12})\exp(-940/T)$ |
| (4) $CH_3O_2 + NO \rightarrow NO_2 + CH_3O$ | $k_4=4.2(10^{-12})\exp(180/T)$ |
| (5) $O(^1D) + H_2O \rightarrow 2OH$ | $k_5=2.2(10^{-10})$ |
| (6) $CO + OH + O_2 \rightarrow CO_2 + HO_2$ | $k_6=1.5(10^{-13})(1+0.6P)$ |
| (7) $O(^1D) + O_2 \rightarrow O_2 + O(^3P)$ | $k_7=3.2(10^{-11})\exp(67/T)$ |
| (8) $O(^1D) + N_2 \rightarrow N_2 + O(^3P)$ | $k_8=1.8(101^{-11})\exp(107/T)$ |
| (9) $O_3 + h\nu \rightarrow O(^1D) + O_2$ | $j_9$ |
| (10) $CH_4 + OH + O_2 \rightarrow H_2O + CH_3O_2$ | $k_{10}=2.4(10^{-12})\exp(-1710/T)$ |
| (11) $CH_3O + O_2 \rightarrow H_2CO + HO_2$ | $k_{11}=8.4(10^{-14})\exp(-1200/T)$ |
| (12) $H_2CO + OH + O_2 \rightarrow H_2O + HO_2 + CO$ | $k_{12}=1.0(10^{-11})$ |
| (13) $H_2CO + h\nu \rightarrow 1/2(2HO_2 + H_2) + CO$ | $j_{13}=8.5(10^{-5})$ |
| (14) $HO_2 + HO_2 \rightarrow H_2O_2 + O_2$<br>$HO_2 + HO_2 + M \rightarrow H_2O_2 + O_2 + M$ | $k_{14}=2.3(10^{-13})\exp(590/T) +$<br>$1.7(10^{-33})\exp(1000/T)xM$ |
| (15) $H_2O_2 + h\nu \rightarrow 2OH$ | $j_{15}=1.0(10^{-5})$ |
| (16) $NO_2 + h\nu \rightarrow NO + O(^3P)$ | $j_{16}$ |
| (17) $O_3 + NO \rightarrow NO_2 + O_2$ | $k_{17}=1.8(10^{-12})\exp(-1370/T)$ |
| (18) $O(^3P) + O_2 \rightarrow O_3$ | $k_{18}=6.0(10^{-3})(T/300)^{-2.7}xM$ |
| (19) $OH + HO_2 \rightarrow H_2O + O_2$ | $k_{19}=1.0(10^{-11})(7+4P)$ |
| (20) $HO_2 + NO_2 + M \rightarrow HO_2NO_2 + M$ | $k_{20}=2.0(10^{-31})(T/300)^{-2.7}xM$ |
| (21) $HO_2NO_2 + M \rightarrow HO_2 + NO_2 + M$ | $k_{21}=k_{20}/(2.33(10^{-27})x$<br>$\exp(10870/T))$ |
| (22) $OH + NO_2 + M \rightarrow HNO_3 + M$ | $k_{22}=2.6(10^{-30})(T/300)^{-3.2}xM$ |
| (23) $CH_3O_2 + HO_2 \rightarrow CH_3OOH + O_2$ | $k_{23}=7.7(10^{-14})\exp(1300/T)$ |
| (24) $CH_3OOH + 1/2OH \rightarrow H_2O$<br>$+ 1/2H_2CO + 1/2CH_3O_2$ | $k_{24}=1.0(10^{-11})$ |
| (25) $H_2O_2 + OH \rightarrow H_2O + HO_2$ | $k_{25}=3.1(10^{-12})\exp(1300/T)$ |
| (26) $H_2O_2 \rightarrow$ rainout | $k_{26}=4.0(10^{-7})$ |

Source of rate constants is NASA (1985), except for reaction 26, which is estimated from a lifetime of one month.

and destruction. Pickering (1987) used a subset of the most important reactions (reactions 1-10 on Table 4), to derive an analytical solution to the $O_3$ production problem. The full set of reactions greatly complicates the steady state analysis that follows, and requires a numerical solution. Calculations were first done using the analytical model below. Then some results were compared to a complete numerical solution using a model recently developed by Pickering and Dickerson (1988, personal communication). (Note, reaction numbers refer to those in Table 4, not the previous text.) $O_3$ concentration changes according to the following:

$$d[O_3]/dt = [NO]\,([HO_2]k_1 + [RO_2]k_4) - [O(^1D)][H_2O]k_5 - [O_3]\,([HO_2]k_2 + [OH]k_3) \quad (6)$$

$HO_2$ concentration can be estimated from:

$$[HO_2] = \frac{k_6[CO][OH] + 2k_{10}[CH_4][OH]}{k_1[NO] + k_2[O_3]} \quad (7)$$

And the concentration of $RO_2$ can be approximated by:

$$[CH_3O_2] = \frac{k_{10}[CH_4][OH]}{k_4[NO]} \quad (8)$$

Also, OH concentration is estimated from the following:

$$[OH] = \frac{2k_8[O(^1D)][H_2O]}{k_6[CO]} \quad (9)$$

It remains to estimate the concentration of $O(^1D)$ by:

$$[O(^1D)] = \frac{j_9[O_3]}{k_7[O_2] + k_8[N_2] + k_5[H_2O]} \quad (10)$$

All that remains unknown is $j_9$, the photolysis rate of $O_3$ by radiation with wavelength less than 318 nm. This was measured and discussed by Dickerson et al. (1982). This quantity is highly variable, and is a function primarily of altitude, temperature, pressure, solar angle (and therefore time of day and year), aerosol loading, cloudiness,

total column ozone and surface albedo. Total column ozone was about 300 Du (from TOMS data). Tropospheric ozone was assumed to be 10 percent, and the effective ozone column density was calculated by dividing 300 Du minus a fraction of 10 percent, based on altitude, by the cosine of the solar zenith angle for the aircraft location and flight time. Figure 4 in Dickerson et al. (1982), a graph of effective ozone column density versus photolysis frequency for Boulder, Colorado in summer, shows that measurements and calculations from several sources fall close to a narrow band. This figure was assumed to be valid for this flight location as well. The photolysis frequency from this curve was increased to include the effect of upwelling radiation (or surface albedo) by multiplying by the net (upwelling plus downwelling) radiation and dividing by downwelling radiation (both components were measured on the Sabreliner with two Epply UV radiometers). The inclusion of upwelling radiation increased $j_e$ by about 20 percent in most cases, but went as high as a 55 percent increase at high altitude on the first flight.

Once $[O(^1D)]$ is estimated, one can estimate [OH], then $[HO_2]$ and $[RO_2]$, and calculate the net production of $O_3$.

The atmosphere was divided into layers to perform the vertical integration (see Figures 10 and 21). Layers were used because continuous data did not exist for all the species needed in the reaction scheme and estimates for smaller layers did not seem valid. This introduces error into the model as the product of two means is generally not the same as the mean of the products (Chameides et al.,

1987). All data measured within a layer were averaged without regard to exact altitude to obtain layer averages of temperature, pressure, CO, $O_3$ and $H_2O$ concentrations. For example, where many data in a layer were collected at a constant altitude, the variables may be biased to that level and are not corrected to better represent the center of the layer. When NO was not measured at all in a layer, 15 percent of $NO_x$ concentration was used. Liu et al. (1987) used a $[NO]/[NO_x]$ ratio of 1/3, based on measurements made by Williams et al. (1984) at Niwot Ridge. Their instrument did not have a PAN interference, nonetheless 15 percent is a conservative estimate. This estimate inputs substantial error into the calculation of $O_3$ production, as the production of $O_3$ goes up with the ratio $NO_2$ to NO. The tropospheric column production is an underestimate, since the troposphere above 10.5 km was not included in the calculation as it was not sampled. This is partially balanced by the PBL values, which may be too high, as no attempt was made to include surface loss of $O_3$.

Although NMHC concentrations are usually several orders of magnitude lower than that of $CH_4$, their effect on atmospheric chemistry is important because they react much more quickly than $CH_4$ (Greenberg and Zimmerman, 1984). Unlike the remote Pacific (Chameides et al., 1987), NMHC concentrations were significant in the free troposphere of the central US, and neglecting NMHCs can underestimate $O_3$ production (Liu et al., 1987). Estimates by Zimmermann et al. (1978) and Hanst et al. (1980), indicate the atmospheric breakdown of NMHCs from vegetation is a major source of atmospheric CO. No grab samples of hydrocarbons were collected during either flight on 22 June 1985,

but throughout the PRE-STORM Project twelve different samples were collected under various conditions and analyzed by J.P. Greenberg and P.R. Zimmerman of NCAR. The samples were analyzed using gas chromatography with a flame ionization detector, as discussed in Greenberg and Zimmerman (1984). Basically the technique consists of passing the sample through various analytical columns along with a carrier gas. Each hydrocarbon moves through the column at a different rate, and will show up as a peak on a chromatogram at a representative retention time. The mixing ratio can be inferred from the height of the peak or the area under the peak.

Using the measured hydrocarbon concentrations, the following simple scheme was used to approximate the effective methane concentration:

$$[CH_4]_{eff} = [CH_4] + \sum (n[C_nH] \times k_{cn}/k_{cH4}) \qquad (11)$$

Where $n[C_nH]$ indicates the concentration of a specific hydrocarbon multiplied by the number of carbon atoms it contains, $k_{cn}$ is the rate of reaction of that hydrocarbon with OH, and $k_{cH4}$ is the rate of reaction of $CH_4$ with OH. Table 5 lists the number of times each hydrocarbon was found in a sample and the rate constants used. The gas chromatography technique fails to detect NMHCs with more than 10 carbon atoms or oxygenated hydrocarbons (Liu et al., 1987) The assumption is that the hydrogen atom extraction is the rate determining step, and after that the rest of the molecule reacts almost instantaneously. Analysis of the initial results found that where propylene was detected, it had an extremely large effect on this calculation. The propylene reaction with the first OH is extremely

TABLE 5

HYDROCARBON ANALYSIS

| SPECIES | NUMBER OF SAMPLES | RATE CONSTANT |
|---|---|---|
| Methane | 12 | $8.0(10^{-15})\exp(-1710/T)$ k |
| CO | 12 | n/a |
| Ethane | 12 | $1.1(10^{-11})\exp(-1090/T)$ n |
| Ethylene | 9 | $8.4(10^{-12})\exp(8.39/T)$ k |
| Acetylene | 10 | $2.0(10^{-12})\exp(-250/T)$ h |
| Propane | 12 | $1.6(10^{-11})\exp(-800/T)$ n |
| Propylene | 8 | see below e,k |
| Isobutane | 11 | $2.4(10^{-12})\exp(-390/T)$ k |
| N-Butane | 12 | $2.6(10^{-12})\exp(-560/T)$ k |
| Isopentane | 10 | $4.1(10^{-12})\exp(-530/T)$ e |
| Neopentane | 11 | $4.1(10^{-12})\exp(-530/T)$ e |
| N-Pentane | 12 | $4.1(10^{-12})\exp(-530/T)$ k |
| Isoprene | 2 | $9.9(10^{-11})\exp(500/T)$ k |
| 1-Pentene | 2 | $10^{-10}$ e |
| Neohexane | 10 | $5.7(10^{-12})\exp(-530/T)$ e |
| 4-Me-1-Pentene | 4 | $10^{-10}$ e |
| 2-Me-Pentane | 10 | $5.7(10^{-12})\exp(-530/T)$ e |
| 3-Me-Pentane | 9 | $5.7(10^{-12})\exp(-530/T)$ e |
| 1-Hexene | 3 | $10^{-10}$ e |
| N-Hexane | 11 | $5.7(10^{-12})\exp(-530/T)$ k |
| Benzene | 12 | $7.57(10^{-12})\exp(-529/T)$ p |
| Cyclohexane | 9 | $5.7(10^{-12})\exp(-530/T)$ e |
| 2,4Di-Me-Pentane | 1 | $7.3(10^{-12})\exp(-530/T)$ e |
| 3-Me-Hexane | 1 | $7.3(10^{-12})\exp(-530/T)$ e |
| 2,3-Di-Me-Pentane | 2 | $7.3(10^{-12})\exp(-530/T)$ e |
| 1-Heptene | 3 | $10^{-10}$ e |
| N-Heptane | 9 | $7.3(10^{-12})\exp(-530/T)$ k |
| Me-Cyclohexane | 7 | $7.3(10^{-12})\exp(-530/T)$ e |
| Toluene | 10 | $10^{-10}$ e |
| 2,2,4Tri-Me-Pentane | 2 | $9.0(10^{-12})\exp(-530/T)$ e |
| 2,3,4Tri-Me-Pentane | 1 | $9.0(10^{-12})\exp(-530/T)$ e |
| 3-Me-Heptane | 2 | $9.0(10^{-12})\exp(-530/T)$ e |
| N-Octane | 8 | $9.0(10^{-10})\exp(-530/T)$ k |
| 1-Octene | 6 | $10^{-10}$ e |
| Ethyl-Benzene | 2 | $10^{-11}$ e |
| P-Xylene | 4 | $2.4(10^{-11})$ k |
| M-Xylene | 1 | $2.4(10^{-11})$ k |
| O-Xylene | 3 | $2.4(10^{-11})$ k |
| 1-Nonene | 7 | $10^{-10}$ e |
| N-Nonane | 9 | $10^{-11}$ e |
| Isopropylbenzene | 2 | $10^{-10}$ e |
| N-Propyl-Benzene | 3 | $10^{-10}$ e |
| 1,3,5-Tri-Me-Tol | 2 | $10^{-11}$ e |
| 1-Decene | 1 | $10^{-10}$ e |
| N-Decane | 8 | $10^{-11}$ e |
| Alpha-Pinene | 1 | $5.6(10^{-11})$ k |
| Beta-Pinene | 2 | $10^{-10}$ e |
| Delta-3-Carene | 3 | $10^{-10}$ e |

| | | |
|---|---|---|
| Delta-4-Carene | 1 | $10^{-10}$ e |
| Betaphellandrene | 3 | $10^{-10}$ e |
| Myrcene | 1 | $10^{-10}$ e |
| Butanal | 6 | $2.5(10^{-11})\exp(250/T)$ k |
| Pentanal | 9 | $1.6(10^{-11})\exp(260/T)$ k |
| Hexanal | 6 | $10^{-11}$ e |
| 3-Heptanone | 3 | $10^{-11}$ e |
| Heptanal | 8 | $10^{-11}$ e |
| Octanal | 2 | $10^{-11}$ e |
| Methychloroform | 12 | $5.4(10^{-12})\exp(-1820/T)$ h |

e - estimated
k - Kerr and Calvert (1984)
h - Hampson (1980)
p - Finlayson-Pitts and Pitts (1986)
n - NASA (1985)
(Rate constant for propylene used : $1/3[1.6(10^{-11})\exp(260/T) + 10^{-11} + 2.9(10^{-11})\exp(540/T)]$)

fast (better than $2(10^{-10})$ $s^{-1}$ at room temperature and pressure). It was decided to slow the breakdown rate by averaging this rate with the breakdown rates of two possible stable intermediates; this is the rate given for propylene as a footnote to Table 5.

The total NMHC concentrations and the ratios of effective methane to measured methane concentration are listed for each sample in Table 6. The smallest ratio was 1.8 for a very clean sample and the largest was a tremendous 549 from an extremely dirty sample.

Certainly this scheme is an over simplification. Exact calculations of the effect of NMHCs would require a detailed scheme of the complete breakdown rate of each hydrocarbon, checking especially for stable intermediates. Also, some NMHCs may breakdown to $CO_2$ without becoming CO. Nevertheless, this exercise suggests their effect is far from negligible in increasing $[CH_4]_{eff}$. The ratios showed tremendous variation, but were not correlated with altitude or CO concentration. Despite their relatively short lifetimes, NMHCs were observed at high enough concentrations in the free troposphere to greatly increase $[CH_4]_{eff}$ in most samples. Most hydrocarbons have longer lifetimes at the lower temperatures and pressures at high altitudes. Some past studies only included the effect of NMHCs on PBL $O_3$ production (Vukavich et al., 1985; Trainer et al., 1987). Data suggest that NMHCs may effect $O_3$ production throughout the free troposphere when they escape the PBL by means such as convection.

Methane concentrations, because of its long atmospheric lifetime,

## TABLE 6

## EFFECTIVE METHANE CALCULATION

| SAMPLE | ALTITUDE (km) | TOTAL NMHC (ppbC) | $[CH_4]_{eff}/[CH_4]$ | [CO] (ppb) | $[CH_4]$ (ppm) |
|---|---|---|---|---|---|
| 1011 | 10.7 | 7.2 | 1.8 | 85 | 1.69 |
| 1022 | 5.5 | 9.8 | 4.8 | 103 | 1.68 |
| 1043 | .9 | 18.9 | 12 | 122 | 1.71 |
| 1013 | 5.8 | 18.9 | 19 | 134 | 1.71 |
| 1049 | 2.4 | 15.7 | 21 | 94 | 1.65 |
| 1012 | 10.7 | 29.6 | 25 | 123 | 1.73 |
| 201 | .9 | 20.6 | 27 | 87 | 1.68 |
| 1006 | .9 | 26.7 | 57 | 202 | 1.96 |
| 200 | 10.1 | 5.8 | 64 | 108 | 1.66 |
| 1000 | 7.6 | 53.0 | 150 | 103 | 1.72 |
| 202 | 10.7 | 11.5 | 167 | 97 | 1.68 |
| 1042 | 6.7 | 80.3 | 549 | 118 | 1.68 |

are almost always close to 1.6 ppm in the troposphere. For the $O_3$ column production, it was decided to try three effective methane concentrations, 1.6 ppm (ignoring the effect of NMHCs), 2.9 ppm (a ratio of 1.8, equal to the cleanest case measured) and 120 ppm (a ratio of 75, but cleaner than the three dirtiest samples measured). The same $[CH_4]_{eff}$ was used in all four layers, and three calculations were done for each flight. It is reasonable to expect at least moderate values of man-made NMHCs in all layers of the first flight and the lowest two layers of the second flight; low level wind trajectories were from the south through southwest, bringing the air from the Gulf of Mexico through east Texas and Louisiana, which has many refineries and power plants. As reported in the 1980 NAPAP (National Air Pollution Assessment Program) emission inventories by Wagner et al. (1986), this region has high emissions of $NO_x$ and $SO_2$; which suggests accompanying high anthropogenic hydrocarbon emissions. As discussed, this low level air was mixed to the higher layers by convection.

In all six calculations, local photochemistry produced $O_3$ in every layer. Table 7 shows the net production rate in each layer and the sum for the column in each case.

Production during the later flight, as solar zenith angle was rapidly increasing, is less than 1/7 of that during the first flight, when the sun was nearly overhead. To make a rough estimate of the diurnal average production rates, the calculations were redone with zenith angle of 45 degrees, and the results were divided by two. The

TABLE 7

NET OZONE COLUMN PRODUCTION

Units : $10^{12}$ molec/($cm^2$s)

Flight 1

| $[CH_4]_{eff}$ (ppm) | 1.6 | 2.9 | 120. |
|---|---|---|---|
| Layer 1: | 3.3 | 5.4 | 200. |
| Layer 2: | 1.3 | 2.2 | 90. |
| Layer 3: | .75 | 1.2 | 42. |
| Layer 4: | .17 | .25 | 6.8 |
| Total: | 5.5 | 9.1 | 340. |
| Diurnal Average: | 1.8 | 2.9 | 110. |
| Numerical Model: | 1.0 | 1.3 | 4.2 |

Flight 2

| $[CH_4]_{eff}$ (ppm) | 1.6 | 2.9 | 120. |
|---|---|---|---|
| Layer 1: | .47 | .76 | 27. |
| Layer 2: | .19 | .31 | 12. |
| Layer 3: | .052 | .086 | 3.2 |
| Layer 4: | .024 | .037 | 1.2 |
| Total: | .73 | 1.2 | 43. |
| Diurnal Average: | 1.4 | 2.2 | 81. |
| Numerical Model: | 1.3 | 1.7 | 5.5 |

correction for upwelling radiation was not changed, which assumes the surface albedo is independent of zenith angle. The results of these calculations are also presented in Table 7.

To check the accuracy of this simple model, the diurnal averages were also calculated using the numerical model which includes the 26 reactions in Table 4. The model numerically solves the differential equations necessary to arrive at the $O_3$ production. One must make initial guesses of OH, $HO_2$, $CH_3O$, $H_2CO$, $CH_3O_2$, $O(^3P)$, $HO_2NO_2$, and $CH_3OOH$ concentration, but the model recalculates these quantities and seems to be stable to small changes of these input parameters. The greatest source of uncertainty in the model comes from the necessity to guess $NO_2$ concentration from the measurement of $NO_x$ (this is complicated by the PAN interference). At higher altitudes, more odd nitrogen would be expected to be in one of the reservoir species such as PAN than as $NO_2$, so I used a decreasing percentage with altitude of the layer average $NO_x$ to estimate $NO_2$ (60 percent in layer I, 50 percent in layer II, 40 percent in layer III, and 20 percent in layer IV). The photolysis rate of $NO_2$, $j_{16}$, was estimated from an equation based on zenith angle in Dickerson et al. (1982).

The results of the numerical model are also presented in Table 7. For the case with only $CH_4$, the results of the analytical and numerical solution agree quite well. At the higher $[CH_4]_{eff}$ ratios, the numerical solution tends to moderate the effect of high NMHCs. It appears high concentrations of NMHCs may increase net column $O_3$ production by a factor of 4 or 5 over that expected with only $CH_4$,

rather than by more than an order of magnitude as suggested by the analytical model.

The production estimates using the lowest two $[CH_4]_{eff}$ ratios are of about the same magnitude as the estimate given above by Liu et al. (1987) (sum of anthropogenic and natural production), who assumed no NMHCs in the free troposphere; inclusion of high NMHCs increases the column production by a factor of two to four over that estimated by Liu et al. (1987). These results are two orders of magnitude larger than the $O_3$ production calculated for the remote Pacific by Chameides et al. (1987). To get a feel for the importance of tropospheric production, $2(10^{12})$ molec/cm$^2$s in the mid-troposphere (600mb, 270K) corresponds to production of about 10 ppb/day. The average tropospheric $O_3$ concentration is around 50 ppb, so for the day sampled, tropospheric production of $O_3$ was significant.

# VI. SUMMARY AND CONCLUSIONS

This study presents some of the first aircraft data analyzed from flights over non-urban North America where $O_3$, CO and odd nitrogen were measured concurrently in the free troposphere. The two flights presented complement each other; the first shows a troposphere well mixed by recent convection, and the second shows a stable stratification several hours later. The flight area did not experience a frontal passage; low-level winds were from the south through southwest, shifting to westerly aloft for both flights.

Analysis of the first flight showed that immediately after intense convection, large areas (the flight traversed more than 500 km) of the atmosphere are disturbed by mesoscale mixing. The troposphere is not thoroughly mixed, but large volumes of air have been displaced vertically, resulting in profiles very different than those predicted by eddy diffusion. When there is a large amount of convection, horizontal variations will be large, otherwise vertical variations will predominate as on the second flight. The effects of thunderstorms and convection should not be ignored in models of tropospheric trace gas concentrations.

The depth of tropospheric air with concentrations typical of the PBL can be very deep (greater than 5 km), during summer in the Central US. Long-range transport is increased at these higher altitudes, and the lifetimes of $O_3$ precursors, such as $NO_y$, are greater. Like thunderstorms, the mechanism that causes this raised PBL has potential

to increase net tropospheric $O_3$ production.

A strong gradient in $O_3$, caused by neither tropopause fold or a thunderstorm, was observed at 10.6 km on the second flight in eastern Oklahoma. The mesoscale gradient was not correlated with CO or potential temperature, but was strongly correlated with winds, showing that synoptic scale dynamic phenomena causing confluence of air parcels can dramatically alter trace gas concentrations in the upper free troposphere.

Tropical tropospheric $O_3$ features studied by Fishman et al. (1986) were often the dominant features in the $TCo_3$. But in this case, analysis of TOMS data, after correction for the cloud compensation algorithm, failed to provide evidence to either support or refute whether the tropospheric $O_3$ features sampled on these missions caused the gradients in $TCo_3$ seen on TOMS imagery. The TOMS imagery can be used with other data to understand the large scale synoptic features; however, it must be used with caution. Over continental areas in summer, the cloud algorithm tends to underestimate the contribution of tropospheric $O_3$ by neglecting the very high cloud tops from thunderstorm activity and underestimating the background tropospheric $O_3$ concentration. As a result, clear areas will tend to show up as maxima, and cloudy areas as minima, where no real gradient exists. This effect should be considered when TOMS data are used for applications other than estimating total global column $O_3$ or comparing the dominant stratospheric features.

A simple photochemical model found in-situ production possible at all altitudes under the conditions measured on each flight. Net tropospheric column production without NMHCs was close to the estimate of Liu et al. (1987). Consideration of NMHCs in a simplified "effective $CH_4$" scheme shows that NMHCs have an effect on tropospheric $O_3$ production due to their strong reactivity, and increased production by a factor of two to four over Liu et al. (1987). Tropospheric production appeared to be an important source of tropospheric $O_3$ on this day, and was enhanced by the strong convective mixing of $O_3$ precursors and very deep PBL. NMHC concentrations were not correlated with altitude and high NMHC concentrations were measured above the PBL.

## APPENDIX A. DATA PROCESSING

Computer programs described by Pickering (1987) were used initially to process the minimally-processed data received on tape from NCAR. The output of these programs was reviewed and the data quality improved as described below.

### 1. Nitrogen Oxides

The raw data were processed by subtracting the recorded voltages from the baseline made by linearly interpolating between the average values of two consecutive backgrounds. Outgassing from the converters was checked by cycling zero air through the channels. Ideally, any deviations of the zero air from the background should be subtracted from the appropriate channel. It was determined that the zero air values were negligible, but there was enough noise in the zero air reading to cause high uncertainty in measurements near the detection limit. Due to the linear interpolation and the background noise, some of the NO values were calculated to be negative after the first processing. When this happened, the data were analyzed by hand, and corrections were made to account for any erroneously high voltages in the background or what appeared to be an obvious non-linear drop in background values when the instrument was still warming up. Positive, but small values were extracted for NO. Several strong spikes were eliminated from the analyzed data; most were $NO_y$, immediately after a mode change. One very sharp spike of NO (suspected to be caused by a faulty solenoid) on the second flight at 1809 CDT in clear air was eliminated as well. At the end of the second flight, during the

second penetration into the boundary layer, it was determined some zero air was getting into the sample flow. The measurements were not used for correlations or calculations. Before the first background and after the last background, the data were not processed.

2. Ozone

Little additional processing was required on the continuous $O_3$ data set. Some measurements at the beginning of each flight were ignored while the detector was warming up. Due to spiking in the data acquisition system, several points on each flight were cut: on the first flight near 1717 and 1806 CDT, and on the second flight near 1304 and 1454 CDT.

3. Carbon Monoxide

As with the nitrogen oxide detector, data had to be processed by subtracting the voltages from the baseline drawn between the average values of two consecutive backgrounds. A 30 second response time was assumed when processing the data to account for the time required to pump air through the detector ($O_3$ and odd nitrogen detection are nearly instantaneous). This lag was checked against $O_3$ and water vapor in cases where the Sabreliner was entering and leaving the boundary layer (ie., where a rapid change would be expected in each variable). The changes in the three variables showed a reasonable match.

For the first flight, data were eliminated near 1828, between 1834 and 1842, and after 1851 CDT. For the second flight, a spike in

one background, caused by a sudden change in aircraft attitude (Dickerson and Delany, 1988), was replaced with a more reasonable value so CO concentrations would be positive.

APPENDIX B

Average data for every 1 minute. Missing data is indicated by 0.0. The NO column contains NO (status 1.), NOx (status 2.) and NOy (status 3.).

FLIGHT 1

| HR | MIN | ALT (M) | LAT (DEG N) | LONG (DEG E) | TEMP (C) | TD (C) | WD (DEG) | WS (M/S) | O3 (PPB) | CO (PPB) | NO (PPT) | STAT |
|---|---|---|---|---|---|---|---|---|---|---|---|---|
| 12 | 19 | 363.1 | 0.00 | 0.00 | 30.2 | 17.7 | 0. | 0.0 | 0.0 | 0.0 | 0. | 0. |
| 12 | 20 | 418.8 | 0.00 | 0.00 | 27.8 | 20.0 | 210. | 4.2 | 0.0 | 0.0 | 0. | 0. |
| 12 | 21 | 990.5 | 35.34 | -97.60 | 21.8 | 18.0 | 189. | 5.2 | 21.5 | 0.0 | 0. | 0. |
| 12 | 22 | 1682.3 | 35.33 | -97.54 | 18.4 | 10.6 | 169. | 5.8 | 26.8 | 0.0 | 0. | 0. |
| 12 | 23 | 2263.9 | 35.35 | -97.46 | 15.9 | 6.3 | 142. | 3.0 | 32.6 | 0.0 | 0. | 0. |
| 12 | 24 | 2801.2 | 35.38 | -97.37 | 12.5 | 1.7 | 119. | 5.2 | 33.3 | 0.0 | 0. | 0. |
| 12 | 25 | 3485.3 | 35.39 | -97.28 | 8.2 | -5.7 | 51. | 4.5 | 46.1 | 0.0 | 0. | 0. |
| 12 | 26 | 4057.5 | 35.38 | -97.19 | 2.8 | -7.9 | 183. | 5.6 | 49.5 | 0.0 | 0. | 0. |
| 12 | 27 | 4568.4 | 35.36 | -97.08 | -1.5 | -7.6 | 330. | 5.6 | 46.4 | 0.0 | 0. | 0. |
| 12 | 28 | 4991.3 | 35.34 | -96.97 | -3.3 | -14.2 | 308. | 5.7 | 41.4 | 124.4 | 0. | 0. |
| 12 | 29 | 5480.0 | 35.34 | -96.88 | -5.0 | -22.0 | 245. | 4.1 | 31.1 | 113.1 | 0. | 0. |
| 12 | 30 | 5892.8 | 35.34 | -96.76 | -7.7 | -25.1 | 253. | 4.8 | 38.5 | 98.8 | 0. | 0. |
| 12 | 31 | 6140.3 | 35.32 | -96.65 | -10.1 | -26.9 | 325. | 5.6 | 42.7 | 93.5 | 0. | 0. |
| 12 | 32 | 6480.0 | 35.31 | -96.54 | -13.1 | -28.4 | 293. | 7.3 | 52.0 | 89.6 | 0. | 0. |
| 12 | 33 | 6872.3 | 35.30 | -96.44 | -16.3 | -26.2 | 277. | 8.2 | 63.9 | 91.2 | 0. | 0. |
| 12 | 34 | 7184.5 | 35.29 | -96.32 | -18.5 | -24.5 | 297. | 6.6 | 46.2 | 98.3 | 0. | 0. |
| 12 | 35 | 7406.7 | 35.28 | -96.19 | -20.1 | -25.4 | 291. | 7.0 | 42.9 | 99.2 | 0. | 0. |
| 12 | 36 | 7603.2 | 35.27 | -96.08 | -22.0 | -26.2 | 284. | 8.5 | 47.6 | 0.0 | 0. | 0. |
| 12 | 37 | 7595.8 | 35.23 | -95.96 | -22.1 | -26.0 | 288. | 8.3 | 46.3 | 0.0 | 0. | 0. |
| 12 | 38 | 7590.5 | 35.18 | -95.82 | -21.8 | -26.2 | 286. | 7.1 | 48.5 | 0.0 | 0. | 0. |
| 12 | 39 | 7840.7 | 35.14 | -95.71 | -23.5 | -27.3 | 294. | 8.2 | 48.8 | 92.4 | 0. | 0. |
| 12 | 40 | 8250.3 | 35.11 | -95.60 | -26.5 | -29.0 | 279. | 7.0 | 51.0 | 124.2 | 0. | 0. |
| 12 | 41 | 8502.3 | 35.10 | -95.46 | -27.4 | -31.9 | 261. | 8.5 | 56.0 | 121.3 | 0. | 0. |
| 12 | 42 | 8663.4 | 35.09 | -95.32 | -27.8 | -35.2 | 254. | 11.9 | 53.2 | 120.2 | 0. | 0. |
| 12 | 43 | 8829.8 | 35.08 | -95.21 | -29.1 | -38.0 | 254. | 12.8 | 48.9 | 125.4 | 0. | 0. |
| 12 | 44 | 8804.6 | 35.06 | -95.06 | -29.0 | -39.3 | 253. | 12.4 | 52.3 | 128.4 | 0. | 0. |
| 12 | 45 | 8810.6 | 35.04 | -94.92 | -29.3 | -37.3 | 259. | 11.1 | 54.8 | 116.3 | 0. | 0. |
| 12 | 46 | 8802.0 | 35.03 | -94.79 | -29.4 | -36.3 | 267. | 9.9 | 51.5 | 124.7 | 1964. | 3. |
| 12 | 47 | 8796.7 | 35.00 | -94.65 | -29.2 | -36.3 | 274. | 8.7 | 48.5 | 121.1 | 1497. | 3. |
| 12 | 48 | 8787.3 | 34.98 | -94.50 | -29.1 | -35.4 | 276. | 7.6 | 45.6 | 0.0 | 1612. | 3. |
| 12 | 49 | 8787.4 | 34.97 | -94.35 | -29.3 | -36.3 | 272. | 6.3 | 43.8 | 0.0 | 0. | 0. |
| 12 | 50 | 8794.0 | 34.95 | -94.22 | -29.4 | -36.5 | 275. | 7.6 | 47.0 | 0.0 | 0. | 0. |
| 12 | 51 | 8791.9 | 34.93 | -94.08 | -29.4 | -35.0 | 282. | 6.7 | 45.0 | 115.5 | 0. | 0. |
| 12 | 52 | 8792.9 | 34.91 | -93.93 | -29.4 | -35.6 | 290. | 5.4 | 45.3 | 92.6 | 87. | 1. |
| 12 | 53 | 8792.3 | 34.90 | -93.81 | -29.5 | -34.5 | 283. | 5.4 | 45.8 | 96.2 | 91. | 1. |
| 12 | 54 | 8791.4 | 34.88 | -93.68 | -29.5 | -34.2 | 253. | 6.6 | 41.5 | 93.6 | 155. | 1. |
| 12 | 55 | 8789.9 | 34.86 | -93.53 | -29.7 | -33.7 | 241. | 6.1 | 37.9 | 94.2 | 517. | 2. |
| 12 | 56 | 8796.6 | 34.85 | -93.40 | -29.9 | -33.9 | 244. | 8.3 | 38.4 | 92.4 | 626. | 2. |
| 12 | 57 | 8804.1 | 34.83 | -93.26 | -30.0 | -33.5 | 243. | 9.7 | 39.6 | 88.0 | 1064. | 2. |
| 12 | 58 | 9047.4 | 34.82 | -93.13 | -30.9 | -34.3 | 265. | 10.4 | 39.6 | 96.6 | 1593. | 3. |
| 12 | 59 | 9460.7 | 34.81 | -92.99 | -33.9 | -39.1 | 269. | 15.8 | 38.4 | 104.4 | 1281. | 3. |
| 13 | 0 | 9752.6 | 34.79 | -92.88 | -36.6 | -42.5 | 272. | 19.9 | 43.1 | 0.0 | 1174. | 3. |
| 13 | 1 | 9955.0 | 34.78 | -92.78 | -38.9 | -42.9 | 266. | 20.6 | 39.5 | 0.0 | 0. | 0. |
| 13 | 2 | 10040.6 | 34.77 | -92.65 | -39.9 | -43.8 | 268. | 21.6 | 39.2 | 0.0 | 0. | 0. |
| 13 | 3 | 10024.4 | 34.75 | -92.53 | -39.8 | -44.5 | 270. | 19.2 | 38.2 | 102.5 | 0. | 0. |
| 13 | 4 | 10029.0 | 34.74 | -92.42 | -39.8 | -44.1 | 265. | 17.3 | 38.3 | 111.6 | 588. | 1. |
| 13 | 5 | 10021.5 | 34.72 | -92.28 | -39.9 | -43.2 | 262. | 17.8 | 35.7 | 104.6 | 688. | 1. |
| 13 | 6 | 10012.6 | 34.70 | -92.14 | -40.3 | -42.8 | 271. | 12.8 | 39.2 | 101.3 | 305. | 1. |
| 13 | 7 | 10004.6 | 34.67 | -92.01 | -40.4 | -43.3 | 282. | 10.4 | 49.3 | 91.7 | 548. | 2. |
| 13 | 8 | 10274.0 | 34.64 | -91.89 | -41.8 | -45.7 | 302. | 17.7 | 48.5 | 115.8 | 480. | 2. |
| 13 | 9 | 10611.4 | 34.61 | -91.76 | -44.6 | -49.8 | 293. | 24.7 | 44.3 | 116.2 | 651. | 2. |
| 13 | 10 | 10634.4 | 34.59 | -91.63 | -45.1 | -50.9 | 279. | 23.4 | 46.5 | 102.6 | 1754. | 3. |
| 13 | 11 | 10632.9 | 34.58 | -91.50 | -45.2 | -52.2 | 277. | 18.5 | 42.8 | 121.1 | 1279. | 3. |
| 13 | 12 | 10631.6 | 34.57 | -91.36 | -45.3 | -53.2 | 271. | 16.7 | 45.4 | 0.0 | 1168. | 3. |
| 13 | 13 | 10626.4 | 34.55 | -91.22 | -45.5 | -51.0 | 280. | 16.7 | 45.4 | 0.0 | 0. | 0. |
| 13 | 14 | 10625.7 | 34.53 | -91.10 | -45.5 | -50.5 | 293. | 19.0 | 53.8 | 0.0 | 0. | 0. |
| 13 | 15 | 10620.4 | 34.50 | -90.97 | -45.7 | -50.9 | 298. | 17.3 | 54.1 | 112.3 | 0. | 0. |
| 13 | 16 | 10613.5 | 34.47 | -90.84 | -45.7 | -51.4 | 305. | 15.0 | 56.0 | 99.2 | 884. | 1. |
| 13 | 17 | 10615.4 | 34.44 | -90.69 | -45.7 | -52.3 | 308. | 15.0 | 55.2 | 114.6 | 918. | 1. |
| 13 | 18 | 10613.1 | 34.41 | -90.56 | -45.9 | -53.5 | 311. | 14.7 | 53.3 | 119.4 | 700. | 1. |
| 13 | 19 | 10612.0 | 34.38 | -90.42 | -45.8 | -53.7 | 310. | 14.0 | 55.2 | 126.5 | 1047. | 2. |

| | | | | | | | | | | | | |
|---|---|---|---|---|---|---|---|---|---|---|---|---|
| 13 | 20 | 10599.8 | 34.35 | -90.28 | -45.6 | -54.1 | 273. | 21.4 | 54.1 | 127.2 | 1025. | 2. |
| 13 | 21 | 10618.7 | 34.26 | -90.24 | -45.5 | -54.5 | 309. | 32.5 | 52.0 | 130.4 | 0. | 0. |
| 13 | 22 | 10610.2 | 34.21 | -90.33 | -45.7 | -54.5 | 144. | 21.7 | 53.1 | 123.2 | 2036. | 3. |
| 13 | 23 | 10628.2 | 34.24 | -90.46 | -45.9 | -54.5 | 288. | 5.3 | 54.6 | 121.9 | 1940. | 3. |
| 13 | 24 | 10640.2 | 34.29 | -90.57 | -46.2 | -54.5 | 344. | 6.2 | 52.8 | 0.0 | 1939. | 3. |
| 13 | 25 | 10641.2 | 34.34 | -90.68 | -46.2 | -54.5 | 340. | 5.6 | 53.3 | 0.0 | 0. | 0. |
| 13 | 26 | 10625.0 | 34.39 | -90.80 | -46.2 | -53.2 | 335. | 6.3 | 54.3 | 0.0 | 0. | 0. |
| 13 | 27 | 10358.4 | 34.44 | -90.93 | -43.9 | -50.5 | 318. | 7.3 | 57.2 | 130.4 | 0. | 0. |
| 13 | 28 | 10021.3 | 34.47 | -91.04 | -41.0 | -46.3 | 318. | 10.1 | 58.4 | 109.9 | 0. | 0. |
| 13 | 29 | 9759.9 | 34.49 | -91.17 | -38.4 | -37.2 | 289. | 7.1 | 40.9 | 106.0 | 0. | 0. |
| 13 | 30 | 9420.0 | 34.51 | -91.29 | -35.2 | -36.5 | 294. | 6.3 | 44.5 | 99.4 | 0. | 0. |
| 13 | 31 | 9434.5 | 34.53 | -91.42 | -34.9 | -38.8 | 283. | 7.6 | 42.4 | 88.2 | 931. | 2. |
| 13 | 32 | 9431.5 | 34.56 | -91.53 | -34.8 | -39.7 | 285. | 6.5 | 41.9 | 93.9 | 645. | 2. |
| 13 | 33 | 9433.3 | 34.58 | -91.66 | -35.3 | -43.4 | 282. | 6.8 | 49.9 | 110.1 | 501. | 2. |
| 13 | 34 | 9429.6 | 34.61 | -91.78 | -35.3 | -39.3 | 275. | 7.8 | 55.5 | 96.2 | 1734. | 3. |
| 13 | 35 | 9429.6 | 34.63 | -91.90 | -35.3 | -40.0 | 277. | 8.6 | 54.0 | 105.5 | 1210. | 3. |
| 13 | 36 | 9418.8 | 34.65 | -92.01 | -35.3 | -37.6 | 268. | 8.6 | 37.3 | 0.0 | 788. | 3. |
| 13 | 37 | 9433.2 | 34.67 | -92.13 | -35.1 | -38.2 | 277. | 11.4 | 43.0 | 0.0 | 0. | 0. |
| 13 | 38 | 9432.2 | 34.75 | -92.17 | -35.1 | -38.6 | 257. | 9.1 | 42.6 | 0.0 | 0. | 0. |
| 13 | 39 | 9429.6 | 34.79 | -92.06 | -35.1 | -38.7 | 245. | 13.1 | 38.9 | 115.3 | 0. | 0. |
| 13 | 40 | 9426.6 | 34.75 | -91.94 | -35.0 | -38.4 | 264. | 12.0 | 42.0 | 93.5 | 215. | 1. |
| 13 | 41 | 9436.4 | 34.68 | -91.83 | -35.2 | -38.6 | 277. | 8.9 | 52.2 | 96.0 | 207. | 1. |
| 13 | 42 | 9437.4 | 34.62 | -91.74 | -35.3 | -40.4 | 284. | 7.7 | 58.3 | 90.4 | 397. | 1. |
| 13 | 43 | 9435.4 | 34.57 | -91.63 | -35.2 | -39.9 | 298. | 7.7 | 54.8 | 96.5 | 478. | 2. |
| 13 | 44 | 9427.8 | 34.55 | -91.49 | -34.8 | -41.0 | 284. | 5.6 | 46.5 | 93.7 | 799. | 2. |
| 13 | 45 | 9405.8 | 34.51 | -91.36 | -34.4 | -37.6 | 289. | 5.9 | 43.5 | 107.9 | 2114. | 2. |
| 13 | 46 | 9065.8 | 34.48 | -91.25 | -32.4 | -34.3 | 275. | 7.1 | 44.6 | 96.9 | 2196. | 3. |
| 13 | 47 | 8324.0 | 34.40 | -91.24 | -27.2 | -31.0 | 205. | 6.3 | 42.8 | 96.2 | 2332. | 3. |
| 13 | 48 | 7919.9 | 34.40 | -91.35 | -23.3 | -25.7 | 277. | 8.2 | 45.3 | 0.0 | 1422. | 3. |
| 13 | 49 | 7930.8 | 34.43 | -91.45 | -23.2 | -25.5 | 273. | 6.2 | 46.7 | 0.0 | 0. | 0. |
| 13 | 50 | 7927.6 | 34.48 | -91.54 | -23.3 | -26.2 | 277. | 5.4 | 43.8 | 0.0 | 0. | 0. |
| 13 | 51 | 7931.4 | 34.53 | -91.64 | -23.3 | -26.2 | 259. | 3.1 | 47.3 | 105.3 | 0. | 0. |
| 13 | 52 | 7937.9 | 34.57 | -91.75 | -23.3 | -26.9 | 287. | 6.0 | 47.6 | 98.7 | 136. | 1. |
| 13 | 53 | 7940.6 | 34.60 | -91.85 | -23.2 | -26.3 | 263. | 8.6 | 45.3 | 102.3 | 174. | 1. |
| 13 | 54 | 7923.8 | 34.63 | -91.97 | -23.1 | -25.7 | 265. | 10.4 | 41.0 | 100.9 | 274. | 1. |
| 13 | 55 | 7930.5 | 34.65 | -92.08 | -23.1 | -25.9 | 262. | 11.3 | 44.8 | 102.3 | 626. | 2. |
| 13 | 56 | 7935.3 | 34.67 | -92.18 | -23.3 | -26.4 | 260. | 11.6 | 50.5 | 107.8 | 533. | 2. |
| 13 | 57 | 7936.2 | 34.69 | -92.28 | -23.2 | -26.8 | 254. | 11.3 | 49.1 | 106.4 | 622. | 2. |
| 13 | 58 | 7931.5 | 34.71 | -92.39 | -23.4 | -27.2 | 275. | 10.4 | 46.1 | 118.9 | 2505. | 3. |
| 13 | 59 | 7938.8 | 34.72 | -92.50 | -23.9 | -26.1 | 264. | 10.0 | 43.0 | 98.2 | 1828. | 3. |
| 14 | 0 | 7943.0 | 34.75 | -92.60 | -23.9 | -26.5 | 252. | 9.2 | 46.1 | 0.0 | 1513. | 3. |
| 14 | 1 | 7935.7 | 34.76 | -92.72 | -23.6 | -26.5 | 239. | 10.1 | 46.0 | 0.0 | 0. | 0. |
| 14 | 2 | 7934.3 | 34.78 | -92.83 | -23.7 | -26.7 | 252. | 9.0 | 47.1 | 0.0 | 0. | 0. |
| 14 | 3 | 7924.3 | 34.80 | -92.94 | -23.7 | -26.7 | 246. | 10.3 | 51.3 | 0.0 | 0. | 0. |
| 14 | 4 | 7737.1 | 34.82 | -93.04 | -22.3 | -26.6 | 278. | 8.6 | 54.2 | 108.8 | 62. | 1. |
| 14 | 5 | 7380.5 | 34.84 | -93.16 | -20.3 | -23.7 | 315. | 10.2 | 54.0 | 107.0 | 57. | 1. |
| 14 | 6 | 7123.4 | 34.86 | -93.27 | -18.4 | -22.0 | 302. | 10.1 | 52.8 | 107.5 | 44. | 1. |
| 14 | 7 | 6537.0 | 34.88 | -93.37 | -14.6 | -22.4 | 284. | 13.5 | 51.3 | 110.2 | 170. | 2. |
| 14 | 8 | 5935.2 | 34.90 | -93.47 | -10.6 | -21.5 | 279. | 14.2 | 47.3 | 99.3 | 109. | 2. |
| 14 | 9 | 5493.3 | 34.93 | -93.58 | -7.9 | -16.4 | 282. | 12.6 | 47.0 | 105.8 | 191. | 2. |
| 14 | 10 | 5473.1 | 34.95 | -93.67 | -8.2 | -10.7 | 280. | 15.5 | 47.7 | 99.5 | 267. | 2. |
| 14 | 11 | 5469.1 | 34.97 | -93.76 | -7.7 | -11.0 | 281. | 16.0 | 45.1 | 103.4 | 0. | 0. |
| 14 | 12 | 5465.5 | 34.99 | -93.86 | -7.1 | -11.8 | 276. | 15.2 | 45.3 | 0.0 | 0. | 0. |
| 14 | 13 | 5482.1 | 35.01 | -93.96 | -6.8 | -12.6 | 281. | 13.7 | 47.1 | 0.0 | 0. | 0. |
| 14 | 14 | 5475.7 | 35.03 | -94.06 | -6.8 | -12.7 | 283. | 12.9 | 47.0 | 0.0 | 0. | 0. |
| 14 | 15 | 5475.1 | 35.06 | -94.16 | -7.1 | -12.6 | 288. | 11.3 | 48.8 | 0.0 | 0. | 0. |
| 14 | 16 | 5473.1 | 35.08 | -94.27 | -6.6 | -13.3 | 295. | 9.7 | 49.4 | 89.5 | 0. | 0. |
| 14 | 17 | 5479.0 | 35.10 | -94.36 | -6.1 | -16.7 | 303. | 9.8 | 46.6 | 90.4 | 0. | 0. |
| 14 | 18 | 5479.6 | 35.12 | -94.46 | -6.5 | -19.6 | 294. | 9.7 | 58.1 | 92.8 | 0. | 0. |
| 14 | 19 | 5476.8 | 35.14 | -94.57 | -6.3 | -27.3 | 293. | 9.8 | 68.2 | 116.7 | 0. | 0. |
| 14 | 20 | 5462.4 | 35.15 | -94.69 | -6.2 | -28.6 | 293. | 8.5 | 68.3 | 142.5 | 0. | 0. |
| 14 | 21 | 5467.1 | 35.15 | -94.79 | -6.4 | -32.7 | 305. | 8.4 | 78.1 | 148.2 | 0. | 0. |
| 14 | 22 | 5464.0 | 35.15 | -94.90 | -6.4 | -34.2 | 322. | 7.7 | 86.8 | 145.6 | 0. | 0. |
| 14 | 23 | 5479.1 | 35.15 | -95.01 | -6.5 | -34.1 | 313. | 6.4 | 79.7 | 137.3 | 0. | 0. |
| 14 | 24 | 5463.2 | 35.13 | -95.11 | -6.5 | -33.7 | 318. | 6.0 | 59.3 | 0.0 | 0. | 0. |
| 14 | 25 | 5462.6 | 35.10 | -95.22 | -6.4 | -31.5 | 318. | 5.7 | 49.9 | 0.0 | 0. | 0. |
| 14 | 26 | 5468.6 | 35.08 | -95.33 | -6.4 | -31.9 | 313. | 5.4 | 46.4 | 0.0 | 0. | 0. |
| 14 | 27 | 5463.7 | 35.06 | -95.44 | -7.1 | -20.4 | 310. | 5.5 | 42.9 | 0.0 | 0. | 0. |
| 14 | 28 | 5471.3 | 35.04 | -95.55 | -7.0 | -20.0 | 319. | 5.6 | 43.8 | 120.3 | 0. | 0. |

| | | | | | | | | | | | | |
|---|---|---|---|---|---|---|---|---|---|---|---|---|
| 14 | 29 | 5462.3 | 35.03 | -95.67 | -6.8 | -16.9 | 312. | 6.1 | 45.7 | 78.9 | 46. | 1. |
| 14 | 30 | 5467.7 | 35.02 | -95.78 | -6.5 | -17.5 | 318. | 5.7 | 45.5 | 80.9 | 39. | 1. |
| 14 | 31 | 5461.7 | 35.01 | -95.89 | -6.5 | -17.3 | 315. | 5.0 | 46.1 | 75.0 | 0. | 0. |
| 14 | 32 | 5465.0 | 35.00 | -95.99 | -6.6 | -16.3 | 313. | 5.7 | 45.4 | 81.3 | 0. | 0. |
| 14 | 33 | 5430.7 | 34.99 | -96.11 | -6.2 | -17.3 | 316. | 4.7 | 45.4 | 87.6 | 0. | 0. |
| 14 | 34 | 5208.8 | 34.98 | -96.23 | -5.1 | -13.6 | 249. | 1.9 | 48.1 | 84.1 | 181. | 2. |
| 14 | 35 | 4969.0 | 34.98 | -96.33 | -3.5 | -13.9 | 281. | 2.4 | 49.6 | 96.5 | 169. | 2. |
| 14 | 36 | 4640.4 | 34.98 | -96.44 | -2.0 | -14.5 | 339. | 6.9 | 56.9 | 0.0 | 277. | 2. |
| 14 | 37 | 4292.2 | 35.00 | -96.53 | -0.2 | -17.4 | 219. | 5.8 | 66.2 | 0.0 | 279. | 2. |
| 14 | 38 | 3851.2 | 35.02 | -96.62 | 2.9 | -12.9 | 43. | 5.1 | 72.0 | 0.0 | 461. | 2. |
| 14 | 39 | 3372.4 | 35.04 | -96.71 | 7.2 | -8.9 | 82. | 6.0 | 73.6 | 121.7 | 466. | 2. |
| 14 | 40 | 2980.6 | 35.07 | -96.81 | 10.1 | -1.7 | 107. | 7.8 | 64.7 | 139.6 | 449. | 2. |
| 14 | 41 | 2552.2 | 35.10 | -96.90 | 13.8 | 2.1 | 119. | 7.3 | 53.1 | 111.2 | 422. | 2. |
| 14 | 42 | 2160.9 | 35.13 | -96.99 | 15.3 | 5.9 | 126. | 5.0 | 49.4 | 95.0 | 580. | 2. |
| 14 | 43 | 1728.0 | 35.17 | -97.08 | 16.5 | 9.9 | 142. | 5.2 | 50.6 | 110.7 | 684. | 2. |
| 14 | 44 | 1183.4 | 35.20 | -97.16 | 19.1 | 16.1 | 157. | 6.4 | 45.9 | 135.7 | 1087. | 2. |
| 14 | 45 | 860.5 | 35.23 | -97.23 | 22.3 | 18.4 | 170. | 6.4 | 38.1 | 139.8 | 1371. | 2. |
| 14 | 46 | 862.2 | 35.25 | -97.30 | 22.3 | 18.2 | 166. | 7.0 | 36.5 | 117.8 | 863. | 2. |
| 14 | 47 | 869.4 | 35.27 | -97.38 | 22.5 | 18.5 | 156. | 6.7 | 45.8 | 130.5 | 670. | 2. |
| 14 | 48 | 870.0 | 35.32 | -97.44 | 22.6 | 19.5 | 158. | 7.4 | 48.5 | 0.0 | 728. | 2. |
| 14 | 49 | 873.6 | 35.38 | -97.47 | 23.1 | 18.9 | 155. | 6.5 | 47.9 | 0.0 | 0. | 0. |
| 14 | 50 | 863.5 | 35.44 | -97.51 | 23.5 | 18.5 | 157. | 6.2 | 50.5 | 0.0 | 0. | 0. |
| 14 | 51 | 787.1 | 35.46 | -97.57 | 24.4 | 18.4 | 155. | 6.0 | 46.7 | 0.0 | 0. | 0. |
| 14 | 52 | 763.9 | 35.45 | -97.62 | 24.7 | 18.4 | 155. | 6.3 | 41.5 | 0.0 | 0. | 0. |
| 14 | 53 | 545.4 | 35.42 | -97.60 | 26.7 | 18.5 | 148. | 7.0 | 45.0 | 0.0 | 0. | 0. |
| 14 | 54 | 368.5 | 35.40 | -97.59 | 29.8 | 19.6 | 249. | 2.9 | 42.9 | 0.0 | 0. | 0. |
| 14 | 55 | 365.4 | 0.00 | 0.00 | 30.9 | 19.7 | 0. | 0.0 | 44.6 | 0.0 | 0. | 0. |

FLIGHT 2

| HR | MIN | ALT (M) | LAT (DEG N) | LONG (DEG E) | TEMP (C) | TD (C) | WD (DEG) | WS (M/S) | O3 (PPB) | CO (PPB) | NO (PPT) | STAT |
|---|---|---|---|---|---|---|---|---|---|---|---|---|
| 17 | 3 | 368.0 | 35.40 | -97.61 | 31.8 | 18.3 | 0. | 0.0 | 32.8 | 0.0 | 0. | 0. |
| 17 | 4 | 368.4 | 35.41 | -97.61 | 31.0 | 19.3 | 0. | 0.0 | 32.6 | 0.0 | 0. | 0. |
| 17 | 5 | 368.8 | 35.41 | -97.60 | 31.1 | 20.2 | 0. | 0.0 | 32.5 | 0.0 | 0. | 0. |
| 17 | 6 | 369.8 | 35.41 | -97.60 | 30.7 | 20.3 | 0. | 0.0 | 29.0 | 0.0 | 0. | 0. |
| 17 | 7 | 515.1 | 35.39 | -97.60 | 28.3 | 20.2 | 147. | 6.4 | 22.6 | 0.0 | 0. | 0. |
| 17 | 8 | 1159.5 | 35.35 | -97.57 | 22.3 | 18.2 | 161. | 6.6 | 32.9 | 0.0 | 0. | 0. |
| 17 | 9 | 1919.1 | 35.36 | -97.50 | 16.1 | 12.0 | 171. | 8.6 | 34.2 | 0.0 | 0. | 0. |
| 17 | 10 | 2472.3 | 35.38 | -97.42 | 14.1 | 4.2 | 164. | 5.9 | 38.6 | 0.0 | 0. | 0. |
| 17 | 11 | 3212.1 | 35.39 | -97.32 | 10.2 | -3.1 | 143. | 5.3 | 47.9 | 0.0 | 0. | 0. |
| 17 | 12 | 3968.3 | 35.39 | -97.22 | 4.1 | -4.7 | 266. | 3.5 | 46.7 | 0.0 | 0. | 0. |
| 17 | 13 | 4428.1 | 35.37 | -97.14 | 1.6 | -13.7 | 341. | 9.6 | 44.5 | 0.0 | 0. | 0. |
| 17 | 14 | 4880.0 | 35.35 | -97.04 | -1.4 | -17.3 | 341. | 8.8 | 44.4 | 0.0 | 0. | 0. |
| 17 | 15 | 5469.5 | 35.34 | -96.93 | -5.3 | -22.0 | 319. | 3.3 | 33.0 | 0.0 | 0. | 0. |
| 17 | 16 | 5837.9 | 35.33 | -96.83 | -8.6 | -25.0 | 303. | 2.9 | 33.2 | 92.1 | 0. | 0. |
| 17 | 17 | 6170.9 | 35.32 | -96.74 | -11.3 | -27.3 | 327. | 2.8 | 40.2 | 96.0 | 0. | 0. |
| 17 | 18 | 6616.3 | 35.31 | -96.62 | -14.5 | -29.3 | 92. | 4.9 | 42.2 | 94.5 | 0. | 0. |
| 17 | 19 | 6976.8 | 35.29 | -96.50 | -17.7 | -31.2 | 93. | 5.1 | 37.1 | 107.1 | 0. | 0. |
| 17 | 20 | 7001.9 | 35.28 | -96.40 | -18.5 | -33.2 | 330. | 5.3 | 43.9 | 96.4 | 0. | 0. |
| 17 | 21 | 6994.3 | 35.27 | -96.28 | -18.6 | -33.2 | 346. | 6.2 | 46.3 | 100.2 | 0. | 0. |
| 17 | 22 | 6989.5 | 35.25 | -96.15 | -18.5 | -29.7 | 343. | 6.6 | 46.3 | 96.3 | 0. | 0. |
| 17 | 23 | 6986.4 | 35.24 | -96.02 | -18.4 | -29.7 | 340. | 6.7 | 47.6 | 94.8 | 0. | 0. |
| 17 | 24 | 6983.7 | 35.22 | -95.90 | -18.3 | -29.9 | 342. | 6.5 | 48.4 | 0.0 | 0. | 0. |
| 17 | 25 | 6983.9 | 35.21 | -95.78 | -18.3 | -32.4 | 337. | 6.2 | 44.8 | 0.0 | 0. | 0. |
| 17 | 26 | 6989.9 | 35.16 | -95.68 | -18.0 | -37.2 | 347. | 4.9 | 47.6 | 0.0 | 0. | 0. |
| 17 | 27 | 6996.1 | 35.08 | -95.70 | -17.7 | -39.0 | 349. | 5.6 | 49.7 | 79.4 | 93. | 1. |
| 17 | 28 | 7002.3 | 35.06 | -95.81 | -17.9 | -39.4 | 353. | 5.5 | 50.0 | 90.3 | 109. | 1. |
| 17 | 29 | 7012.3 | 34.99 | -95.87 | -18.1 | -39.7 | 38. | 4.7 | 46.2 | 85.5 | 0. | 0. |
| 17 | 30 | 6999.3 | 34.89 | -95.88 | -18.0 | -40.1 | 16. | 4.7 | 44.7 | 87.5 | 182. | 2. |
| 17 | 31 | 7002.6 | 34.80 | -95.90 | -17.9 | -40.4 | 18. | 5.1 | 47.0 | 91.5 | 165. | 2. |
| 17 | 32 | 6999.6 | 34.71 | -95.94 | -17.9 | -37.4 | 15. | 5.8 | 50.7 | 92.3 | 137. | 2. |
| 17 | 33 | 7017.7 | 34.68 | -96.04 | -18.2 | -25.6 | 9. | 5.7 | 55.8 | 103.0 | 2727. | 3. |
| 17 | 34 | 7005.3 | 34.75 | -96.07 | -18.4 | -34.0 | 18. | 6.5 | 46.2 | 95.7 | 1702. | 3. |
| 17 | 35 | 7016.1 | 34.84 | -96.07 | -18.5 | -40.8 | 17. | 7.0 | 44.0 | 0.0 | 938. | 3. |
| 17 | 36 | 7004.2 | 34.93 | -96.07 | -18.5 | -41.4 | 12. | 6.5 | 45.6 | 0.0 | 0. | 0. |
| 17 | 37 | 7002.7 | 35.01 | -96.02 | -18.6 | -41.5 | 8. | 6.6 | 49.1 | 0.0 | 0. | 0. |
| 17 | 38 | 7013.3 | 35.08 | -95.96 | -18.6 | -32.1 | 294. | 7.4 | 49.8 | 0.0 | 0. | 0. |
| 17 | 39 | 6989.7 | 35.15 | -95.89 | -18.6 | -29.6 | 351. | 6.7 | 50.1 | 77.5 | 31. | 1. |
| 17 | 40 | 6978.9 | 35.24 | -95.81 | -18.3 | -30.3 | 343. | 6.5 | 49.6 | 78.0 | 34. | 1. |

| | | | | | | | | | | | | |
|---|---|---|---|---|---|---|---|---|---|---|---|---|
| 17 | 41 | 7492.8 | 35.30 | -95.72 | -21.4 | -32.9 | 332. | 5.8 | 49.9 | 84.7 | 77. | 1. |
| 17 | 42 | 8063.7 | 35.28 | -95.63 | -24.3 | -30.2 | 285. | 6.6 | 57.5 | 95.7 | 245. | 2. |
| 17 | 43 | 8253.3 | 35.19 | -95.63 | -25.5 | -31.1 | 274. | 9.6 | 66.5 | 91.7 | 294. | 2. |
| 17 | 44 | 8695.9 | 35.09 | -95.65 | -27.9 | -35.2 | 250. | 12.6 | 67.7 | 99.6 | 379. | 2. |
| 17 | 45 | 8842.4 | 35.01 | -95.68 | -29.5 | -43.1 | 254. | 13.1 | 56.3 | 82.8 | 2723. | 3. |
| 17 | 46 | 8820.9 | 34.91 | -95.71 | -29.5 | -45.2 | 256. | 13.0 | 54.1 | 86.1 | 1324. | 3. |
| 17 | 47 | 8814.9 | 34.80 | -95.73 | -29.5 | -45.8 | 258. | 13.1 | 67.4 | 0.0 | 1142. | 3. |
| 17 | 48 | 8802.8 | 34.70 | -95.76 | -29.4 | -45.1 | 260. | 12.6 | 66.3 | 0.0 | 0. | 0. |
| 17 | 49 | 8788.9 | 34.63 | -95.84 | -29.3 | -45.9 | 263. | 12.5 | 66.1 | 0.0 | 0. | 0. |
| 17 | 50 | 8785.3 | 34.65 | -95.96 | -29.3 | -45.7 | 266. | 13.4 | 68.1 | 0.0 | 0. | 0. |
| 17 | 51 | 8773.0 | 34.76 | -95.99 | -29.2 | -45.2 | 263. | 13.6 | 59.0 | 82.5 | 100. | 1. |
| 17 | 52 | 8948.2 | 34.87 | -95.96 | -30.4 | -44.9 | 264. | 13.9 | 60.9 | 86.5 | 98. | 1. |
| 17 | 53 | 9401.7 | 34.99 | -95.94 | -34.9 | -44.9 | 257. | 14.0 | 71.7 | 110.8 | 117. | 1. |
| 17 | 54 | 9408.0 | 35.09 | -95.96 | -35.2 | -45.6 | 254. | 14.5 | 68.7 | 112.1 | 511. | 2. |
| 17 | 55 | 9410.3 | 35.11 | -96.07 | -35.2 | -46.5 | 250. | 15.1 | 66.5 | 103.5 | 410. | 2. |
| 17 | 56 | 9660.5 | 35.09 | -96.19 | -36.9 | -47.2 | 247. | 16.0 | 64.5 | 111.1 | 375. | 2. |
| 17 | 57 | 10122.9 | 35.07 | -96.31 | -40.3 | -48.0 | 254. | 15.5 | 56.4 | 92.6 | 1325. | 3. |
| 17 | 58 | 10246.3 | 35.11 | -96.39 | -41.8 | -49.3 | 262. | 14.1 | 37.8 | 75.6 | 538. | 3. |
| 17 | 59 | 10437.7 | 35.20 | -96.37 | -43.3 | -50.8 | 257. | 13.9 | 43.1 | 0.0 | 420. | 3. |
| 18 | 0 | 10604.3 | 35.28 | -96.28 | -45.1 | -52.4 | 255. | 13.9 | 42.9 | 0.0 | 0. | 0. |
| 18 | 1 | 10650.7 | 35.37 | -96.22 | -45.9 | -53.9 | 258. | 14.0 | 59.8 | 0.0 | 0. | 0. |
| 18 | 2 | 10645.5 | 35.47 | -96.18 | -45.6 | -54.5 | 261. | 13.2 | 88.5 | 0.0 | 0. | 0. |
| 18 | 3 | 10636.3 | 35.56 | -96.13 | -45.6 | -54.5 | 265. | 12.8 | 100.7 | 57.9 | 574. | 3. |
| 18 | 4 | 10640.0 | 35.62 | -96.02 | -45.3 | -54.5 | 260. | 12.4 | 108.3 | 70.2 | 596. | 3. |
| 18 | 5 | 10622.2 | 35.55 | -95.98 | -45.0 | -54.5 | 254. | 13.0 | 91.8 | 64.8 | 480. | 3. |
| 18 | 6 | 10626.0 | 35.46 | -96.06 | -45.3 | -54.5 | 250. | 13.6 | 77.9 | 61.2 | 221. | 2. |
| 18 | 7 | 10618.8 | 35.38 | -96.11 | -45.4 | -54.5 | 248. | 14.3 | 59.5 | 71.6 | 153. | 2. |
| 18 | 8 | 10613.7 | 35.28 | -96.15 | -45.1 | -54.5 | 245. | 14.6 | 43.3 | 62.7 | 119. | 2. |
| 18 | 9 | 10617.1 | 35.20 | -96.24 | -44.8 | -54.5 | 245. | 15.1 | 39.5 | 70.1 | 54. | 1. |
| 18 | 10 | 10617.7 | 35.22 | -96.35 | -45.2 | -54.5 | 251. | 14.8 | 47.2 | 85.7 | 108. | 1. |
| 18 | 11 | 10618.6 | 35.32 | -96.37 | -45.6 | -54.5 | 255. | 14.1 | 60.8 | 0.0 | 68. | 1. |
| 18 | 12 | 10624.5 | 35.43 | -96.34 | -45.7 | -54.5 | 256. | 13.4 | 78.3 | 0.0 | 0. | 0. |
| 18 | 13 | 10625.3 | 35.54 | -96.31 | -45.4 | -54.5 | 256. | 11.8 | 114.4 | 0.0 | 0. | 0. |
| 18 | 14 | 10622.2 | 35.66 | -96.28 | -44.6 | -54.5 | 253. | 10.6 | 127.1 | 82.2 | 0. | 0. |
| 18 | 15 | 10632.1 | 35.73 | -96.19 | -44.5 | -54.5 | 255. | 11.1 | 132.6 | 88.9 | 557. | 3. |
| 18 | 16 | 10637.0 | 35.71 | -96.06 | -44.7 | -54.5 | 248. | 10.9 | 123.8 | 83.0 | 470. | 3. |
| 18 | 17 | 10619.8 | 35.60 | -96.02 | -45.1 | -54.5 | 253. | 13.0 | 103.1 | 81.5 | 431. | 3. |
| 18 | 18 | 10619.3 | 35.51 | -96.05 | -45.3 | -54.5 | 249. | 14.3 | 84.3 | 85.0 | 177. | 2. |
| 18 | 19 | 10626.4 | 35.42 | -96.09 | -45.3 | -54.5 | 245. | 14.6 | 72.2 | 76.1 | 154. | 2. |
| 18 | 20 | 10625.0 | 35.31 | -96.13 | -45.2 | -54.5 | 246. | 14.9 | 52.8 | 87.3 | 118. | 2. |
| 18 | 21 | 10619.8 | 35.21 | -96.19 | -44.9 | -54.5 | 245. | 15.7 | 41.8 | 78.0 | 92. | 1. |
| 18 | 22 | 10626.7 | 35.19 | -96.29 | -45.1 | -54.5 | 250. | 15.8 | 43.8 | 91.6 | 193. | 1. |
| 18 | 23 | 10572.5 | 35.28 | -96.36 | -45.3 | -54.5 | 254. | 15.1 | 56.8 | 0.0 | 99. | 1. |
| 18 | 24 | 9798.8 | 35.40 | -96.35 | -40.2 | -54.5 | 252. | 14.6 | 54.5 | 0.0 | 0. | 0. |
| 18 | 25 | 8461.2 | 35.50 | -96.33 | -29.6 | -44.0 | 277. | 10.9 | 68.1 | 0.0 | 0. | 0. |
| 18 | 26 | 7264.2 | 35.61 | -96.32 | -21.4 | -42.7 | 319. | 6.7 | 47.3 | 0.0 | 0. | 0. |
| 18 | 27 | 6401.6 | 35.71 | -96.28 | -14.5 | -41.0 | 195. | 5.6 | 40.0 | 77.4 | 1506. | 3. |
| 18 | 28 | 5694.0 | 35.73 | -96.19 | -8.9 | -36.5 | 253. | 4.4 | 40.7 | 65.2 | 872. | 3. |
| 18 | 29 | 5104.0 | 35.67 | -96.16 | -4.0 | -29.2 | 343. | 7.0 | 43.2 | 68.8 | 436. | 3. |
| 18 | 30 | 4734.4 | 35.64 | -96.23 | -1.7 | -25.7 | 347. | 9.9 | 39.1 | 75.5 | 253. | 3. |
| 18 | 31 | 4389.2 | 35.63 | -96.32 | 0.9 | -30.0 | 355. | 9.1 | 47.9 | 109.7 | 327. | 3. |
| 18 | 32 | 4060.5 | 35.61 | -96.41 | 2.3 | -15.1 | 341. | 7.8 | 52.5 | 128.7 | 0. | 0. |
| 18 | 33 | 3686.8 | 35.59 | -96.49 | 4.7 | -6.3 | 201. | 3.1 | 51.4 | 127.7 | 0. | 0. |
| 18 | 34 | 3339.1 | 35.58 | -96.58 | 7.8 | -6.9 | 112. | 2.3 | 59.8 | 145.0 | 0. | 0. |
| 18 | 35 | 3006.2 | 35.58 | -96.68 | 10.7 | -9.1 | 147. | 5.5 | 63.0 | 130.8 | 391. | 2. |
| 18 | 36 | 2691.2 | 35.58 | -96.77 | 12.7 | -8.6 | 153. | 6.9 | 62.5 | 0.0 | 249. | 2. |
| 18 | 37 | 2342.9 | 35.58 | -96.86 | 13.7 | 1.9 | 166. | 8.5 | 53.4 | 0.0 | 314. | 2. |
| 18 | 38 | 2023.4 | 35.58 | -96.96 | 14.7 | 10.2 | 172. | 9.4 | 47.5 | 133.6 | 531. | 2. |
| 18 | 39 | 1665.3 | 35.58 | -97.04 | 17.2 | 13.5 | 173. | 8.9 | 46.9 | 134.1 | 645. | 2. |
| 18 | 40 | 1243.6 | 35.56 | -97.12 | 19.9 | 16.8 | 169. | 8.3 | 41.6 | 138.4 | 866. | 2. |
| 18 | 41 | 937.7 | 35.54 | -97.21 | 22.7 | 19.0 | 163. | 6.5 | 42.0 | 153.9 | 1257. | 2. |
| 18 | 42 | 1147.1 | 35.56 | -97.29 | 21.3 | 18.0 | 173. | 7.6 | 38.0 | 160.9 | 1232. | 2. |
| 18 | 43 | 1503.0 | 35.62 | -97.29 | 18.8 | 15.5 | 192. | 7.8 | 38.4 | 148.7 | 977. | 2. |
| 18 | 44 | 1784.1 | 35.65 | -97.20 | 16.8 | 14.0 | 189. | 8.3 | 39.6 | 138.4 | 1209. | 2. |
| 18 | 45 | 2118.3 | 35.66 | -97.11 | 14.7 | 10.7 | 184. | 9.1 | 44.5 | 129.7 | 1193. | 2. |
| 18 | 46 | 2543.5 | 35.67 | -97.03 | 14.1 | -4.4 | 175. | 7.0 | 55.4 | 129.1 | 1178. | 2. |
| 18 | 47 | 2939.1 | 35.67 | -96.95 | 12.1 | -12.1 | 169. | 5.8 | 61.6 | 154.7 | 1151. | 2. |
| 18 | 48 | 3264.1 | 35.68 | -96.87 | 9.2 | -8.5 | 184. | 2.5 | 62.9 | 159.7 | 1099. | 2. |
| 18 | 49 | 3686.9 | 35.68 | -96.77 | 5.4 | -4.8 | 314. | 2.5 | 56.2 | 155.2 | 1049. | 2. |
| 18 | 50 | 4179.4 | 35.68 | -96.68 | 1.9 | -10.0 | 332. | 8.8 | 50.1 | 145.5 | 966. | 2. |
| 18 | 51 | 4640.0 | 35.68 | -96.58 | 0.1 | -23.4 | 345. | 12.0 | 41.5 | 112.1 | 673. | 2. |
| 18 | 52 | 5048.4 | 35.68 | -96.48 | -2.6 | -27.7 | 334. | 9.5 | 39.9 | 81.6 | 510. | 2. |
| 18 | 53 | 5293.9 | 35.67 | -96.39 | -4.3 | -29.4 | 334. | 6.0 | 40.9 | 0.0 | 0. | 0. |
| 18 | 54 | 5294.2 | 35.67 | -96.29 | -4.5 | -30.6 | 334. | 6.4 | 41.0 | 0.0 | 0. | 0. |

| | | | | | | | | | | | | |
|---|---|---|---|---|---|---|---|---|---|---|---|---|
| 18 | 55 | 5288.3 | 35.64 | -96.21 | -4.5 | -31.7 | 330. | 6.0 | 42.4 | 0.0 | 0. | 0. |
| 18 | 56 | 5292.0 | 35.58 | -96.25 | -4.5 | -32.5 | 320. | 5.6 | 42.5 | 0.0 | 139. | 2. |
| 18 | 57 | 5298.3 | 35.56 | -96.33 | -4.7 | -32.5 | 318. | 5.6 | 42.6 | 0.0 | 119. | 2. |
| 18 | 58 | 5262.3 | 35.56 | -96.43 | -4.5 | -31.5 | 318. | 5.4 | 43.2 | 0.0 | 88. | 2. |
| 18 | 59 | 4843.9 | 35.54 | -96.52 | -2.2 | -29.8 | 330. | 8.5 | 44.0 | 0.0 | 65. | 2. |
| 19 | 0 | 4338.5 | 35.53 | -96.60 | 1.4 | -29.1 | 346. | 9.0 | 50.3 | 0.0 | 97. | 2. |
| 19 | 1 | 3930.5 | 35.52 | -96.69 | 3.3 | -8.3 | 328. | 6.5 | 55.1 | 0.0 | 203. | 2. |
| 19 | 2 | 3437.7 | 35.51 | -96.78 | 6.9 | -6.2 | 247. | 1.7 | 61.0 | 0.0 | 341. | 2. |
| 19 | 3 | 2845.2 | 35.50 | -96.87 | 11.4 | -8.1 | 154. | 5.7 | 66.8 | 0.0 | 259. | 2. |
| 19 | 4 | 2321.4 | 35.50 | -96.95 | 13.3 | 4.9 | 169. | 8.2 | 55.0 | 0.0 | 193. | 2. |
| 19 | 5 | 1803.4 | 35.49 | -97.04 | 16.4 | 11.4 | 177. | 8.7 | 47.8 | 0.0 | 211. | 2. |
| 19 | 6 | 1288.0 | 35.49 | -97.13 | 19.6 | 16.7 | 184. | 7.8 | 44.3 | 0.0 | 357. | 2. |
| 19 | 7 | 1032.3 | 35.48 | -97.20 | 22.0 | 19.0 | 181. | 6.6 | 38.6 | 0.0 | 530. | 2. |
| 19 | 8 | 1026.6 | 35.48 | -97.28 | 22.1 | 19.0 | 176. | 6.5 | 38.2 | 0.0 | 0. | 0. |
| 19 | 9 | 1035.0 | 35.48 | -97.37 | 22.3 | 19.0 | 174. | 7.4 | 41.7 | 0.0 | 0. | 0. |
| 19 | 10 | 1037.7 | 35.47 | -97.44 | 22.5 | 19.0 | 177. | 7.4 | 43.5 | 0.0 | 0. | 0. |
| 19 | 11 | 936.8 | 35.46 | -97.51 | 23.3 | 19.4 | 174. | 7.3 | 47.8 | 0.0 | 0. | 0. |

## REFERENCES


Altshuller, A.P., The role of nitrogen oxides in nonurban ozone formation in the planetary boundary layer over N. America, W. Europe, and adjacent areas of ocean, Atmos. Environ. 20, 245-268, 1986.

Chameides, W.L., D.D. Davis, M.O. Rodgers, J. Bradshaw, S. Sandholm, G. Sachse, G. Hill, G. Gregory, and R. Rasmussen, Net ozone photochemical production over the eastern and central N. Pacific as inferred from GTE/CITE 1 observations during fall 1983, J. Geophys. Res., 92, 2131-2152, 1987.

Chameides, W.L. and J.G. Walker, A photochemical theory of tropospheric ozone, J. Geophys. Res., 78, 8751-8760, 1973.

Chatfield, R.B. and P.J. Crutzen, Sulfur dioxide in remote oceanic air: cloud transport of reactive precursors, J. Geophys. Res., 89, 7111-7132, 1984.

Condon, E.P., E.F. Danielson, G.W. Sachse, and G.F. Hill, Carbon monoxide measurements over the eastern Pacific during GTE/CITE 1, J. Geophys. Res., 92, 2095-2104, 1987.

Crutzen, P.J., A discussion of the chemistry of some minor contituents in the stratosphere and troposphere, Pure Applied Geophysics, 106-108, 1385-1399, 1973.

Crutzen, P.J. and L.T. Gidel, A two-dimensional photochemical model of the atmosphere, 2, the tropospheric budgets of the anthropogenic chlorocarbons, CO, CH4, CH3Cl, and the effect of the various NOx sources on tropospheric ozone, J. Geophys. Res. , 88, 6641-6661, 1983.

Danielson, E.F., S.E. Gaines, R.S. Hipskind, G.L. Gregory, G.W. Sachse and G.F. Hill, Meteorological context for fall experiments including distributions of water vaper, ozone, and carbon monoxide, J. Geophys. Res., 92, 1986-1994, 1987.

Davis, D.D., J.D. Bradshaw, M.O. Rodgers, S.T.Sandholm, and S.KeSheng, Free tropospheric and boundary layer measurements of NO over the central and eastern N. Pacific Ocean, J. Geophys. Res., 92, 2049-2070, 1987.

Delany, A.C., R.R. Dickerson, F.L. Melchoir, and A.F. Wartburg, Modification of a commercial NOx detector for high sensitivity, Rev. Sci. Instrum., 53, 1899-1902, 1982.

Dickerson, R.R., D.H. Stedman, and A.C. Delany, Direct measurements of ozone and nitrogen dioxide photolysis rates in the troposphere, J. Geophys. Res., 87, 4933-4946, 1982.

Dickerson, R.R., A.C. Delany, and A.F.Wartburg, Further modification of a commercial NOx detector for high sensitivity, Rev. Sci. Instrum., 55, 1995-1998, 1984.

Dickerson, R.R. and A.C. Delany, Modification of a commercial gas filter correlation CO detector for enhanced sensitivity. To appear in J. Atmos. Oceanic Technol., 1988.

Dickerson, R.R., G.J. Huffman, W.T. Luke, L.J. Nunnermacker, K.E. Pickering, A.C.D. Leslie, C.G. Lindsey, W.G.N. Slinn, T.J. Kelly, A.C. Delany, J.P. Greenberg, P.R. Zimmerman, J.F. Boatman, J.D. Ray, and D.H. Stedman, Thunderstorms: An important mechanism in the transport of air pollutants, Science, 235, 460-465, 1987.

Droppo, J.G., Concurrent measurements of ozone dry deposition using eddy correlation and profile flux methods, J. Geophys. Res., 90, 2111-2118, 1985.

Fahey, D.W., G. Hubler, D.D. Parrish, E.J. Williams, R.E. Norton, B.A. Ridley, H.B. Singh, S.C. Liu, and F.C. Fehsenfeld, Reactive nitrogen species in the troposphere: Measurements of NO, NO2, HNO3, particulate nitrate, peroxyacetyl nitrate (PAN), O3, and total reactive odd nitrogen (NOy) at Niwot Ridge, Colorado, J. Geophys. Res., 91, 9781-9793, 1986.

Fehsenfeld, F.C., R.R. Dickerson, G. Hubler, W.T. Luke, L. Nunnermacker, J. Roberts, E.J. Williams, J.G. Calvert, C. Curran, A.C. Delany, C.S. Eubank, D.W. Fahey, A. Fried, B. Gandrud, A. Langford, P. Murphy, R.B. Norton, K.E. Pickering, and B. Ridley, A ground-based intercomparison of NO, NOx, and NOy measurement techniques, J. Geophys. Res., 92, 14710-14722, 1987.

Finlayson-Pitts, B.J., and J.N. Pitts, Atmospheric Chemistry: Fundamentals and Experimental Techniques, John Wiley & Sons, New York, 1986.

Fishman, J., W. Seiler, and P. Haagenson, Simultaneous presence of O3 and CO bands in the troposphere, Tellus, 32, 456-463, 1980.

Fishman, J. and W. Seiler, Correlative nature of ozone and carbon monoxide in the troposphere: implications for the tropospheric ozone budget, J. Geophys. Res., 88, 3662-3670, 1983.

Fishman, J., Ozone in the troposphere, in Ozone in the Free Atmosphere, edited by R.C. Whitton and S.S. Prasad, pp. 161-194, Van Nostrand Reinhold, New York, 1985.

Fishman, J., P. Minnis, and H.G. Reichle, Use of satellite data to study tropospheric ozone in the tropics, J. Geophys. Res., 91, 14451-14465, 1986.

Fishman, J., G.L. Gregory, G.W. Sachse, S.M. Beck, and G.F. Hill, Vertical profiles of ozone, carbon monoxide, and dew-point temperature obtained during GTE/CITE 1, October-November 1983, J. Geophys. Res., 92, 2083-2094, 1987.

Gidel, L.T., Cumulus cloud transport of transient tracers, J. Geophys. Res., 88, 6587-6599, 1983.

Greenberg, J.P., and P.R. Zimmerman, Nonmethane hydrocarbons in remote tropical, continental, and marine atmospheres, J. Geophys. Res., 89, 4767-4778, 1984.

Hampson, R.F., Chemical kinetic and photochemical data sheets for atmospheric reactions, Report No. FAA-EE-80-17, Federal Aviation Administration, Washington, D.C., 1980.

Hanst, P.L., J.W. Spence, and E.O. Edney, Carbon monoxide production in photooxidation of organic molecules in the air, Atmos. Environ., 14, 1077-1088, 1980.

Holton, J.R., An Introduction to Dynamic Meteorology, 2nd. ed., Academic Press, New York, 1979.

Isaac, G.A., P.L. Joe, and P.W. Summers, The vertical transport and redistribution of pollutants by clouds, in The Meteorology of Acid Deposition, edited by P.J. Samson, pp. 496-512, Air Pollution Control Association, Pittsburgh, 1984.

Junge, C.E., Global ozone budget and exchange between stratosphere and troposphere, Tellus, 14, 364-377, 1962.

Kerr, J.A., and J.G. Calvert, Chemical transformation modules for Eulerian acid deposition models - Vol 1: The gas-phase chemistry, U.S. Environmentral Protection Agency, Research Triangle Park, NC, 1984.

Leighton, P.A., Photochemistry of Air Pollution, Academic Press, New York, 1961.

Levy II, H., Normal atmosphere: Large radical and formaldehyde concentrations predicted, Science, 173, 141-143, 1971.

Liu, S.C., M. Trainer, F.C. Fehsenfeld, D.D Parrish, E.J. Williams, D.W. Fahey, G. Hubler, and P.C. Murphy, Ozone production in the rural troposphere and the implications for regional and global ozone distributions, J. Geophys. Res., 92, 4191-4207, 1987.

Logan, J.A., Nitrogen oxides in the troposphere: global and regional budgets, J. Geophys. Res., 88, 10785-10807, 1983.

Logan, J.A., M.J. Prather, S.C. Wolfsy and M.B. McElroy, Tropospheric chemistry: a global perspective, J. Geophys. Res., 86, 7210-7254, 1981.

Lyons, W.A., R.H. Calby and C.S. Keen, The impact of mesoscale convective systems on regional visibility and oxidant distributions during persistent elevated pollution episodes, J. Clim. Appl. Met., 25, 1518-1531, 1986.

Lyons, W.A. and R.H. Calby, Further case studies on the impact of mesoscale convective systems on regional ozone and haze distributions, paper presented at the 79th. annual meeting of the Air Pollut. Contr. Assoc., Minneapolis, Minnesota, June 2-27, 1986.

Meitin, J.G., and J.B. Cunning, The Oklahoma-Kansas Preliminary Regional Experiment for Storm-Central (O-K Pre-Storm), Vol. I. Daily Operations Summary, NOAA Technical Memorandum ERL-ESG- 20, Environmental Sciences Group, Boulder, Colorado, 1985.

National Center for Atmospheric Research (NCAR), Research Aviation Facility, The NCAR Sabreliner: Overview and Summary of Capabilities, Bul. No. 3, Boulder, Colorado, 1984.

Panofsky, H.A., and G.W. Brier, Some Applications of Statistics to Meteorology, The Pennsylvania State University, 1968.

Pickering, K.E., Observations of Tropospheric Trace Gases and Techniques for Assessing the Regional Transport of Air Pollutants, doctoral dissertation, Univ. of Maryland, 1987.

Pickering, K.E., R.R. Dickerson, G.J. Huffman, J.F. Boatman, and A. Schanot, Trace gas transport in the vicinity of frontal convective clouds, J. Geophys. Res., 93, 759-773, 1988a.

Pickering, K.E., R.R. Dickerson, W.T. Luke, and L.T. Nunnermacker, Clear-sky vertical profiles of trace gases as influenced by upstream convective activity, submitted to J. Geophys. Res., 1988b.

Quenouille, M.H., Associated Measurements, Butterworth Scientific Publications, London, 1952.

Ridley, B.A., M.A. Corrall, G.L. Gregory, Measurements of nitric oxide in the boundary layer and free troposphere over the Pacific Ocean, J. Geophys. Res., 92, 2025-2047, 1987.

Stedman, D.H., E.E. Darby, F. Stuhl, and H. Niki, Analysis of ozone and nitric oxide by a chemluminescent method in laboroatory and atmospheric studies of photochemical smog, J. Air Pollut. Contr. Assoc., 22, 260-263, 1972.

Stedman, D.H. and R.E. Shetter, The global budget of atmospheric nitrogen species, in Trace Atmospheric Constituents, Advan. in Environ. Sci. and Tech., vol. 12, edited by S.E. Schwartz, John Wiley, New York, 1983.

Stull, R.B., Models and measurements of the interaction between the mixed layer and fair weather cumulus clouds, in The Meteorology of Acid Deposition, edited by P.J. Samson, pp. 167-175, Air Pollution Control Association, 1984.

Thompson, A.M. and R.J. Cicerone, Possible pertibations to atmospheric CO, $CH_4$, and OH, J. Geophys. Res., 91, 10853-10864, 1986.

US Air Force, Weather for Aircrews, AFM 51-12, Vol 1, Washington, DC., 1982.

Vukovich, F.M., J. Fishman, and E.V. Browell, The reservoir of ozone in the boundary layer of the eastern U.S., and its potential impact on the global tropospheric ozone budget, J. Geophys. Res., 90, 5687-5698, 1985.

Wagner, J.A., R.A. Walters, L.J. Maiocco, and D.R. Neal, Development of the NAPAP Emission Inventory for 1980, Report Number EPA-600/7-86/057a, U.S. Environmental Protection Agency, Research Traingle Park, N.C., 1986.

Williams, E.J., D.H. Fahey, G. Hubler, D.D. Parrish, P.C. Murphy, R.B. Norton, C.S. Eubank, D.L. Albritton, and F.C. Fehsenfeld, Measurements of NO, NOx and O3 at Niwot Ridge, Colorado, Eos Trans AGU, 65, 833, 1984.

Zimmerman P.R., R.B. Chatfiled, J. Fishman, P.J. Crutzen and P.L. Hanst, Estimates on the production of CO and $H_2$ from the oxidation of hydrocarbon emissions from vegetation, Geophys. Res. Lett., 5, 679-682, 1978.